

RICE UNIVERSITY


**Design and Control of an Exoskeletal  
Rehabilitation Device for Stroke and Spinal Cord  
Injury Patients**

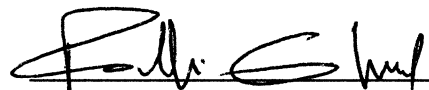
by

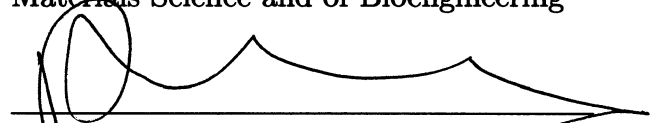
**Ali Utku Pehlivan**

A THESIS SUBMITTED  
IN PARTIAL FULFILLMENT OF THE  
REQUIREMENTS FOR THE DEGREE  
**Master of Science**

APPROVED, THESIS COMMITTEE:

  
\_\_\_\_\_  
Marcia K. O'Malley, Chair  
Associate Professor of Mechanical  
Engineering and of Computer Science

  
\_\_\_\_\_  
Fathi H. Ghorbel  
Professor of Mechanical Engineering and  
Materials Science and of Bioengineering

  
\_\_\_\_\_  
Pol D. Spanos  
Lewis B. Ryon Professor of Mechanical  
Engineering and of Civil Engineering

Houston, Texas

December, 2011

## ABSTRACT

### Design and Control of an Exoskeletal Rehabilitation Device for Stroke and Spinal Cord Injury Patients

by

Ali Utku Pehlivan

Robotic rehabilitation has gained significant traction in recent years, due to the clinical demonstration of its efficacy in restoring function for upper extremity movements and locomotor skills, demonstrated primarily in stroke populations. In this thesis, I present the design of MAHI Exo-II, a robotic exoskeleton for rehabilitation of the upper extremity after stroke, spinal cord injury, or other brain injuries. The five degree-of-freedom robot enables elbow flexion-extension, forearm pronation-supination, wrist flexion-extension, and radial-ulnar deviation.

In the first part of this thesis, hardware design of the system is presented. The device offers several significant design improvements compared to its predecessor, MAHI Exo I. Specifically, issues with backlash and singularities in the wrist mechanism have been resolved, torque output has been increased in the forearm and elbow joints, a passive degree of freedom has been added to allow shoulder abduction thereby improving alignment especially for users who are wheelchairbound, and the hardware now enables simplified and fast swapping of treatment side. These modifications are discussed in the thesis, and results for the range of motion and maximum torque output capabilities of the new design and its predecessor are presented.

In the second part of this thesis, I present the modification and implementation of

a previously reported linear position and force control to MAHI Exo-II. The modified controller includes three different modes which are designed for use with patients with different levels of severity of injury. These modes either completely assist or resist the patient during the movement. Next, I present the implementation of a previously proposed nonlinear control algorithm in simulation for the forearm and wrist module of MAHI Exo-II. The proposed nonlinear controller aims to provoke a compliant characteristic to the device and assist the patient only as much as needed. Finally, the result of clinical testing of the feasibility of the mechanical design and the efficacy of the control modes with a 28-year-old female SCI patient are presented.

# Contents

Abstract	ii
List of Illustrations	vi
List of Tables	ix
<b>1 Introduction</b>	<b>1</b>
1.1 Hardware Design . . . . .	2
1.2 Controller Design . . . . .	6
1.3 Thesis Outline . . . . .	7
<b>2 MAHI Exo-II: Kinematic Structure and Mechanical Design</b>	<b>8</b>
2.1 Introduction . . . . .	9
2.2 Literature Review . . . . .	9
2.3 System Description . . . . .	12
2.3.1 Kinematic Structure . . . . .	12
2.3.2 Design Description . . . . .	25
2.4 Results . . . . .	30
<b>3 Control Implementations</b>	<b>35</b>
3.1 Introduction . . . . .	35
3.2 Literature Review . . . . .	36
3.3 Control Modes, Modifications and Clinical Testing . . . . .	38
3.3.1 Passive Mode . . . . .	39
3.3.2 Triggered Mode . . . . .	40

3.3.3	Constrained Mode . . . . .	41
3.3.4	Graphical User Interface . . . . .	42
3.3.5	Pilot Clinical Testing and Results . . . . .	44
3.4	Assist-As-Needed Control . . . . .	47
3.4.1	Adaptive Controller . . . . .	48
3.4.2	Simulation Results . . . . .	54
<b>4</b>	<b>Conclusions and Future Work</b>	<b>59</b>
<b>A</b>	<b>Technical Drawings</b>	<b>61</b>
<b>B</b>	<b>Autolev and C-Codes for Kinematic and Dynamic Equations</b>	<b>79</b>
B.1	Autolev Code for Kinematic Equations . . . . .	79
B.1.1	Position Level . . . . .	79
B.1.2	Velocity Level . . . . .	83
B.2	Autolev Code for Dynamics Equations . . . . .	93
	<b>Bibliography</b>	<b>106</b>

# Illustrations

1.1	(a) End-effector based two DOF MIT-MANUS. (b) ARMin, a six DOF exoskeletal rehabilitation device. . . . .	3
1.2	(a) Grounded exoskeleton, MAHI-Exo-I. (b) An ungrounded exoskeleton, X-Arm 2, attached to the operator's body. . . . .	4
2.1	MAHI Exo-II – Elbow, forearm and wrist exoskeleton for stroke and spinal cord injury (SCI) rehabilitation. . . . .	8
2.2	[Human arm kinematics . . . . .	15
2.3	Kinematic structure of MAHI Exo II – A 3-RPS (Revolute-Prismatic-Spherical) platform constitutes the wrist degrees-of-freedom of the robot and is in serial configuration with forearm and elbow degrees-of-freedom. (Adopted from [1]) . . . . .	16
2.4	(a) CAD model of the wrist ring with inclined surface to increase wrist range of motion. (b) Manufactured inclined wrist ring attached to the spherical joint. . . . .	27
2.5	(a) Forearm mechanical design CAD model for MAHI Exo I. Forearm encoder ring ran along the circumference of the forearm and was prone to misalignment errors. A frameless brushless motor inside an aluminum encasing actuated the joint. (b) Forearm mechanical design CAD model for MAHI Exo II. Current design employs a Maxon DC motor with cable drive mechanism, and the encoder is coupled to the motor shaft at the bottom end (not shown in this model). . . . .	28

2.6	(a) A tapered pin connects the capstan to the elbow shaft on both sides. (b) The tapered pin can be easily removed to allow driving the elbow joint from the other side. By changing the side of the counterweight, the device can be used for the desired arm. . . . .	29
2.7	(a) In MAHI Exo-I, elbow motor and counterweight fixed on one side allowed only rehabilitation of the right arm. (b) In MAHI Exo-II, counterweight can be attached on either side to allow both left and right arm therapy. (c) A passive DOF that tilts the whole device in the coronal plane provides improved patient comfort and posture during therapy. . . . .	30
2.8	(a) CAD model of the MAHI Exo-II complete assembly. (b) Manufactured MAHI Exo-II complete assembly with motors, handle and counterweight attached. . . . .	33
3.1	Target Hitting Task– Subject must move the cursor to the highlighted target (left target in this case) . . . . .	42
3.2	(a) Triggered mode and passive mode can be operated over the same GUI. (b) The GUI for the constrained mode, allows therapist to run a mini trial prior to main trial to measure the ROM capabilities of the patients . . . . .	43
3.3	Subject – MAHI Exo-II is being used by a 28-year-old SCI patient. .	45
3.4	(a) 4 DOF RiceWrist employs a 3-RPS (revolute-prismatic-spherical) parallel mechanism at the wrist module and a revolute joint at the forearm (b) CAD model of RiceWrist. . . . .	48
3.5	Trajectory tracking for both adaptive and PD controllers. (a) and (b) shows the rotation around $x_4$ for adaptive and PD controllers respectively, and (c) and (d) shows the rotation around $z_4$ for adaptive and PD controllers respectively . . . . .	55

3.6	Trajectory tracking with increased $K_p$ gains. (a) and (b) shows the rotation around $x_4$ for adaptive and PD controllers respectively . . .	58
A.1	Wrist Ring . . . . .	62
A.2	Wrist Link Base . . . . .	63
A.3	Wrist Motor Mount . . . . .	64
A.4	Bottom Plate to motor connector . . . . .	65
A.5	Bottom Plate to motor connector Reversed . . . . .	66
A.6	Wrist Bearing Spacer . . . . .	67
A.7	Bottom Plate Ring . . . . .	68
A.8	Forearm Inner Drum . . . . .	69
A.9	Forearm Outer Drum . . . . .	70
A.10	Forearm Elbow Connector Right . . . . .	71
A.11	Forearm Elbow Connector Left . . . . .	72
A.12	Elbow to Forearm Joint . . . . .	73
A.13	Forearm Motor Mount . . . . .	74
A.14	Elbow to Ground Joint . . . . .	75
A.15	Ground Block . . . . .	76
A.16	Elbow Capstan Arc . . . . .	77
A.17	Elbow Motor Mount . . . . .	78



# Tables

2.1	The torque and workspace capabilities of human arm extracted from [2].	13
2.2	The torque and workspace capabilities of human arm for 19 activities of daily living (ADL) . . . . .	14
2.3	Link parameters for the Elbow and Forearm joints . . . . .	17
2.4	Achievable joint ranges of motion (ROM) and maximum continuous joint torque output values for MAHI Exo I and MAHI Exo II. Maximum joint ROM and torque values for 19 activities of daily living (ADL) as extracted from [3] are also given for comparison. . . .	31
3.1	Clinical testing results . . . . .	46
3.2	Control Effort . . . . .	57

# Chapter 1

## Introduction

In the United States, each year about 795,000 people experience a stroke. Stroke is the leading cause of long-term disability and has a significant social and economic impact on the United States with a \$68.9 billion total estimated cost for 2009 [4]. There are approximately 12,000 incidences of Spinal Cord Injury (SCI) in the US each year [5]. With the average age of injury as low as 40.2 years, a much younger population is effected by SCI than by stroke, leading to estimated yearly direct and indirect costs of \$14.5 billion and \$5.5 billion, respectively [6].

Rehabilitation of patients with impairments due to neurological lesions mostly includes task-oriented repetitive movements which can improve muscle strength and movement co-ordination in these patients [7]. The goal of rehabilitation is to recover the lost brain plasticity and to improve functional outcomes, and to fulfill this goal, therapy has to be intensive with long duration and high repetition numbers [8]. Considering these factors, classical rehabilitation has obvious limitations. First of all, classical rehabilitation is labor intensive and as a consequence expensive, so the duration of the training sessions is generally shorter than the required amount, the main factor that impedes achievement of the optimal therapeutic outcome [9]. Because consistency of training depends on the performance of the therapist, classical rehabilitation is further limited.

Rehabilitation robotics is a branch of robotics which aims to eliminate most of the disadvantages of classical rehabilitation. Utilizing robotics to model machines for

rehabilitation increases the number of training sessions with consistent repetitions and reduces personnel cost by enabling the opportunity to assign one therapist to train two or more patients [10]. Robotics also enables the objective and quantitative performance evaluation of patients, which is not possible with classical rehabilitation, both during and after the therapy sessions. In addition, virtual reality implementations can provide a unique medium where therapy can be provided within a functional and highly motivating context [11], and consequently the intensity of the therapy can be increased.

The results of clinical studies involving robotic rehabilitation protocols support the idea of implementing these devices in treatment of stroke and SCI patients. Due to the clinical demonstrations of its efficacy in restoring function for upper extremity movements and locomotor skills primarily in stroke populations, robotic rehabilitation has gained significant traction in recent years. So far, a number of aspects of robotic rehabilitation have been investigated, including, among others, hardware design and development of control algorithms for upper extremity rehabilitation robots, which are the focus of this thesis. In the following sections first the main consideration points for design and development, and applied methods in upper extremity rehabilitation robotics are explained briefly. Then the applied methods for this work are summarized.

## 1.1 Hardware Design

From a mechanical design point of view, rehabilitation robots can be classified into two groups: end-effector based robots and exoskeletons (see Fig.1.1). MIT-MANUS [12] (Fig. 1.1(a)), a two degree-of-freedom (DOF) planar manipulator with a workspace in the horizontal plane, is an example of an end-effector based robot. Based on

an industrial 6 DOF PUMA robot, Mirror Image Movement Enabler (MIME) [13] constitutes another example of an end-effector based design.

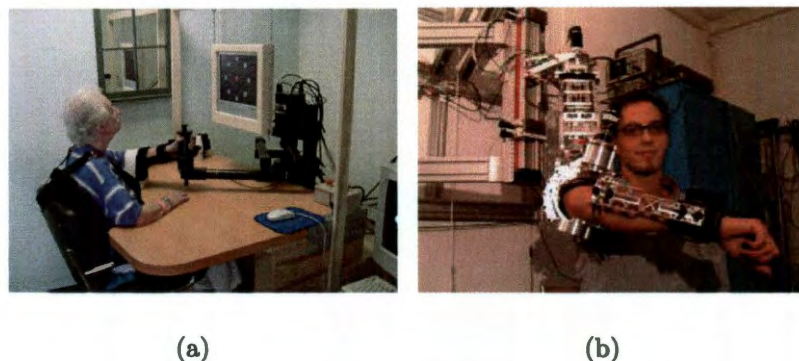


Figure 1.1 : (a) End-effector based two DOF MIT-MANUS. (b) ARMin, a six DOF exoskeletal rehabilitation device.

Although end-effector based robots provide training capability encapsulating a large portion of the functional workspace, they do not possess the ability to apply torques to specific joints of the arm. Exoskeletons, on the other hand, are designed to resemble human anatomy and their structure enables individual actuation of joints. Examples of upper-extremity rehabilitation exoskeletons include 5 DOF MAHI Exo-skeleton [1], 5 DOF Rupert [14], 6 DOF ARMin [9] (Fig. 1.1(b)) and 7 DOF CADEN-7 [3]. Recently, rehabilitation engineering research has increasingly focused on quantitative evaluation of residual motor abilities in an effort to obtain an objective evaluation of rehabilitation and pharmacological treatment effects [15]. Exoskeletons offer the advantage of precisely recording and monitoring isolated joint movements of the arm and wrist and hence are a better-suited design option versus end-effector based designs for this purpose.

Among exoskeletal rehabilitation robots, another classification in terms of mechanical design can be made: grounded and ungrounded robots. Ungrounded robots



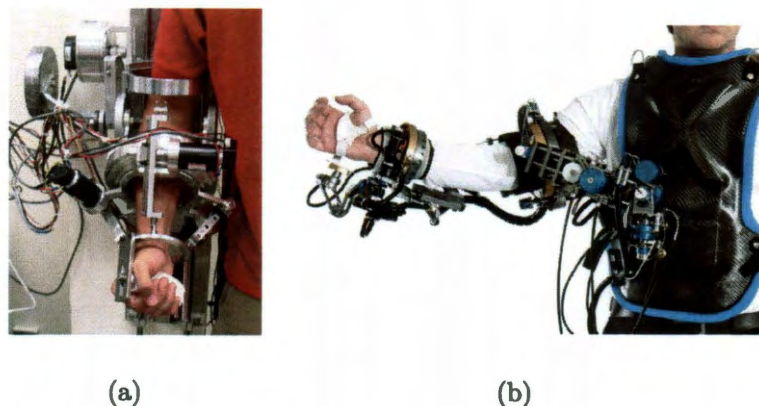


Figure 1.2 : (a) Grounded exoskeleton, MAHI-Exo-I. (b) An ungrounded exoskeleton, X-Arm 2, attached to the operator's body.

can be worn by the patient like a costume and are attached only to the body of the patient. These kinds of devices enable the patient to have more naturalistic movements and allow large workspace capabilities during the movements. The X-Arm 2 [16] is an electrically actuated ungrounded exoskeleton which possesses 14 DOF (8 active and 6 passive), and the authors claim that the design allows interaction with a much bigger portion of the human functional workspace with respect to other currently known systems. However, despite their better movement capability, ungrounded robots can offer limited torque output capability. Because the devices are carried by the patients during the rehabilitation sessions, they have to be lightweight, which limits the chosen actuator sizes and hence the torque output. On the other hand, grounded robots, because of their structure, provide more flexibility in actuator selection. Also, grounded robots offer design simplicity compared to ungrounded robots [1].

The size, weight, force/torque output of and the required control effort for a robotic system are either directly or indirectly affected by the actuation type of the system. Hydraulic, pneumatic and electric actuation are three main actuation types used in robotics. In upper extremity rehabilitation robotics, though, hydraulic actu-

ators are rarely used because of disadvantages such as oil leakage, necessity of wide space and return oil line [17]. Pneumatic actuators offer a high power-to-weight ratio which makes them ideal for light weight applications (for example ungrounded robots). But their highly nonlinear dynamics and low bandwidth make their control challenging and inappropriate for virtual reality application [1]. Electrical actuation is the most commonly used type amongst upper extremity rehabilitation robot applications. Electric actuators, although they possess lower power-to-weight ratio, allow advanced control applications which include virtual reality implementations. Because grounded robots enable one to use larger and heavier motors, electrical actuators are the most important candidates for this kind of device.

A transmission system enables one to transmit the motion from the actuator to the specific part of a system, and while doing so the provided torque/force values can be increased, while the speed of the motion is decreased. Considering that we are dealing with patients with neurological impairments, it is fair to say that upper extremity rehabilitation robots will usually operate at low speeds. So high operation speed is not a crucial design specification for these devices. Torque/force output of a rehabilitation robot, on the other hand, can be considered as one of the performance metrics of the system. Although there are a variety of transmission systems, gear drive and cable drive are the two most frequently used transmission types in rehabilitation robotics. Gear drives are easy to implement but introduce backlash and friction to the system. Both backlash, by causing instability, and friction, by impeding backdrivability, obstruct virtual reality/haptic implementations. Cable drive, on the other hand, allows backdrivability and offers backlash-free transmission system. So, although it increases the design complexity, cable drive is frequently used in haptic devices [18].

MAHI Exo-II, whose mechanical design builds upon its predecessor MAHI Exo-I, is a grounded, exoskeletal device which uses electrical motors for actuation and cable drive for transmission. MAHI Exo-I was designed as a high fidelity haptic interface. Because one of the advantages of robotic rehabilitation over classical rehabilitation is the opportunity of inclusion of the virtual reality/haptic applications in the training sessions, the basic mechanical structure of the MAHI Exo-I is preserved. The motivation to implement an exoskeletal design is to achieve better resemblance to human anatomy and ability of individual actuation of joints. Actuation has been achieved with electric motors, rather than pneumatic actuators, to have a larger bandwidth and consequently have the ability to convey high frequency forces and better sense of touch. The system, because of the load of electric motors, is grounded. MAHI Exo-II employs cable drive to ensure backdrivability and zero backlash.

MAHI Exo-II, as detailed in Chapter 2, proposes significant design improvements over MAHI Exo-I, based on results of pilot clinical testing with SCI patients, and these modifications resulted in reduction of backlash and singularities, increased torque outputs, streamlined interchange between left and right arm configurations and improved ergonomics.

## 1.2 Controller Design

One of the most researched areas in rehabilitation robotics is the development of control algorithms to implement the desired interaction of the device with the patient so that the selected exercises to be performed by the participant provoke motor plasticity, and therefore improve motor recovery [19]. Proposed control strategies vary according to a number of considerations such as the device structure (actuation type) and the intended subject profile (severely injured versus less severely injured

patients), and control structures vary from linear position feedback controllers to nonlinear adaptive control algorithms. In this thesis, I present the modification and implementation of a previously reported linear position and force control to a new hardware system and implement a previously proposed nonlinear control algorithm in simulation for the forearm and wrist module of MAHI Exo-II. The modified controller includes three different modes which are designed for use with patients with different levels of severity of injury. While these modes either completely assist or resist the patient during the movement, the proposed nonlinear controller aims to provoke a compliant characteristic to the device and assist the patient only as much as needed.

### **1.3 Thesis Outline**

The thesis is structured as follows: Chapter 1 provides an overview of upper extremity rehabilitation robotics and presents the applied methods for hardware design and controller development. Chapter 2 gives a detailed description of the hardware design of the system: the deficiencies of the previous design and the introduced design improvements are presented. Chapter 3 details the control modes implemented on MAHI Exo-II and describes the proposed adaptive controller. Chapter 4 summarizes the results of design improvements, the applied control of the system and proposes the future work.



## Chapter 2

### MAHI Exo-II: Kinematic Structure and Mechanical Design

In this chapter, I present the design of MAHI Exo-II (see Fig. 2.1), a robotic exoskeleton for rehabilitation of the upper extremity after stroke, spinal cord injury, or other brain injuries. The five degree-of-freedom robot enables elbow flexion-extension, forearm pronation-supination, wrist flexion-extension, and radial-ulnar deviation.

Portions of this chapter were published in the Proceedings of the IEEE International Conference on Rehabilitation Robotics (ICORR 2011) [20] and I gratefully acknowledge my collaborators in this publication.

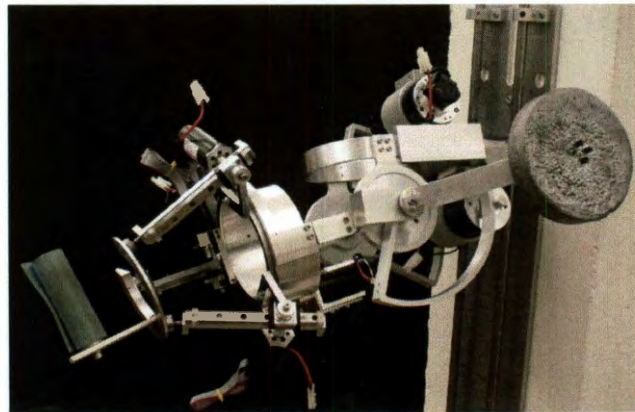


Figure 2.1 : MAHI Exo-II – Elbow, forearm and wrist exoskeleton for stroke and spinal cord injury (SCI) rehabilitation.

## 2.1 Introduction

In this chapter the design of MAHI Exo-II, an elbow, forearm and wrist exoskeleton designed and manufactured for rehabilitation of stroke and SCI patients, is presented. The mechanical design builds upon its predecessor, MAHI Exo-I [1, 21] and has a total of 5 DOF. The device offers several significant design improvements compared to its predecessor, MAHI Exo-I. Specifically, issues with backlash and singularities in the wrist mechanism have been resolved, torque output has been increased in the forearm and elbow joints, a passive degree of freedom has been added to allow shoulder abduction thereby improving alignment especially for users who are wheelchair-bound, and the hardware now enables simplified and fast swapping of treatment side.

## 2.2 Literature Review

To date, various exoskeletal upper extremity rehabilitation robot designs have been proposed. Among these devices, CADEN-7[3] has distinctive features in that can correspond every joint in human arm and has a superior workspace capability compared to other devices. ARMin [9], being an end product of an iterative design process coupled with clinical experiments, is considered as one of the most mature exoskeletal upper extremity rehabilitation device. Although most of those devices are electrically actuated, there are studies in which pneumatic actuation has been used. A clinically tested device [22, 23] called Pneu-WREX [24] is a very successful example of a pneumatically actuated device. First these exoskeleton devices will be introduced, then the common limitations will be discussed.

A cable-actuated dexterous exoskeleton for neurorehabilitation (CADEN-7) [3], developed by Rosen et al., is a seven-degree of freedom (DOF) upper limb exoskeletal

device. The main considerations for this design were the workspace capability and the torque output of the device at every single joint. Further, the design process has been coupled with experimental results of a study on human arm movement during activities of daily living (ADL). The system employs brushed DC motors for actuation and cable drive for transmission. The system aims to control shoulder, elbow, forearm and wrist joints all together, and achieves 99% of the range of motion (ROM) required for activities for ADL.

Another electrically actuated exoskeleton of the arm, the ARMin [9], developed by Mihelj et al., mainly focuses on the proximal part and proposes a new design to handle the shoulder complex. The six-DOF system can achieve shoulder vertical and horizontal rotation, upper arm internal/external rotation, elbow flexion/extension, forearm pronation/supination and wrist flexion/extension. The transmission is achieved by using both cable and gear drives. A specialized type of gear system called Harmonic Drive gear (Harmonic Drive Inc., Japan) is employed at three out of six axes. Although Harmonic Drive gear units are characterized as low-backlash, they still introduce backlash into the system.

Pneu-WREX [24], developed by Reinkensmeyer et al., is a four-DOF upper extremity rehabilitation and training exoskeleton. Mechanical design is based on Wilmington Robotic Exoskeleton (WREX), a passive arm support developed for children. The system's four degrees of freedom accommodate shoulder horizontal flexion/extension, upper arm internal/external rotation, elbow flexion/extension, forearm pronation/supination. Instead of electrical actuation, pneumatic actuators have been used. Although pneumatic actuators have high power to weight ratio, they introduce control challenges to the system because of their highly nonlinear behavior and slow response [1].

One of the greatest limitations of recent upper limb exoskeleton devices is giving secondary importance to the distal parts of human arm. To achieve the activities of daily living (such as eating, drinking, combing, dressing, etc.), one needs to use the distal parts of his/her arm (forearm, wrist) in coordination with proximal parts (elbow, shoulder), because most daily life activities require coordinated multi-joint movements [25]. However, most of the previous works are either concentrated solely on the rehabilitation of the proximal part of the arm or as in the case of two out of three examples above (namely, ARMin and Pneu-WREX), some or most of the joints at distal part are excluded.

A few groups have sought to design exoskeletal devices for the upper extremity which correspond to as many joints in the human arm as possible (e.g. CADEN-7 and ARMin). This approach resulted in creation of very complex devices. In theory, controlling more axes seems favorable; however, in reality it brings some serious challenges. An exoskeletal device, because it is worn by the user, has to be adjustable for patients with different body sizes. Therefore, the more axes a device incorporates, the more adjustable links have to be added to the design. Because these devices are intended to be used mostly by clinicians, unless the design is very user friendly, the difficulty of the adjustment process increases with the complexity of the device. Also, even if the device is highly adjustable, considering that the majority of brain injury patients have serious spasticity [26], it is extremely difficult, if not impossible, to keep robot axes corresponding to patient axes throughout the operation. In this respect, to both record/monitor isolated joint movements of the arm and apply desired torques/forces at the specified joints of the arm, use of simplified designs is more reasonable.

One of the advantages of robotic rehabilitation over classical rehabilitation is the

possibility of inclusion of virtual reality applications in the training sessions. If an exoskeletal device possesses characteristic features of a high fidelity haptic (force feedback) interface, it can be used as a haptic interface and training sessions can be supported with virtual reality applications. Performance of a haptic interface is mostly limited by physical properties [1], among which backlash, the lost motion in the transmission, is one of the primary source of nonlinearities in the system and can lead to instability in high performance haptic implementations. While transmission using gear trains is the easiest and most popular way, this choice introduces backlash (in turn nonlinearity) to the system even if the gear system is harmonic, as in ARMin. In contrast, capstan drives are backlash-free and can operate successfully even with modest manufacturing and assembly tolerances [18], so the use of capstan drives over gear trains will result a better performing haptic interface.

The structure of the chapter is as follows: Section 2.3 details the kinematic structure of the system and presents the design improvements based on the deficiencies of the previous design. Section 2.4 explains the advantages of the new design over previous design, and presents the capabilities of the new design.

## **2.3 System Description**

### **2.3.1 Kinematic Structure**

The five degree-of-freedom MAHI Exo-II is a robotic exoskeleton that enables elbow flexion-extension, forearm pronation-supination, wrist flexion-extension, and radial-ulnar deviation. Before making a detailed description of the kinematic structure of the exoskeleton, human arm kinematics will be investigated.

### Human Arm Kinematics

It is fair to say that nearly all the activities of daily living (ADL) (eating, drinking, cleaning, dressing, etc.) involve upper extremity movements. So, for a stroke, spinal cord injury or any other brain injury patient, rehabilitation of upper extremities is crucial for restoring the functionality to be able to achieve ADL. Since robotic rehabilitation has been introduced to the field, exoskeletal devices have been drawing attention due to their structural features. They provide the opportunity to apply desired torques/forces throughout the desired range of motion at the specified joints of human limb. Because the limb itself becomes a part of the exoskeletal system during operation, both the capabilities and the limits of the human arm have to be considered carefully, throughout the design process. So, understanding the nature of the human arm is a vital step in the development of upper limb rehabilitation

Joint	ROM(deg)	Torque(Nm)
Shoulder Vertical Flexion/Extension	150	125
Shoulder Horizontal Flexion/Extension	125	110
Upper arm Internal/External Rotation	120	-
Elbow Flexion/Extension	110	72.5
Forearm Pronation/Supination	150	9.1
Wrist Flexion/Extension	120	19.8
Wrist Radial/Ulnar Deviation	70	20.8

Table 2.1 : The torque and workspace capabilities of human arm extracted from [2].

exoskeleton devices.

The human arm includes 7 DOF: shoulder vertical and horizontal flexion/extension, shoulder internal/external rotation, elbow flexion/extension, forearm pronation/supination, wrist flexion/extension and wrist radial/ulnar deviation (as depicted in Fig. 2.2). The torque and workspace capabilities of human arm are shown in Table 2.1. As the primary goal of rehabilitation is to restore function in activities of daily living, defining the torque and workspace capabilities of the human arm as target values for the device is excessive. Instead, setting the target values as the necessary values to complete the activities of daily living will result a more reasonable set of design objectives.

Rosen et al. [27] performed a pilot study to determine the kinematic and dynamic requirements of an exoskeleton arm for functional use. In their study, human

Joint	ROM(deg)	Torque(Nm)
Shoulder Vertical Flexion/Extension	105	9.6
Shoulder Horizontal Flexion/Extension	130	7.2
Upper arm Internal/External Rotation	120	3.2
Elbow Flexion/Extension	150	3.5
Forearm Pronation/Supination	150	0.06
Wrist Flexion/Extension	115	0.35
Wrist Radial/Ulnar Deviation	70	0.35

Table 2.2 : The torque and workspace capabilities of human arm for 19 activities of daily living (ADL) .



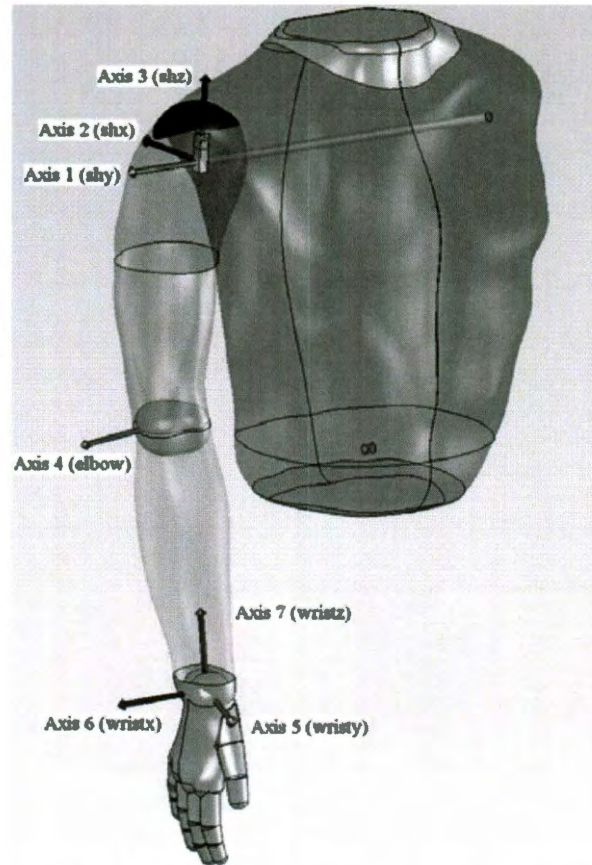


Figure 2.2 : Human arm kinematics – Axis 1: shoulder vertical flexion/extension, Axis 2: shoulder horizontal flexion/extension, Axis 3: shoulder internal/external rotation, Axis 4: elbow flexion/extension, Axis 7: forearm pronation/supination, Axis 5: wrist flexion/extension and Axis 6: wrist radial/ulnar deviation. (Adopted from [27])

arm motions were recorded during 19 ADL, which included eating, drinking, general reaching tasks, functional tasks and hygiene related tasks, by using a motion capture system. Torque values were calculated using both a modeling simulation package (Cosmos/Motion, Solidworks) and an analytical approach (Autolev, Online Dynamics). The resulting torque and ROM values for every joint are given in Table 2.2.

In the development of MAHI Exo-II, the values that are presented in Table 2.2



have been taken as the target specifications, and the achieved values are presented in Section 2.4.

### Robot Kinematics

The basic kinematic structure of the five degree of freedom MAHI Exo-II is depicted in Fig. 2.3. The exoskeleton is comprised of a revolute joint at the elbow, a revolute joint for forearm rotation, and a 3-RPS (revolute-prismatic-spherical) serial-in-parallel wrist. The first two DOF correspond to elbow and forearm rotations. Out of two rotational and one translational (distance of bottom plate from top plate) DOF of the 3-RPS platform, the two rotational DOF correspond to wrist flexion/extension and abduction/adduction. The fifth DOF accounts for minor misalignments of the wrist rotation axes with the device, which may become a problem especially during

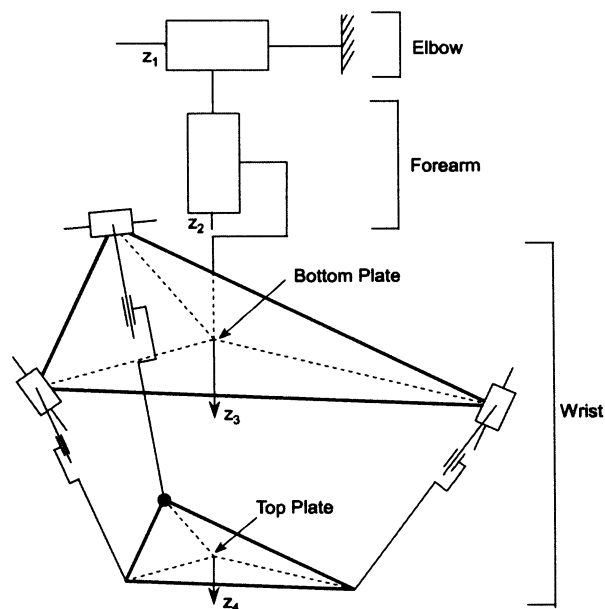


Figure 2.3 : Kinematic structure of MAHI Exo II – A 3-RPS (Revolute-Prismatic-Spherical) platform constitutes the wrist degrees-of-freedom of the robot and is in serial configuration with forearm and elbow degrees-of-freedom. (Adopted from [1])

movement.

### Kinematics of Elbow and Forearm Joints

The coordinate frames assigned to the joints of the system are depicted in Fig. 2.3. Frame {1} is the Newtonian frame (ground), frames {2}, {3} and {4} are fixed to the elbow joint, base and top plate of the wrist platform respectively. The transformation between frame {1} and frame {3} accounts for the rotations at the elbow and the forearm joint (as well as the constant distance from elbow joint to the base plate) and the Denavit-Hartenberg parameters are given in Table 2.3 as

Joint	rot(x)	tr(x)	rot(z)	tr(z)
Elbow	0	0	$\theta_4$	0
Forearm	$-\frac{\pi}{2}$	0	$\theta_5$	d

Table 2.3 : Link parameters for the Elbow and Forearm joints

where  $\theta_4$  and  $\theta_5$  are rotation angles of elbow and forearm joint respectively, and  $(0, -d, 0)^T$  is the location of the base plate of the wrist in frame {2}. Consequently the transformation matrices between frame {1} and frame {2}; and frame {2} and frame {3} are given as

$${}^1T_2 = \begin{bmatrix} \cos \theta_4 & -\sin \theta_4 & 0 & 0 \\ \sin \theta_4 & \cos \theta_4 & 0 & 0 \\ 0 & 0 & 1 & 0 \\ 0 & 0 & 0 & 1 \end{bmatrix} \quad (2.1)$$

$${}^2T_3 = \begin{bmatrix} \cos \theta_5 & -\sin \theta_5 & 0 & 0 \\ 0 & 0 & 1 & -d \\ \sin \theta_5 & \cos \theta_5 & 0 & 0 \\ 0 & 0 & 0 & 1 \end{bmatrix} \quad (2.2)$$

Considering that the elbow and forearm joints of the robot are coincident with the operator's elbow and forearm joints, transformation matrices  ${}^1T_2$  and  ${}^2T_3$  can be used to determine the inverse and forward kinematic measurements of these joints.

### Kinematics of Wrist Module

The wrist module of MAHI Exo-II employs a 3-RPS parallel mechanism (Fig. 2.3), which is first presented by Lee and Shah [28]. The mechanism comprises a base plate, a top plate (which are depicted as frame {3} and frame {4} respectively in Fig. 2.3), and three extensible links (with lengths  $l_1$ ,  $l_2$ ,  $l_3$ ) which connect the base plate to the top plate. The links are connected to the base plate with revolute joints ( $R_1$ ,  $R_2$ ,  $R_3$ ) and to the top plate with spherical joints ( $S_1$ ,  $S_2$ ,  $S_3$ ). Spherical joints are placed  $120^\circ$  apart from each other on the top plate and similarly the revolute joints are placed equally on the base plate. The handle which is held by the patient is attached to the top plate. For the ease of calculations, the coordinate frames  $x_3y_3z_3$  and  $x_4y_4z_4$  are attached to the centers of base plate and top plate, whose radii are  $R$  and  $r$ , respectively. Both  $z_3$ -axis and  $z_4$ -axis are perpendicular to the planes to which they are attached, and  $x_3$ -axis and  $x_4$ -axis point to the revolute joint  $R_1$  and the spherical joint  $S_1$  respectively. The coordinates of the revolute joints in frame {3} are

$$\begin{aligned}
 R_1 &= \begin{bmatrix} R \\ 0 \\ 0 \end{bmatrix} \\
 R_2 &= \begin{bmatrix} -\frac{1}{2}R \\ \frac{\sqrt{3}}{2}R \\ 0 \end{bmatrix} \\
 R_3 &= \begin{bmatrix} -\frac{1}{2}R \\ -\frac{\sqrt{3}}{2}R \\ 0 \end{bmatrix}
 \end{aligned} \tag{2.3}$$

and the coordinates of the spherical joints in the frame {4} are

$$\begin{aligned}
 {}^4S_1 &= \begin{bmatrix} r \\ 0 \\ 0 \end{bmatrix} \\
 {}^4S_2 &= \begin{bmatrix} -\frac{1}{2}r \\ \frac{\sqrt{3}}{2}r \\ 0 \end{bmatrix} \\
 {}^4S_3 &= \begin{bmatrix} -\frac{1}{2}r \\ -\frac{\sqrt{3}}{2}r \\ 0 \end{bmatrix}
 \end{aligned} \tag{2.4}$$

The transformation matrix between frame {3} and frame {4},  ${}^3T_4$  can be written

as

$${}^3T_4 = \begin{bmatrix} n_1 & o_1 & a_1 & p_1 \\ n_2 & o_2 & a_2 & p_2 \\ n_3 & o_3 & a_3 & p_3 \\ 0 & 0 & 0 & 1 \end{bmatrix} \quad (2.5)$$

where  $(p_1, p_2, p_3)^T$  represents the position of the origin of the frame {4} in frame {3}; and  $(n_1, n_2, n_3)^T$ ,  $(o_1, o_2, o_3)^T$  and  $(a_1, a_2, a_3)^T$  are the directional cosines of the unit vectors x, y and z in frame {3}. For simplification of the calculations, all lengths and coordinates are normalized with respect to the base plate's radius R as

$$\begin{aligned} \rho &= \frac{r}{R} \\ L_i &= \frac{l_i}{R} \\ P_i &= \frac{p_i}{R} \end{aligned}$$

In the following sections, forward and inverse kinematic analysis of the 3-RPS mechanism by using the methodology of [28] and [1] are presented. Subsequently, real-time computation of the kinematics of 3-RPS mechanism with a symbol manipulation software, Autolev (Online Dynamics), is introduced.

### Forward Kinematics

The 3-RPS mechanism has two rotational degrees-of-freedom and one translational degree-of-freedom. Because the mechanism is a parallel manipulator, it has multiple constraint equations (three equations for this particular mechanism), and the orientation and the position of the top plate are calculated, in terms of the link lengths, by solving these three configuration constraint equations simultaneously. The angle between the  $R_iS_i$  link and the base plate is  $\theta_i$  and accordingly, the coordinates of the spherical joints with respect to the frame {3} are

$$\begin{aligned}
{}^3S_1 &= \begin{bmatrix} 1 - L_1 \cos \theta_1 \\ 0 \\ L_1 \sin \theta_1 \end{bmatrix} \\
{}^3S_2 &= \begin{bmatrix} -\frac{1}{2}(1 - L_2 \cos \theta_2) \\ \frac{\sqrt{3}}{2}(1 - L_2 \cos \theta_2) \\ L_2 \sin \theta_2 \end{bmatrix} \\
{}^3S_3 &= \begin{bmatrix} -\frac{1}{2}(1 - L_3 \cos \theta_3) \\ -\frac{\sqrt{3}}{2}(1 - L_3 \cos \theta_3) \\ L_3 \sin \theta_3 \end{bmatrix}
\end{aligned} \tag{2.6}$$

Considering that the distance between spherical joints is  $\sqrt{3}r$ , the constraint equations can be written as

$$L_1^2 + L_2^2 - 3 - 3\rho^2 + L_1L_2 \cos \theta_1 \cos \theta_2 - 2L_1L_2 \sin \theta_1 \sin \theta_2 - 3L_1 \cos \theta_1 - 3L_2 \cos \theta_2 = 0 \tag{2.7}$$

$$L_3^2 + L_2^2 - 3 - 3\rho^2 + L_3L_2 \cos \theta_3 \cos \theta_2 - 2L_3L_2 \sin \theta_3 \sin \theta_2 - 3L_3 \cos \theta_3 - 3L_2 \cos \theta_2 = 0 \tag{2.8}$$

$$L_1^2 + L_3^2 - 3 - 3\rho^2 + L_1L_3 \cos \theta_1 \cos \theta_3 - 2L_1L_3 \sin \theta_1 \sin \theta_3 - 3L_1 \cos \theta_1 - 3L_3 \cos \theta_3 = 0 \tag{2.9}$$

The top plate of the mechanism is physically constrained to move on only one side of the base plate, so  $p_3$  is always positive. This brings the following relation:

$$180^\circ > \theta_i > 0^\circ$$

Thus, Equations 2.7-2.9 can be solved numerically for given link lengths, and unique solutions for  $\theta_i$  can be calculated. Considering that the spherical joints are located on the edges of an equilateral triangle on the top plate, the position vector of the top plate can be calculated by using the obtained  $\theta_i$  values and link lengths as

$$P = \begin{bmatrix} P_1 \\ P_2 \\ P_3 \end{bmatrix} = \frac{1}{3} \sum_{i=1}^3 S_i \quad (2.10)$$

The coordinates of the spherical joints, by using transformation matrix  ${}^3T_4$  can be expressed as

$$\begin{bmatrix} {}^3S_i \\ 1 \end{bmatrix} = {}^3T_4 \begin{bmatrix} {}^4S_i \\ 1 \end{bmatrix} \quad (2.11)$$

The elements of directional cosine vectors can be determined by using the Equations 2.4, 2.6 and 2.11. So the components of vector  $\mathbf{n}$  are

$$\begin{aligned} n_1 &= \frac{1 - L_1 \cos \theta_1 - P_1}{\rho} \\ n_2 &= -\frac{P_2}{\rho} \\ n_3 &= \frac{L_1 \sin \theta_1 - P_3}{\rho} \end{aligned} \quad (2.12)$$

and the components of vector  $\mathbf{o}$  are

$$\begin{aligned} o_1 &= n_2 \\ o_2 &= \frac{\sqrt{3} - \sqrt{3}L_2 \cos \theta_2 - 3P_2}{\sqrt{3}\rho} \\ o_3 &= \frac{2L_2 \sin \theta_2 + L_1 \sin \theta_1 - 3P_3}{\sqrt{3}\rho} \end{aligned} \quad (2.13)$$

The orthogonality of the unit vectors  $\mathbf{n}$ ,  $\mathbf{o}$  and  $\mathbf{a}$  allows to determine the components of vector  $\mathbf{a}$

$$\begin{aligned} a_1 &= n_2 o_3 - n_3 o_2 \\ a_2 &= n_3 o_1 - n_1 o_3 \\ a_3 &= n_1 o_2 - n_2 o_1 \end{aligned} \tag{2.14}$$

Equations 2.10 and 2.12-2.14 can be used to determine the transformation matrix  ${}^3T_4$  and subsequently, the Euler-*xyz* angles  $\alpha$ ,  $\beta$  and  $\gamma$  can be represented as

$$\beta = \sin^{-1}(n_3) \tag{2.15}$$

$$\alpha = \text{atan2}(-o_3 / \cos(\beta), a_3 / \cos(\beta)) \tag{2.16}$$

$$\gamma = \text{atan2}(-n_2 / \cos(\beta), n_1 / \cos(\beta)) \tag{2.17}$$

The important point here is that the wrist joint of the patient is coincided with the coordinate center of the top plate during the training sessions and the Euler angles  $\alpha$  and  $\beta$  correspond to the wrist flexion/extension and radial/ulnar deviation respectively. If Euler angle  $\beta = \pm 90^\circ$ , Euler angles  $\alpha$  and  $\gamma$  become indeterminant, as can be seen from Equations 2.16 and 2.17, but the physical constraints prevent this situation from occurring. Another important point to consider is that the top plate can not make any rotation around the  $z_4$ -axis, so  $\gamma = 0$  most of the time.



## Inverse Kinematics

The calculation of the necessary joint space positions to achieve a desired task space position of the end-effector can be carried out using inverse kinematics equations. The position of the end-effector of the 3-RPS mechanism (top plate) can be defined by two rotations, Euler angles  $\alpha$  and  $\beta$ , and a translation,  $P_3$ . Because the Euler angle  $\gamma = 0$ , as stated above, the direction cosine vectors can easily be calculated. The revolute joints constrain the links  $R_1S_1$ ,  $R_2S_2$  and  $R_3S_3$  to move in the planes  $y = 0$ ,  $y = -\sqrt{3}$  and  $y = \sqrt{3}$ . This relation, combined with the right hand side of Equation 2.11, brings

$$n_2\rho + P_2 = 0 \quad (2.18)$$

$$-n_2\rho + \sqrt{3}o_2\rho + 2P_2 = -\sqrt{3}[-n_1\rho + \sqrt{3}o_1\rho + 2P_1] \quad (2.19)$$

$$-n_2\rho - \sqrt{3}o_2\rho + 2P_2 = \sqrt{3}[-n_1\rho - \sqrt{3}o_1\rho + 2P_1] \quad (2.20)$$

Equations 2.19 and 2.20 can further be simplified

$$n_2 = o_1 \quad (2.21)$$

$$P_1 = \frac{\rho}{2}(n_1 - o_2) \quad (2.22)$$

Once  $P_1$  and  $P_2$  are calculated by using Equations 2.18 and 2.22, the transformation matrix  ${}^3T_4$  can be computed. Consequently, the link lengths,  $L_1$ ,  $L_2$  and  $L_3$  can be calculated by using Equation 2.11.

## **Real-Time Computation of the Kinematics of 3-RPS**

The real-time computation of the position of the end-effector for a given set of joint variables (forward kinematics), and the joint variables for a desired end-effector position (inverse kinematics) of a robotic manipulator are crucial for control applications. Although the governing equations for inverse and forward kinematics calculations are derived, as presented in the preceding sections, a powerful and highly-advanced symbolic manipulator software, Autolev (Online Dynamics), has been used for real-time kinematics calculations to generate more robust solutions. Autolev allows one to define a physical mechanism by using the built-in physical objects such as points, particles, frames and bodies. The software includes commands for calculating angles and distances between objects. Furthermore, the software enables one to define the rotations between objects and automatically calculates rotation matrices. The built-in solver for sets of nonlinear algebraic equations allows one to calculate inverse and forward kinematics. Autolev is capable of creating compact C, MATLAB, and Fortran codes for real-time applications. The code piece for kinematic analysis of the 3-RPS system and the output C code are provided at Appendix-B.

### **2.3.2 Design Description**

The new design, while maintaining the basic kinematic structure and grounded nature of the original design, introduces a number of significant design improvements based on the deficiencies of the previous design. The issues and the proposed solutions are presented in detail below, grouped under wrist, forearm and elbow subsections.

### **Wrist Mechanical Design**

Based on the results of pilot clinical testing of spinal cord injury (SCI) patients with MAHI Exo-I, the most important deficiency of the design in the wrist part was identified as the mechanical singularities introduced by the wrist ring connector joints. Because of these singularities, at certain configurations, patients' wrist movements were not being satisfactorily recorded for evaluation. The main reason for the problem was that universal-revolute joints were incapable of providing the intended spherical joint characteristics at some specific configurations of the 3-RPS mechanism. Consequently, we have replaced the universal-revolute joints with Hephaist-Seiko SRJ series high precision spherical joints. Although these spherical joints resolved the problems due to the universal-revolute joints, they led to a decrease in range of motion (ROM). To improve the ROM, we used an inclined surface design on the wrist ring (see Fig. 2.4(a)). This choice also contributed to a considerable reduction in friction and backlash and resulted in a wrist mechanism with significantly more rigid and smooth operation compared to MAHI Exo-I. Besides all of these advantages offered by the use of spherical joints and the inclined wrist ring design, the overall ROM was still slightly reduced in comparison with MAHI Exo-I. A comparison in terms of ROM for both designs for various joints is given in Table 2.4 in Section 2.4. Nevertheless, the new design is still capable of spanning 100% of wrist abduction/adduction ROM and 63% of wrist flexion extension ROM during activities of daily living (ADL).

### **Forearm Mechanical Design**

The improvements for the forearm joint include increasing the torque output while reducing the mechanism complexity and cost. In the previous design, Applimotion 165-A-18 frameless and brushless DC motor actuator with MicroE Systems Mercury

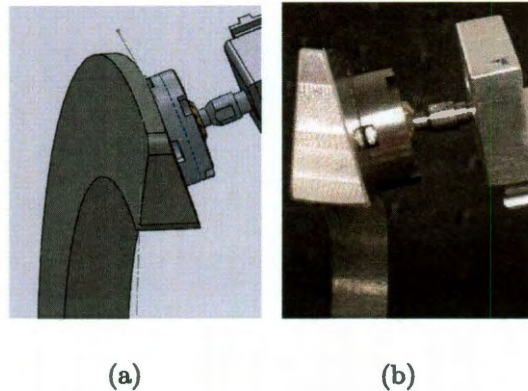


Figure 2.4 : (a) CAD model of the wrist ring with inclined surface to increase wrist range of motion. (b) Manufactured inclined wrist ring attached to the spherical joint.

1500 encoder were used to drive the forearm joint. Although this design enabled implementing the desired mechanism in a limited space, it mainly suffered from low torque output. In the new design, a high torque DC motor (Maxon RE40), with cable drive mechanism is implemented. Use of cable drive mechanism is justified by backdrivable and zero-backlash nature of it and by the considerable reduction in cost. In the new design, desired range of motion is unaltered with an approximately 35% increase in torque output (see Table 2.4), for under one fourth of the cost of the prior design. Another consideration for the new design was eliminating the complexity of the mechanism, more specifically eliminating the issues that emerged due to the misalignment of the optical encoder. In the previous design, the optical encoder was embedded in the forearm joint with the frameless brushless motor, as depicted in Fig. 3.4(a), and was vulnerable to dislocations especially inserting or removing an arm from the exoskeleton. Misalignments in the encoder grating ring required the disassembly of the forearm mechanism and a significant effort to satisfy the  $\mu\text{m}$  level tolerance. Consequently, instead of having the sensor and the actuator be open to effects that would lead to misalignments, in the new design they have been kept out of

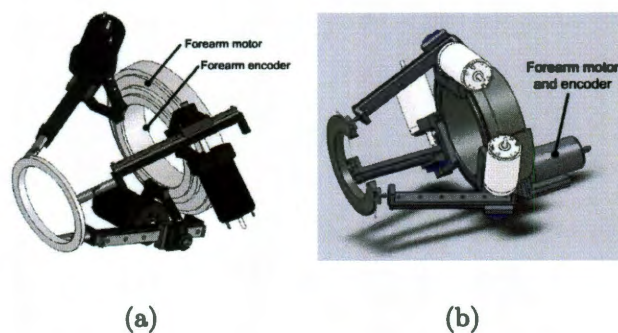


Figure 2.5 : (a) Forearm mechanical design CAD model for MAHI Exo I. Forearm encoder ring ran along the circumference of the forearm and was prone to misalignment errors. A frameless brushless motor inside an aluminum encasing actuated the joint. (b) Forearm mechanical design CAD model for MAHI Exo II. Current design employs a Maxon DC motor with cable drive mechanism, and the encoder is coupled to the motor shaft at the bottom end (not shown in this model).

interference with the arm during attachment or detachment, as shown in Fig. 2.5(b). This solution also enabled easy access to the encoder and the motor in case of a malfunction.

### Elbow Mechanical Design

The primary goal in the new design for the elbow subsystem was to implement a mechanism that allows both left and right arm therapy. In MAHI Exo-I, a Kollmorgen U9D-E pancake DC motor with a cable transmission system was fixed on one side of the elbow mechanism and a counterweight was attached through a moment arm to the motor shaft to provide passive gravity compensation for the forearm assembly. Because the counterweight and elbow motor would be between patient and mechanism as shown in Fig. 2.7(a) for left arm attachment, this configuration only allowed right arm therapy. To overcome this issue, a new design which employs two high torque DC motors (Maxon RE65) with cable drives is developed. Main con-



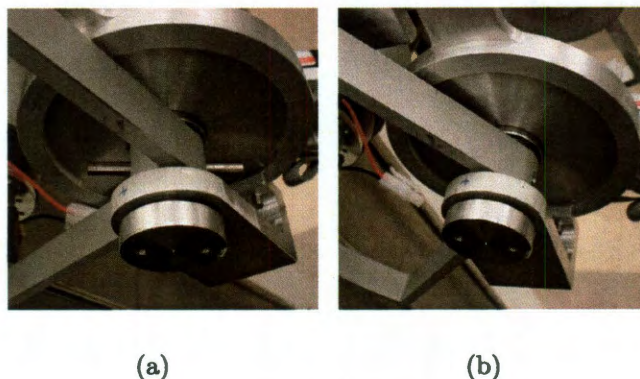


Figure 2.6 : (a) A tapered pin connects the capstan to the elbow shaft on both sides. (b) The tapered pin can be easily removed to allow driving the elbow joint from the other side. By changing the side of the counterweight, the device can be used for the desired arm.

sideration for the new design was to implement a mechanism that will enable one to change the transmission from one side to the other easily and quickly. For this reason coupling/decoupling of the capstans with the driving motor shaft is provided via easily mountable/removable taper pins, as shown in Figs. 2.6(a), 2.6(b). Consequently, changing the transmission from one side to other only requires enabling desired capstan mechanism and mounting the counterweight to the corresponding drive shaft.

New elbow actuation design also led to a considerable improvement in the torque output. Although the initial design was well within the useful range for training and rehabilitation applications, the torque output for the elbow joint was further increased to enable locking of the elbow joint in specified positions for isolated wrist or forearm training. A large capstan with 15:1 transmission ratio allowed a 238% increase in torque output as compared to MAHI Exo-I (see Table 2.4).

One of the most important points to take into account during the mechanical design of a rehabilitation robot is to ensure that the system does not cause any

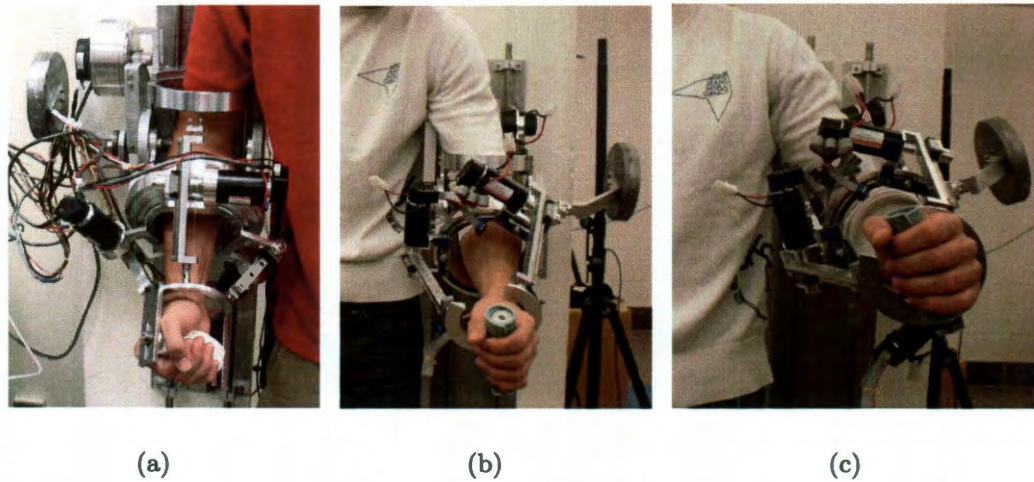


Figure 2.7 : (a) In MAHI Exo-I, elbow motor and counterweight fixed on one side allowed only rehabilitation of the right arm. (b) In MAHI Exo-II, counterweight can be attached on either side to allow both left and right arm therapy. (c) A passive DOF that tilts the whole device in the coronal plane provides improved patient comfort and posture during therapy.

discomfort or safety hazard for the user during the movement [29]. For this reason, a tilting mechanism (as a passive DOF) is implemented to enable the patients to have a better posture during the training/rehabilitation sessions by allowing abduction of the shoulder, as illustrated in Figs. 2.7(b), 2.7(c).

## 2.4 Results

The ranges of motion and maximum achievable torque outputs for the elbow, forearm and wrist joints based on the mechanical design improvements outlined in the previous section are summarized in Table 2.4. Same parameters are given for the previous design (MAHI Exo-I) and for activities of daily living (ADL) as reported by Perry et al. [3] for comparison.

Both MAHI Exo-I and II are capable of providing a ROM exceeding or only

Table 2.4 : Achievable joint ranges of motion (ROM) and maximum continuous joint torque output values for MAHI Exo I and MAHI Exo II. Maximum joint ROM and torque values for 19 activities of daily living (ADL) as extracted from [3] are also given for comparison.

Joint	ADL		MAHI Exo I		MAHI Exo II	
	ROM (deg)	Torque (Nm)	ROM (deg)	Torque (Nm)	ROM (deg)	Torque (Nm)
Elbow Flexion/Extension	150	3.5	90	4.91	>90	11.61
Forearm Pronation/Supination	150	0.06	180	1.69	>180	2.30
Wrist Flexion/Extension	115	0.35	85	2.92	72	1.67
Wrist Abduction/Adduction	70	0.35	85	3.37	72	1.93



slightly below the ROM of ADL for forearm pronation/supination and wrist abduction/adduction. MAHI Exo-I covers 74% of wrist flexion/extension ROM of ADL while MAHI Exo-II covers 63% of it. For the elbow, both designs cover approximately 60% of ADL ROM, from a fully extended posture to a right angle at the elbow. For the joints with a ROM beyond human ROM, both hardware and software stops are implemented for safety.

In terms of torque output capability, both versions of the exoskeleton provide more than sufficient torque to replicate torques involved in ADL, for all four DOF. MAHI Exo-II has a much higher elbow maximum continuous torque output than MAHI Exo-I, but less torque output at the wrist DOF. This is mainly due to use of lighter DC motors (Maxon RE35, 340 g) in MAHI Exo-II, as compared to DC motors used in MAHI Exo-I (Maxon RE40, 480 g). MAHI Exo-II torque output at the forearm DOF is also improved 36% compared to the previous design. The improvements in forearm and elbow torque output serve to enable locking these joints at desired positions in software to allow isolated training of remaining unlocked joints. Despite the decrease in torque output at the wrist joints, the wrist motors are still capable of providing this locking property.

The main goals of the redesign have been enabling the use of the exoskeleton for therapy of both arms and resolving the backlash and singularity issues related to the universal-revolute joints at the wrist ring. To achieve the first goal, two separate DC motors (Maxon RE65) as shown in the complete assembly in Figs. 3.6(a) and 3.6(b) were used. The elbow joint is driven by only one of the motors at a given time, in such a way that the active capstan does not get in the way, specifically between the upper arm and the torso of the patient during elbow movements. Changing of the configuration for using the device for one arm from a configuration for the other arm

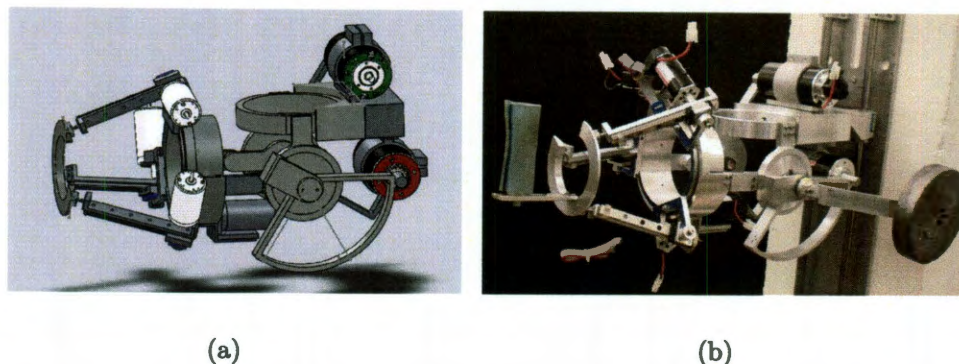


Figure 2.8 : (a) CAD model of the MAHI Exo-II complete assembly. (b) Manufactured MAHI Exo-II complete assembly with motors, handle and counterweight attached.

is handled via installing/removing of a taper pin (see Fig. 2.6(a)) and attaching the counterweight onto the side opposite to the patient. Taper pins provided a practical yet still zero-backlash solution to capstan-shaft coupling and decoupling. The second goal was achieved via use of high precision spherical joints, which led to a slight decrease in ROM after including an inclined wrist ring design that allowed making most use of the available ROM envelope for the spherical joints.

In comparison with other rehabilitation robots, MAHI Exo-II poses several advantages. First, parallel design of the wrist provides increased rigidity and torque output; decreased inertia; and isometric force distribution throughout the workspace, as compared to a serial configuration. Also, the alignment of the biomechanical axes of joint rotation with the controlled DOF of the MAHI Exo-II makes it possible to constrain movement of a desired joints. This is particularly important in rehabilitation, where the therapy exercises may focus on a particular joint.

The new design offered additional benefits in comparison with MAHI Exo-I. One benefit was lowered cost due to use of all DC brush motors for all actuators, by replacing the frameless brushless DC motor on the forearm and the pancake DC motor

on the elbow joint of the earlier version. Another improvement was the additional passive DOF that allowed tilting of the whole device in the coronal plane which significantly added to patient comfort, posture and ease of attachment/detachment.

## Chapter 3

# Control Implementations

This chapter presents both the control/software applications and results of a clinical study carried out in collaboration with The Institute for Rehabilitation and Research (TIRR) and implementation of an advanced control method in simulation level. The presented portion of the work for the study carried out with TIRR included modification of the control modes which were implemented on RiceWrist (a modified version of MAHI Exo-I for wrist and forearm therapy) to include the elbow part of MAHI Exo-II, and development of graphical user interfaces (GUI) for every mode according to the feedback taken from therapists throughout the pilot clinical testings. The results of clinical evaluation of a pilot study, with a 28 year-old SCI patient, are reported. Finally, an advanced assist-as-needed control algorithm to work with severely injured patients is proposed and the simulation results are presented.

### 3.1 Introduction

As the MAHI Exo-II has been designed for training and rehabilitation of stroke and SCI patients, the application of control which dictates the interaction of the device with the patient is a key step for the development of the system. The control modes implemented on MAHI Exo-II were first designed for RiceWrist and are detailed in [30]. RiceWrist, developed at MAHI Lab, is a 4-DOF wrist and forearm rehabilitation robot which possesses the same kinematic structure with the forearm and wrist

module of MAHI Exo-II. Within the scope of this thesis work, this controller was implemented on the 5-DOF MAHI Exo-II, and modified according to the observations during pilot testing with SCI patients. Additionally, a novel adaptive controller proposed by Wolbrecht et al. [31] to provide compliancy is implemented in simulation for the forearm and wrist module of MAHI Exo-II. The main idea is to allow the patient to influence the robot and experience errors which in turn induce motor learning.

### 3.2 Literature Review

Many control algorithms have been proposed for robotic rehabilitation. Given their ad hoc nature [19], categorizing them as assisting and resisting control algorithms will be sufficient for the scope of this work. In assisting control strategies, the robotic device assists a patient to move his/her extremity or limb along a desired path. In resisting control strategies, there is a resistance to the movement of the patient.

The differences among assisting control applications mainly arise at the level of assistance. Lum et al. [32] used the MIME upper extremity rehabilitation robot for shoulder and elbow neurorehabilitation in subacute stroke patients. One of the control strategies they employed during this study was a position feedback assisting controller. Throughout the movement, the subject relaxed his/her arm and the robot moved the limb towards a target with a desired trajectory. A very similar control strategy has been used on MAHI Exo-II, namely passive mode. As will be discussed in latter sections, passive mode employs a proportional-derivative based joint-space trajectory controller [30] and moves the patients limb from an initial position to a final position (both pre-defined). Although this control strategy led to improvements in the studies by both Lum et al. [32] with subacute stroke patients and Feygin et al. [33] with unimpaired patients in physical performance and motor learning

respectively compared to the control groups, Hogan and Krebs et al. [34] state that passively moving patients limb with a robotic device does not produce a significant effect and conclude that recovery requires active participation.

An alternative strategy which aims to increase patient participation level is triggered assistance control. In triggered assistance control, the movement is initiated by the patient according to a predefined measure (such as force/torque treshold or elapsed time during motion) and the robotic device provides assistance for the rest of the movement. Amirabdollahian et al. [35] showed the efficacy of robotic rehabilitation using triggered assistance control as one of their control strategies. The predefined measure was force treshold and the aim was to impose a more challenging exercise mode to more able patients. In the implementation of triggered mode for the MAHI Exo-II, a similar approach is being used for isolated joint movements. Here, the patient has to exceed a predefined treshold force in the direction of movement in order to trigger MAHI Exo-II to move the arm from initial position to final position as in aforementioned passive mode. Although this approach increases the participation of patient with a subject-driven part, the motion still includes a robot driven part [36] during which patient is completely passive.

Because providing too much assistance may have limiting effects on learning, assisting the patient only as much as needed to accomplish a task by employing a controller with adapting parameters based on online measurement of the patient's performance, instead of a controller with static parameters, is a commonly stated goal [19]. In their study, Wolbrecht et al. [31] develop a model-based adaptive controller to provide a mechanical compliance which allows the patient to complete the movement but assists only when it is necessary. Their main motivation to implement a compliant behavior is to allow the patient to influence the robot and experience

errors which in turn induce motor learning. In this chapter, I present the design and simulation results of a similar controller for the forearm and wrist module of MAHI Exo-II.

In contrast to assisting control strategies, in resisting control strategies a resistance is applied to the patient during the motion. The idea is to improve the physical performance of patients with less severity by adding challenge and increasing the required effort. Although Stein and Krebs et al. [37] did not report any significant difference in motor function gains between assisting and resisting robotic treatment, in their study they showed that the subjects receiving robot-aided progressive resistance training did achieve comparable improvements in motor function and maximal force generation. In the constrained mode control strategy used on MAHI Exo-II, a viscous resistance proportional to the velocity of the patient is applied throughout the movement.

The chapter is organized as follows: Section 3.3 details the existing control modes on MAHI Exo-II and the modifications made throughout the clinical testings, then presents the results of pilot clinical testing with an SCI patient. Section 3.4 explains the proposed assistance-as-needed control algorithm and presents the implementation of the algorithm in simulation.

### **3.3 Control Modes, Modifications and Clinical Testing**

As detailed subsequently, the passive mode, triggered, and constrained control modes were designed for patients with different levels of ability. Three control modes were combined with two additional modes, the GoTo Mode, to move the system to specified initial position, and the Wait Mode, to apply a restriction with virtual walls prior to trial start. (figure.control modes) represents the structure of the controller.

The controller runs on a PC with Intel Core Duo 3.00 GHz with 3.21 GB Ram CPU. Matlab Simulink Toolbox from Mathworks and Quarc 2.0 from Quanser are used to build the controller, and Matlab Real Time Workshop Toolbox is used to provide specified control loop frequency. The Quanser Q8 hardware in the loop (HIL) board is used for data acquisition. Accelus ASP-055-18 digital servo amplifiers from Copley Controls are used for signal amplification.

The following sections first discuss the control modes and main modifications in detail, then present the results of the clinical evaluation of an SCI patient after a robotic training protocol with the MAHI Exo-II.

### 3.3.1 Passive Mode

Passive mode was designed mainly for severely injured patients. During the motion, patient keeps his/her arm relaxed and the device moves the patient's limb from an initial position to a final position (both pre-defined). A joint-space proportion-derivative trajectory controller with no gravity compensation is employed. Using the formulation given in [38], the control law can be represented as

$$M(q)\ddot{q} + C(q, \dot{q})\dot{q} + G(q) = u \quad (3.1)$$

$$u = K_p(q_d - q) - K_d\dot{q} \quad (3.2)$$

where  $\mathbf{q}$  is a  $4 \times 1$  vector of joint variables,  $\mathbf{M}$  is the  $4 \times 4$  inertia matrix,  $\mathbf{C}$  is the  $4 \times 4$  matrix which represents Coriolis/centrifugal terms,  $\mathbf{G}$  is the  $4 \times 1$  gravity vector,  $\mathbf{K}_p$  and  $\mathbf{K}_d$  are symmetric positive definite matrices and  $\mathbf{u}$  is the corresponding control input. (Here it should be noted that the system is a serial-in-parallel mechanism, thus representing the equations of motion in the form of Equation 3.1 is not



straightforward. The rationale for this representation will be made in Section 3.4.1.)

At steady state ( $\ddot{\mathbf{q}} = \mathbf{0}$ ,  $\dot{\mathbf{q}} = \mathbf{0}$ )

$$q_d - q = K_p^{-1}G(q) \quad (3.3)$$

Thus, proportional gain values were chosen as high as possible to achieve small steady state error. The desired trajectory was generated by using linear interpolation according to the defined initial and final positions and time scaled to have the flexibility to change the motion speed.

### 3.3.2 Triggered Mode

Triggered mode was designed for use with less severely injured patients who have the ability to initiate movement by applying larger forces than a predefined threshold in the direction of movement. After initiation, the arm is moved from initial position to final position as in passive mode. The control structure consists of two parts, a joint-space impedance force controller used at the motion initiation, and, once the force threshold is exceeded, a joint-space proportional-derivative trajectory controller as described for passive mode.

While using the same controller structure, the strategy has been changed to enable isolated joint movements. Previously, in order to initiate movement, the patient had to trigger all joints at the same time. Because the patient might either lack the required coordination level or not have the same physical capabilities at all of his/her joints, initiation of the movement would be problematic. Another motivation was the reported improvements with isolated joint training in upper extremity functions [39]. The implemented modification enables the therapist to choose the intended joint for therapy and while all other joints are kept locked during the session.

### 3.3.3 Constrained Mode

Constrained mode was designed to apply a viscous resistance proportional to the velocity of the patient throughout the movement, so the patient, different from other two modes, actively moves his/her limb during the motion. The movement of the patient was from a predefined initial position to a predefined final position and was secured to be unidirectional with virtual walls.

One of the modifications that has been implemented is omitting the virtual walls so that the patient could move freely in a viscous friction environment throughout the motion. The reason for this modification was to allow observation of the movement quality (velocity profile) of the patient without any intervention. A modification similar to that in the triggered mode to enable isolated joint movements has been implemented as well, similar justification. A patient, even if able enough to undergo resistive therapy, might have different physical capabilities at different joints of his/her arm and setting a single constraint level for the whole arm movement would cause problems. For example, while the specified constraint level might be appropriate for the elbow joint, it might be excessive for the forearm joint and the patient would not be able to complete the movement because of the weakness at the forearm. Another modification to define initial and final positions was also implemented. Previously, initial and final positions were randomly defined by therapist at the beginning of the trial. Instead, a mini trial prior to the main trial has been implemented. During the mini trial, patient freely moves his/her limb so the neutral, maximum and minimum values for the ROM of the intended joint can be recorded and used at the main trial. The motivation for this modification was to define the trajectory according to the capacities of the patient and to have the ability to compare the ROM values of the patient from different sessions. During both the mini

trial and main trial, visual feedback is provided to the patient through a computer screen (Fig. 3.1).

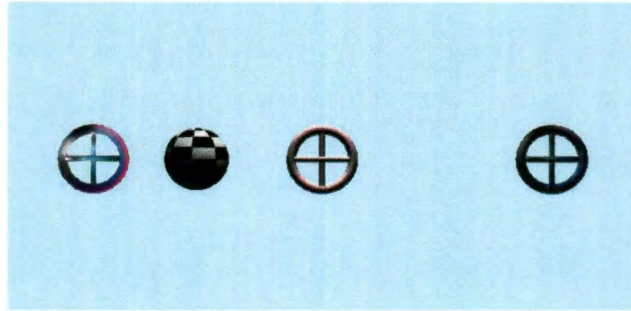


Figure 3.1 : Target Hitting Task– Subject must move the cursor to the highlighted target (left target in this case)

The placements of the three targets are made according to the patient's ROM values, where targets represent the neutral (initial), maximum and minimum values and subjects are supposed to match these targets with the cursor. The aim for providing visual feedback was to encourage the patients to improve their workspace capabilities.

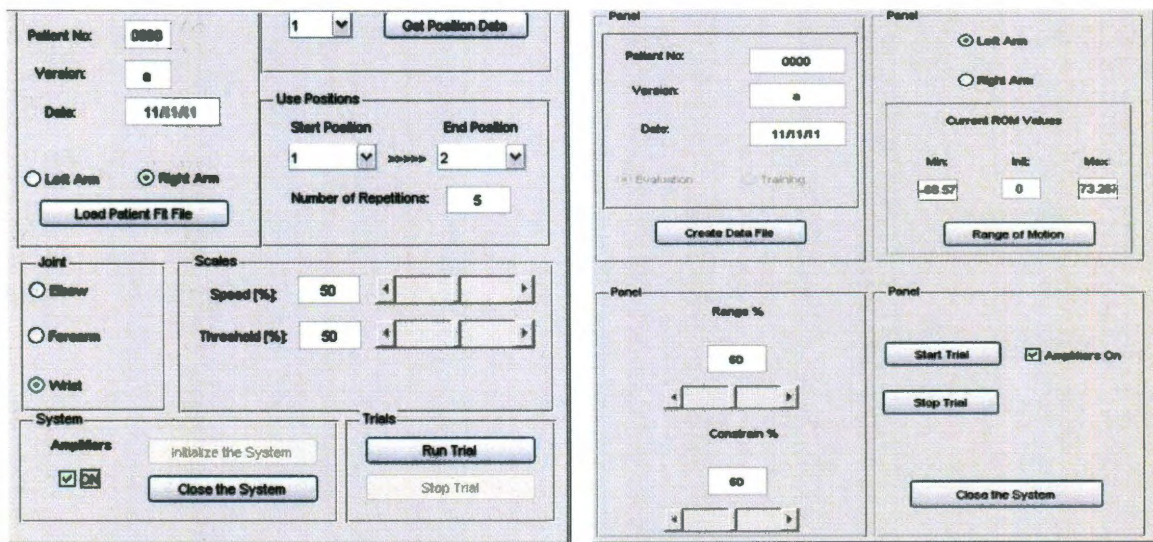
### 3.3.4 Graphical User Interface

In this section the graphical user interfaces (GUIs), which are developed for the individualization of the sessions for every patient, are explained. One of the main goals for the development of MAHI Exo-II was to achieve a device for therapy of patients with different levels of severity, and so the control modes are implemented according to this goal. The aforementioned control modes provide parameters to give the therapist the flexibility to decide on the velocity of the movement and the number of repetitions (for passive and triggered modes); the torque threshold to be overcome (for triggered mode); the applied viscosity and the desired portion of the ROM of



the user (for constrained mode). The selection of these parameters are made through GUIs prior to every session. The GUIs are developed using the Matlab GUI design environment (GUIDE) tool from Mathworks that allow instant modification of the Simulink Model.

The passive and triggered modes can be controlled over the same GUI (Fig. 3.2(b)). The therapist, besides choosing the mentioned parameters for the sessions, has the freedom to specify the desired joint to conduct isolated joint therapy for passive mode and triggered mode through the GUI. For the constrained mode, separate GUIs are prepared for every joint and the therapist chooses the appropriate GUI prior to the therapy session. The GUI for the constrained mode allows the therapist to run a mini trial prior to main trial to measure the ROM capabilities of the patients. The therapist initiates this mini trial with the “Range of Motion” button, and once



(a)

(b)

Figure 3.2 : (a) Triggered mode and passive mode can be operated over the same GUI. (b) The GUI for the constrained mode, allows therapist to run a mini trial prior to main trial to measure the ROM capabilities of the patients

the data is stored the ROM values achieved by the patient are displayed through the GUI on the “Current ROM Values” panel (Fig. 3.2(a)). All the specified session parameters, including the patient’s performance data, are recorded for post-processing and analysis.

### **3.3.5 Pilot Clinical Testing and Results**

In this section results of clinical evaluation of an SCI patient who underwent a robotic training protocol with MAHI Exo-II are presented. The main purpose of the study was to validate the efficacy of MAHI Exo-II, and show that MAHI Exo-II can be safely implemented in treatment of upper extremity motor function of a SCI patient.

#### **Subject**

A 28-year-old female, 29-months after an incomplete SCI at the C2 level, classified as American Spinal Injury Impairment Scale C (AIS) participated in this study (Fig. 3.3). At the time of enrollment she presented with minimum voluntary movements (ASIA motor score 3) of her right upper extremity versus moderate voluntary movements on the left side (ASIA motor score 18). No pain was reported at baseline assessment. The subject signed the consent form approved by the local institutional review board.

#### **Training Protocol**

MAHI Exo-II was used as the robotic rehabilitation device with three therapeutic modes: passive, triggered, and constrained. The total time for each session, including set up and frequent rest intervals, did not exceed three hours. Actual training time for each side, as a portion of the three hour session, increased gradually over four



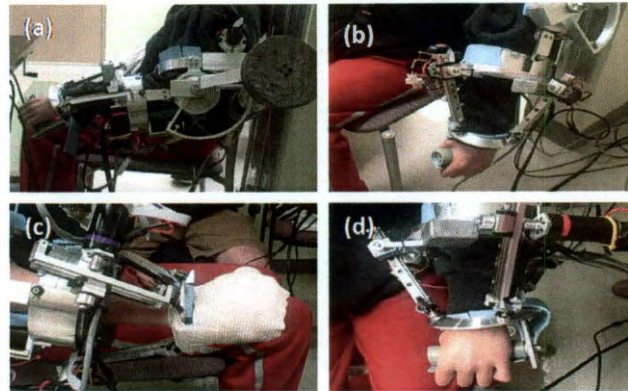


Figure 3.3 : Subject – MAHI Exo-II is being used by a 28-year-old SCI patient.

weeks.

The purpose of the single-joint exercises was to improve strength and active ROM of each joint. Due to severe weakness of the right side, exercises were performed in the triggered mode for elbow flexion, wrist flexion/extension and wrist radial/ulnar deviation. Forearm pronation and supination were exercised in the passive mode. Exercises on the left side were all performed in constrained mode.

During training, a target-hitting task was displayed on the monitor and the subject was asked to move the pointer to hit the active target. After each movement, feedback was given as total number of hits. The treatment was progressed gradually, by increasing number of repetitions, amount of resistance and amount of threshold force applied in the triggered mode. Patient received no additional therapeutic intervention for upper extremity training during the study period.

## Results and Discussion

Extensive discussion of clinical outcomes are beyond the scope of this thesis (for the detailed information the reader is referred to [40]). This single case study demon-

Task	Pre-treatment		Post-treatment	
	Left	Right	Left	Right
ASIA Upper Extremity Motor Score (0-25)	18	7	19	9
ARAT (0-57)	41	3	49	3
JTHFT (total time in seconds)	151.64	1080	80.64	1080

Table 3.1 : Clinical testing results. ASIA: American Spinal Cord Injury Association. The JTHFT was ended after 1080 sec. Lower times represent better performance

strates the preliminary results of a robotic training protocol for training of upper extremity movements after SCI. The results suggest that the MAHI Exo-II can be safely implemented in treatment of upper extremity motor function of a subject with incomplete tetraplegia. Positive gains in arm and hand functions were observed after twelve sessions of treatment on the left side with mild-moderate impairment level, whereas no detectable training effect was observed for the more severely impaired right upper extremity. The current intervention used highly repeatable single-joint movements, focusing on elbow, forearm and wrist. The total number of active repetitive movements on the left side (elbow and wrist flexion/extension, forearm pronation/supination and wrist ulnar/radial deviation) increased from 87 to 800 repetitions. As described before, the treatment was gradually progressed by increasing the number of repetitions and resistance applied, so that at each session the subject was challenged to her maximal effort level. The specific factors that contributed most to the measured gains remain unclear; however, potential mechanisms may include activity-dependent neuroplastic changes, peripheral muscle strengthening which might caused a stronger tenodesis effect and improvement in muscle endurance. Generalization has been demonstrated in similar studies with stroke patients using robotic assisted training as intervention. The gain from the repetitive training could be extended in

overall arm function as it is demonstrated with an improvement in hand functions as measured with the Jebsen-Taylor Hand Function Test (JTHFT), a widely used, well validated test for functional motor assessment that reflects activities of daily living [41], and Action Research Arm Test (ARAT), an observational test used to determine upper limb function [42]. The improvement on left side ARAT score has exceeded the minimally clinical important difference (MCID) limit of 5.7 points (see Table 3.1). Another key factor to consider in the current study was the safety of robotic training in subjects with SCI. Based on the findings of this pilot study, no adverse events were observed and use of the repetitive robotic exercises did not result in significant fatigue or discomfort as reported by the subject. This case report presents a rationale for performing larger controlled clinical studies to further evaluate the safety, feasibility and efficacy of using robotic-assisted training in patients with incomplete SCI in the future.

### **3.4 Assist-As-Needed Control**

The fact that the recovery of stroke, SCI or any other neurologic impairment patients requires active participation [34] makes implementation of controllers with adapting control gains according to the patient's performance, rather than "stiff" controllers with fixed control gains, more desirable. Patient involvement can be increased by implementing a compliant behavior to the robotic device so that the device allows the patient to influence the device whenever they are able to carry out the movement by themselves, and assists them to complete the movement only when they need assistance. A passivity-based adaptive controller, proposed by Slotine and Li [43] is used to develop assistance-as-needed control algorithm by Wolbrecht et al. [31]. The implementation of this controller to the forearm and wrist module of MAHI Exo-II



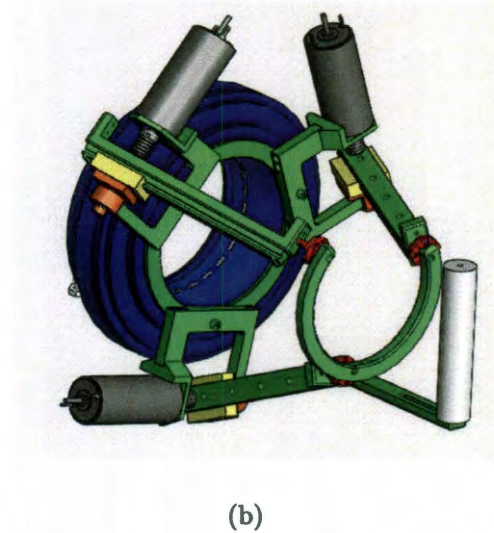
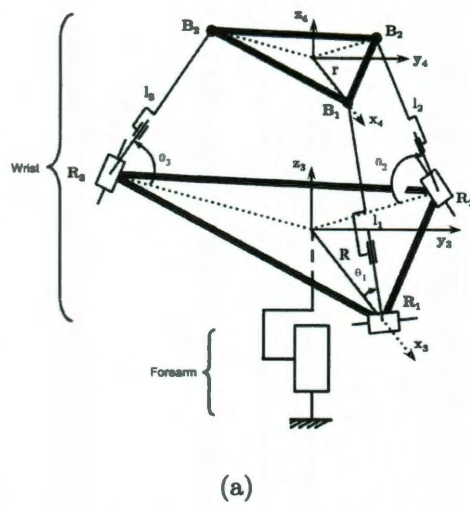


Figure 3.4 : (a) 4 DOF RiceWrist employs a 3-RPS (revolute-prismatic-spherical) parallel mechanism at the wrist module and a revolute joint at the forearm (b) CAD model of RiceWrist.

in simulation is presented subsequently.

### 3.4.1 Adaptive Controller

The control algorithm is developed for wrist and forearm exoskeleton device RiceWrist (see Fig.3.4(b)) which possesses the same serial-in-parallel kinematic structure with the wrist-forearm module of MAHI Exo-II. The mechanism has three rotational and one translational degree-of-freedom. The dynamic equations of the system can be shown as

$$M(q)\ddot{q} + C(q, \dot{q})\dot{q} + G(q) = F_r + F_p \quad (3.4)$$

where  $\mathbf{q}$  is a  $4 \times 1$  vector of joint variables,  $\mathbf{M}$  is the  $4 \times 4$  inertia matrix,  $\mathbf{C}$  is the  $4 \times 4$  matrix which represents Coriolis/centrifugal terms,  $\mathbf{G}$  is the  $4 \times 1$  gravity vector,  $\mathbf{F}_r$  is the  $4 \times 1$  vector of forces applied by the actuators and  $\mathbf{F}_p$  is the  $4 \times 1$  vector of

forces applied by patient at the end-effector (handle) which is mapped to the joint space by the transpose of the inverse of the Jacobian of the mechanism.

It should be noted that the system employs a closed-chain parallel mechanism, namely 3-RPS (revolute-prismatic-spherical), and because of the implicit nature of the loop equations, representing the equations of motion in the form of Equation 3.4 is not straightforward [44]. However, using the formulation in [44] it could be shown that the dynamical equations of the RiceWrist can be expressed in the form of Equation 3.4 and posses identical properties as open-chain serial mechanisms. The important distinction, however, is that the given dynamical equations are valid only locally, i.e. the domain of the generalized coordinates ( $\mathbf{q}$ ) is a bounded and closed set ( $\Omega$ ) rather than the whole  $n$ -dimensional ( $n$  corresponds to the number of DOF of the device, our case  $n = 4$ ) real space [44]:

$$\mathbf{q} \in \Omega, \text{ where } \Omega \subset \mathfrak{R}^n$$

The explicit characterization of the bounds of the domain of the generalized coordinates is out of the scope of this work, but the domain is a subset of the workspace that is free of structural singularities [44]. Consequently, it can be said that the 4-DOF serial-in-parallel mechanism possesses two important properties:

- **Skew – symmetry property**, the matrices  $\mathbf{M}$  and  $\mathbf{C}$  are not independent from each other. The matrix  $\dot{\mathbf{M}} - 2\mathbf{C}$  is skew symmetric and using this property the passivity of the system can be proven [45].
- **Linearity – in – the – parameters property**, the equations of motion are linear in terms of suitable selected robot and load parameters [43].

Another point to clarify about Equation 3.4 is the effect of coupling of the robot with human arm on the dynamics of the system is not modelled for the simulations,

so Equation 3.4 represents the dynamics of the robot itself rather than the dynamics of the robot connected to the human arm.

The following adaptive control law is developed by Slotine and Li [43], and we adopted the formulation presented in [38] and [45] which exploit the passivity property of the robotic devices.

Let us define the tracking error as  $\tilde{q}(t) = q(t) - q_d(t)$ , where  $\mathbf{q}(t)$  is  $4 \times 1$  actual joint position and  $\mathbf{q}_d(t)$  is at least twice differentiable desired trajectory and both  $\mathbf{q}(t), \mathbf{q}_d(t) \in \Omega$  such that Equation 3.4 is valid. Consider the following control law:

$$F_r = \hat{M}(q)a + \hat{C}(q, \dot{q})v + \hat{G} - \hat{F}_p - K_D r \quad (3.5)$$

where  $\hat{M}$ ,  $\hat{C}$  and  $\hat{G}$  are the estimates of the dynamics of the system,  $\hat{F}_p$  is the estimates of the forces coming from the patient,  $K_D$  is a symmetric positive definite matrix, and

$$\begin{aligned} r &= \dot{\tilde{q}} + \Lambda \tilde{q} = (\dot{q} - \dot{q}_d) + \Lambda(q - q_d) \\ v &= \dot{q}_d - \Lambda \tilde{q} = \dot{q}_d - \Lambda(q - q_d) \\ a &= \dot{v} \end{aligned} \quad (3.6)$$

where  $\Lambda$  is a  $4 \times 4$  constant, positive definite, symmetric matrix. Note that desired position, velocity and acceleration are all bounded. The substitution of control input into Equation 3.4 will bring

$$M(q)\ddot{q} + C(q, \dot{q})\dot{q} + G(q) - F_p = \hat{M}(q)a + \hat{C}(q, \dot{q})v + \hat{G} - \hat{F}_p - K_D r \quad (3.7)$$

As stated above, system dynamics are linear in terms of system parameters, and they can be modelled as

$$Y\hat{\mathbf{b}} = \hat{M}\dot{w} + \hat{C}w + \hat{G} \quad (3.8)$$

where  $\mathbf{Y}$  is a  $4 \times m$  regressor matrix which contains known functions of  $\mathbf{q}$ ,  $\dot{\mathbf{q}}$ ,  $\mathbf{v}$  and  $\mathbf{a}$ , and  $\hat{\mathbf{b}}$  is  $m \times 1$  estimates of unknown system parameters. Here it is going to be assumed that the estimates of the forces coming from the patient can be modelled as

$$Y\hat{\mathbf{h}} = \hat{F}_p \quad (3.9)$$

where  $\mathbf{Y}$  is the regressor matrix used in Equation 3.10 and  $\mathbf{h}$  is the vector of parameters that represent patients ability and effort. Furthermore define overall system parameters,  $\theta$ , as  $\theta = \mathbf{b} - \mathbf{h}$  so that

$$Y\hat{\theta} = Y\hat{\mathbf{b}} - Y\hat{\mathbf{h}} \quad (3.10)$$

This relationship represents the difference between forces required to move the patient's limb, and the forces generated by the patient [31], and subsequently a further discussion for both  $\mathbf{Y}$  and  $\theta$  will be conducted.

Then by using Equation 3.12 and considering that  $\ddot{q} = \dot{r} + a$  and  $\dot{q} = r + v$ , Equation 3.9 can be written as

$$\begin{aligned} M(q)\dot{r} + C(q, \dot{q})r + K_D r &= \tilde{M}(q)a + \tilde{C}(q, \dot{q})v + \tilde{G} - \tilde{F}_p \\ &= Y(q, \dot{q}, v, a)\tilde{\theta} := \Psi \end{aligned} \quad (3.11)$$

where  $\tilde{(\cdot)} = \hat{(\cdot)} - (\cdot)$ . Next, the adaptation law is defined such that the mapping in Equation 3.13 from  $-r$  to  $\Psi$  is passive.

$$\dot{\tilde{\theta}} = -\Gamma Y^T r \quad (3.12)$$

where  $\tilde{\theta}$  is the parameter estimation error and  $\Gamma$  is a symmetric positive definite matrix. Then, by using Equation 3.13 and 3.14 the passivity of the mapping from  $-r$  to  $\Psi$  can be shown as follows:

$$r^T Y \tilde{\theta} = -\dot{\tilde{\theta}}^T \Gamma \tilde{\theta} \quad (3.13)$$

hence,

$$\begin{aligned} -\int_0^t r^T \Psi d\tau &= \int_0^t \dot{\tilde{\theta}}^T \Gamma \tilde{\theta} d\tau \\ &= \frac{1}{2} \int_0^t \frac{d}{d\tau} (\tilde{\theta}^T \Gamma \tilde{\theta}) d\tau \\ &= \frac{1}{2} \tilde{\theta}^T(t) \Gamma \tilde{\theta}(t) - \frac{1}{2} \tilde{\theta}^T(0) \Gamma \tilde{\theta}(0) \\ &\geq -\frac{1}{2} \tilde{\theta}^T(0) \Gamma \tilde{\theta}(0) \end{aligned} \quad (3.14)$$

Because the equations of motion are valid locally for our system, a local stability analysis is required. This analysis, in principle, can be conducted based on the existing global stability analyses of the aforementioned control algorithm in the literature ([45], [46]), with considering the necessary additional arguments to show local stability. But because of the lack of the explicit closed form equations of motions for our system, the stability analysis is beyond the scope of this work.

The parametrization of both the system dynamics and the forces coming from the patient (Equations 3.10-3.12) indicates that the matrix of known functions,  $Y$ , consists of both the inertia components, which represent the known functions of the system dynamics, and the components that represent known functions of the patient's ability and effort. The inertia components can be acquired by separating out the linear parameters from the equations of motion but as a matter of fact, separating these parameters is difficult especially for the systems that include parallel mechanisms in their structure, because of the existence of multiple closed-chains. However, the

movements in the rehabilitation of patients with impairments due to neurological lesions are at low speeds and the assumption of being in a quasi-static condition can be made. Consequently, the method proposed in [31] has been adopted and simple models  $\mathbf{I}\dot{\mathbf{w}}$  and  $\mathbf{I}\mathbf{w}$  have been chosen to represent the inertia components of the regressor matrix  $\mathbf{Y}$ .

Considering that the capability of a patient to apply forces depends on the location of the hand, Gaussian radial basis functions are used to model the ability and effort of the patient. Gaussian radial basis functions are real-valued functions whose values depend on the distance from the origin [47]. Gaussian radial basis functions are bounded, strictly positive, and absolutely integrable. Any continuous function, not necessarily infinitely smooth, can be uniformly approximated by linear combinations of Gaussian radial basis functions [48] which are defined as

$$g_n = \exp(-\|x - \mu_n\|^2 / 2\sigma^2) \quad (3.15)$$

where  $g_n$  is the  $n^{\text{th}}$  Gaussian radial basis function,  $\mathbf{x}$  is the current location of the RiceWrist's end-effector,  $\mu_n$  is the location of the  $n^{\text{th}}$  Gaussian radial basis function, and  $\sigma$  is a smoothing constant. In total, 96 Gaussian radial basis functions are assigned to the workspace of RiceWrist. The forces coming from the patient are parameterized using these 96 known functions. The vector of Gaussian radial basis functions is defined as

$$\mathbf{g} = [g_1 \ g_2 \ \dots \ g_{96}]^T \quad (3.16)$$

Consequently the regressor matrix which represent both the known functions of the system dynamics (simple models  $\mathbf{I}\dot{\mathbf{w}}$  and  $\mathbf{I}\mathbf{w}$ ) and known functions of patient's ability and effort (Gaussian radial basis functions) is defined as

$$\mathbf{Y}^{4 \times 392} = \begin{bmatrix} & \mathbf{g}^T & 0 & 0 & 0 \\ \mathbf{I}\dot{\mathbf{w}}, & \mathbf{I}\mathbf{w}, & 0 & \mathbf{g}^T & 0 & 0 \\ & & 0 & 0 & \mathbf{g}^T & 0 \\ & & 0 & 0 & 0 & \mathbf{g}^T \end{bmatrix} \quad (3.17)$$

The unknown parameter vector  $\mathbf{a}$  is a  $392 \times 1$  vector which is estimated using Equation 3.14.

$$\dot{\hat{W}} = (\Gamma_1 \hat{\sigma}' \hat{V}^T \dot{x}_d e_2^T) \quad (3.18)$$

$$\dot{\hat{V}} = (\Gamma_2 \dot{x}_d ((\hat{\sigma}')^T \hat{W} e_2)^T) \quad (3.19)$$

### 3.4.2 Simulation Results

The assist-as-needed control designed for severely injured patients is the same as the control strategy presented in Section 3.3.1, which uses a proportional-derivative controller. The difference between these two control strategies is that the assist-as-needed control employs a controller with adapting parameters based on online measurement of the patient's performance, instead of a controller with static parameters. The controller brings compliance to the mechanical system and allows the patient to influence the mechanism when he/she is capable of performing the movement.

The goals of the simulations are twofold: first, the trajectory tracking performance of the implemented adaptive controller will be investigated, then the control effort of the controller will be compared with a proportional-derivative (PD) controller.

The position and velocity level inverse and forward kinematics, and the forward dynamics equations for the 4-DOF RiceWrist were formulated using Autolev (Online

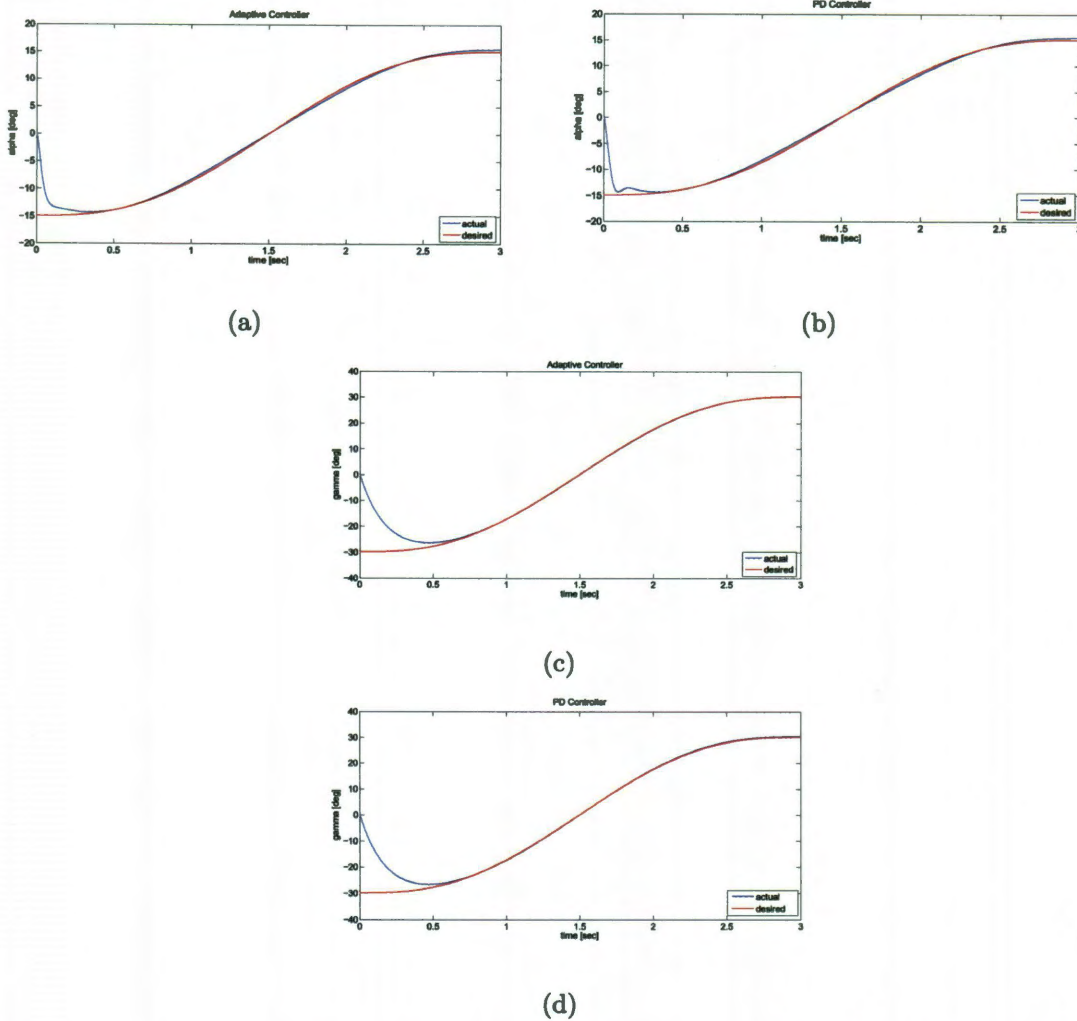


Figure 3.5 : Trajectory tracking for both adaptive and PD controllers. (a) and (b) shows the rotation around  $x_4$  for adaptive and PD controllers respectively, and (c) and (d) shows the rotation around  $z_4$  for adaptive and PD controllers respectively

Dynamics), a symbolic manipulator software designed to both derive the equations of motion for multi-body systems by using Kane's method and generate compact C, MATLAB, and Fortran codes for real-time applications [49]. Autolev allows one to define a physical mechanism by using the built-in physical objects such as points, particles, frames and bodies.



In order to simulate human movements, we defined a 1 kg virtual load at the end-effector of the system during the formulation of the forward dynamics equations to mimic the situation through which the patient keeps his/her hand relaxed. A combined movement which includes rotation of the end-effector both around  $x_4$  ( $\alpha$ ) and  $z_4$  ( $\gamma$ ) (Fig. 3.4 (a)) is chosen as a defined trajectory. The rotations are defined by fifth order polynomials. The trajectory tracking performances of the controller for two axes are presented in Fig. 3.5.

The control effort of the adaptive controller is compared with a PD controller. The  $K_p$  and  $K_d$  values of the PD controller are picked identical to the gains of the feedback part of the adaptive controller (see Equation 3.5-3.6). The trajectory tracking performance of the PD controller (maximum position error for  $\alpha=0.43^\circ$ ) is very close to the performance of the adaptive controller (maximum position error for  $\alpha=0.40^\circ$ ) (see Fig 3.5 (a)-(b)). The control efforts are compared by calculating the work done by the actuators which is the provided energy to every actuator by the controllers. It should be considered that the three wrist motors are responsible for the rotation around  $x_4$  and only the forearm motor is responsible for the rotation around  $z_4$ . Hence the work done for the rotation around  $x_4$  is equal to the total work done by the wrist motors and the work done for the rotation around  $z_4$  is equal to the work done by only the forearm motor. Because the forces applied by the actuators are changing over time, the calculations are done for every time step (0.001 sec) and summed. The work done by wrist motors during the motion are given in Table 3.2.

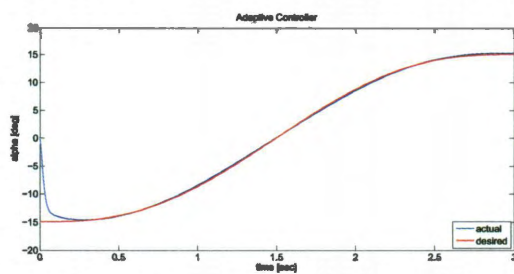
The provided energy by adaptive controller is approximately 10% less than the energy provided by PD controller. The work done by the forearm motor for both controllers are not significantly different from each other.

To further investigate the capabilities of the adaptive controller with different

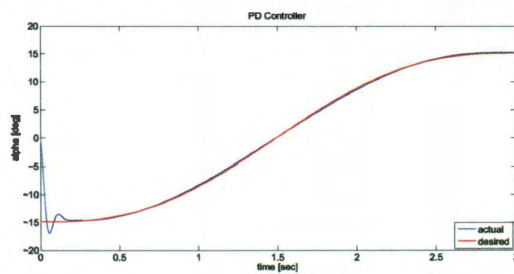
Actuator	Provided Energy (J)	
	PD Controller	Assist as needed controller
wrist motor 1	0.156	0.1483
wrist motor 2	0.09611	0.07838
wrist motor 3	0.09194	0.08687
total	0.344	0.313

Table 3.2 : Provided energy to wrist actuators for mentioned desired trajectory.

sets of controller gains the  $K_p$  values for  $\alpha$  and  $\gamma$  are increased equally in both controllers. The trajectory tracking performances of both controller for  $\alpha$  are given in Fig. 3.6. Besides providing better tracking performance, the adaptive controller provides almost 17.5% less energy to the wrist actuators for this particular case. Both the tracking performance for  $\gamma$  and the provided energy to the forearm motor are not significantly different from each other for these controllers.



(a)



(b)

Figure 3.6 : Trajectory tracking with increased  $K_p$  gains. (a) and (b) shows the rotation around  $x_4$  for adaptive and PD controllers respectively

## Chapter 4

### Conclusions and Future Work

Rehabilitation robots have been drawing attention due to their advantages over classical rehabilitation, such as training sessions with increased number of repetitions, longer duration and consistent delivery; reduction in personnel cost; inclusion of virtual reality into the training; and objective performance evaluation of the patients. This thesis presents the design of MAHI Exo-II, a robotic exoskeleton for the rehabilitation of upper extremity after stroke, spinal cord injury, or other brain injuries. The mechanical design builds upon its predecessor MAHI Exo-I, and proposes significant design improvements to achieve clinical use.

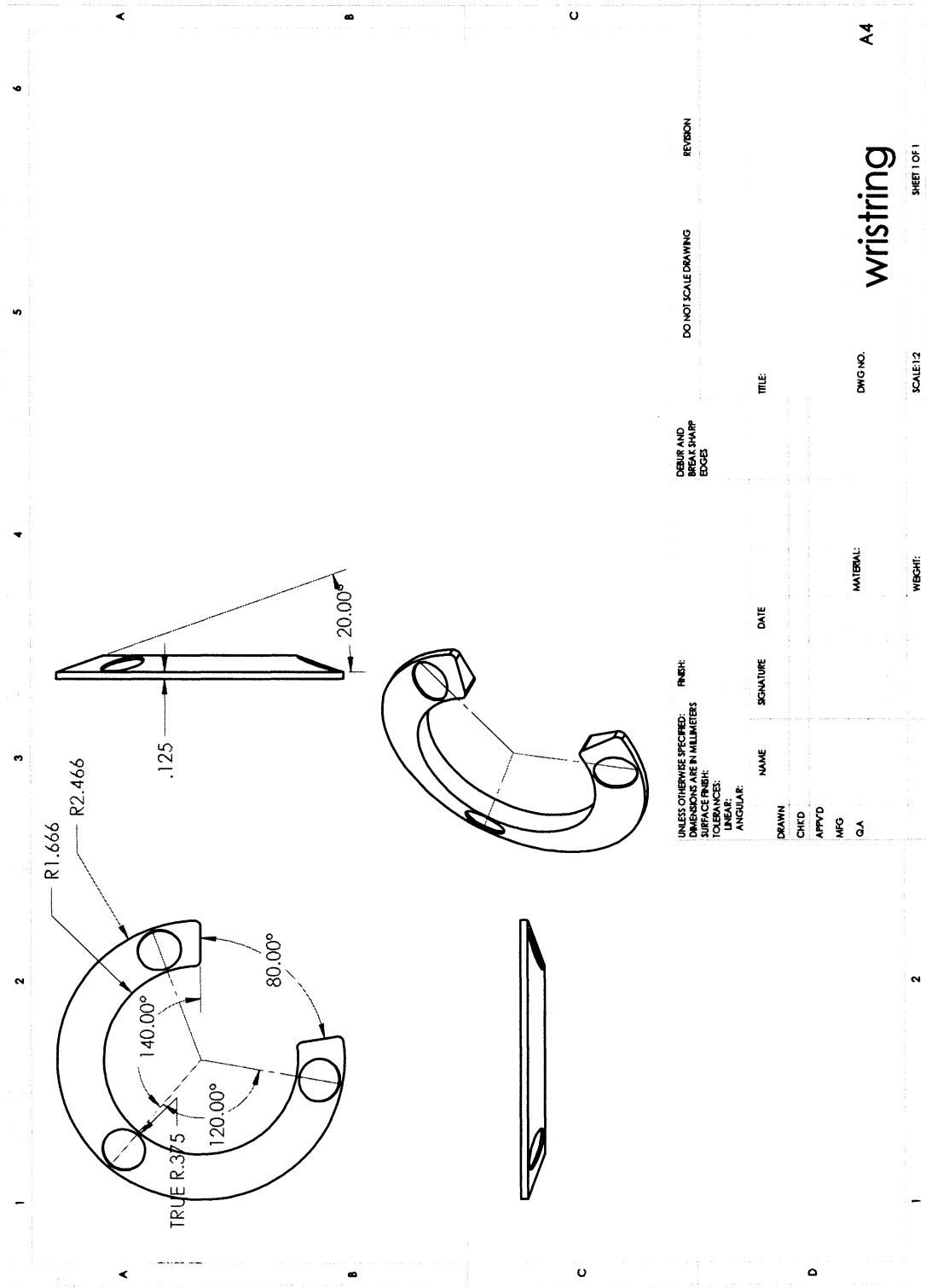
Chapter 2 presented the kinematical structure of the system in detail and discussed the design improvements introduced in the new design. The design improvements included solution of the mechanical problems that cause undesired mechanism configurations at the wrist, redesign of the elbow joint to enable easy donning for both left and right arm, and implementation of a mechanism for better posture during the training/rehabilitation sessions. Additionally, these improvements resulted in increase in torque output at the forearm and elbow part, and reduction of the device cost.

Chapter 3 detailed the control of the exoskeletal mechanism and presented the implementation of an advanced assistance-as-needed control algorithm in simulation. The control modes presented in Chapter 3 were first designed for RiceWrist, a 4-DOF forearm and wrist rehabilitation device. The control modes were implemented on the

5-DOF MAHI Exo-II and with some modifications, justified in the thesis. Chapter 3 also presented the results of the clinical testing of the efficacy of the control modes and the feasibility of the mechanical design.

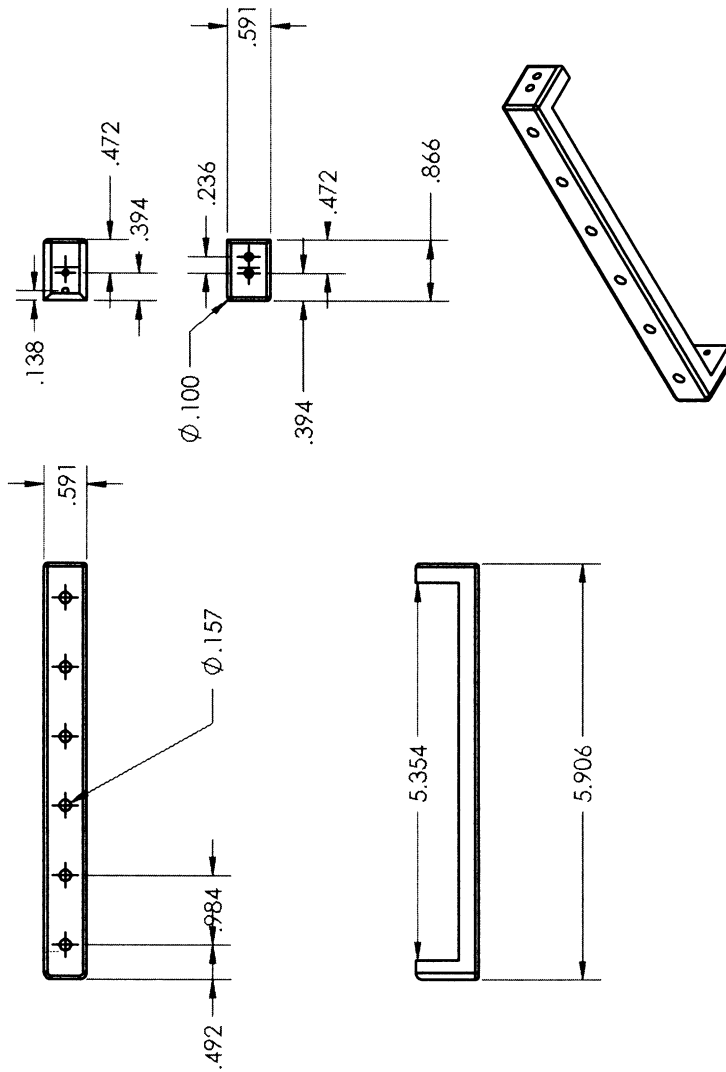
Future work includes the experimental testing of the assistance-as-needed control algorithm with the RiceWrist as an initial test bed prior to implementation of the controller on MAHI Exo-II. Alternative designs for the wrist module, specifically a serial mechanism design, are also being explored in order to overcome workspace limitations of the parallel wrist design.

**Appendix A**  
**Technical Drawings**



UNLESS OTHERWISE SPECIFIED:		FINISH:		DO NOT SCALE DRAWING		REVISION	
DIMENSIONS ARE IN MILLIMETERS		SURFACE FINISH:		DEBUR AND BREAK SHARP EDGES		SHEET 1 OF 1	
TOLERANCES:				TITLE		DWG NO.	
UNLESS ANGLE:				MATERIAL:		SCALE: 1:2	
ANGULAR:				WEIGHT:		A4	
DRAWN	NAME	SIGNATURE	DATE				
CHEK							
APP'D							
MFG							
Q.A.							

Figure A.1 : Wrist Ring



<p><b>UNLESS OTHERWISE SPECIFIED:</b></p> <p>DIMENSIONS ARE IN INCHES</p> <p>FRACTIONAL:                      CHECKED</p> <p>ANGULAR: MACH:                  ENG. APPR.</p> <p>TWO PLACE DECIMAL            MFG APPR.</p> <p>THREE PLACE DECIMAL        G.A.</p> <p>INTERPRET GEOMETRIC TOLERANCING PER:        COMMENTS:</p> <p>MATERIAL</p> <p>FINISH</p> <p>DO NOT SCALE DRAWING</p>		<p>NAME</p> <p>DATE</p>	<p>TITLE:</p> <p>SIZE DWG. NO.                      REV</p> <p><b>A sliderbase</b>                      1</p> <p>SCALE: 1:2                      WEIGHT:                      SHEET 1 OF 1</p>
<p>PROPRIETARY AND CONFIDENTIAL</p> <p>THE INFORMATION CONTAINED IN THIS DRAWING IS THE SOLE PROPERTY OF &lt;INSERT COMPANY NAME HERE&gt;. ANY REPRODUCTION IN PART OR AS A WHOLE WITHOUT THE WRITTEN PERMISSION OF &lt;INSERT COMPANY NAME HERE&gt; IS PROHIBITED.</p>	<p>NEXT ASSY</p> <p>USED ON</p> <p>APPLICATION</p>	<p>2</p>	<p>1</p>
<p>5</p>	<p>4</p>	<p>3</p>	<p>1</p>

Figure A.2 : Wrist Link Base



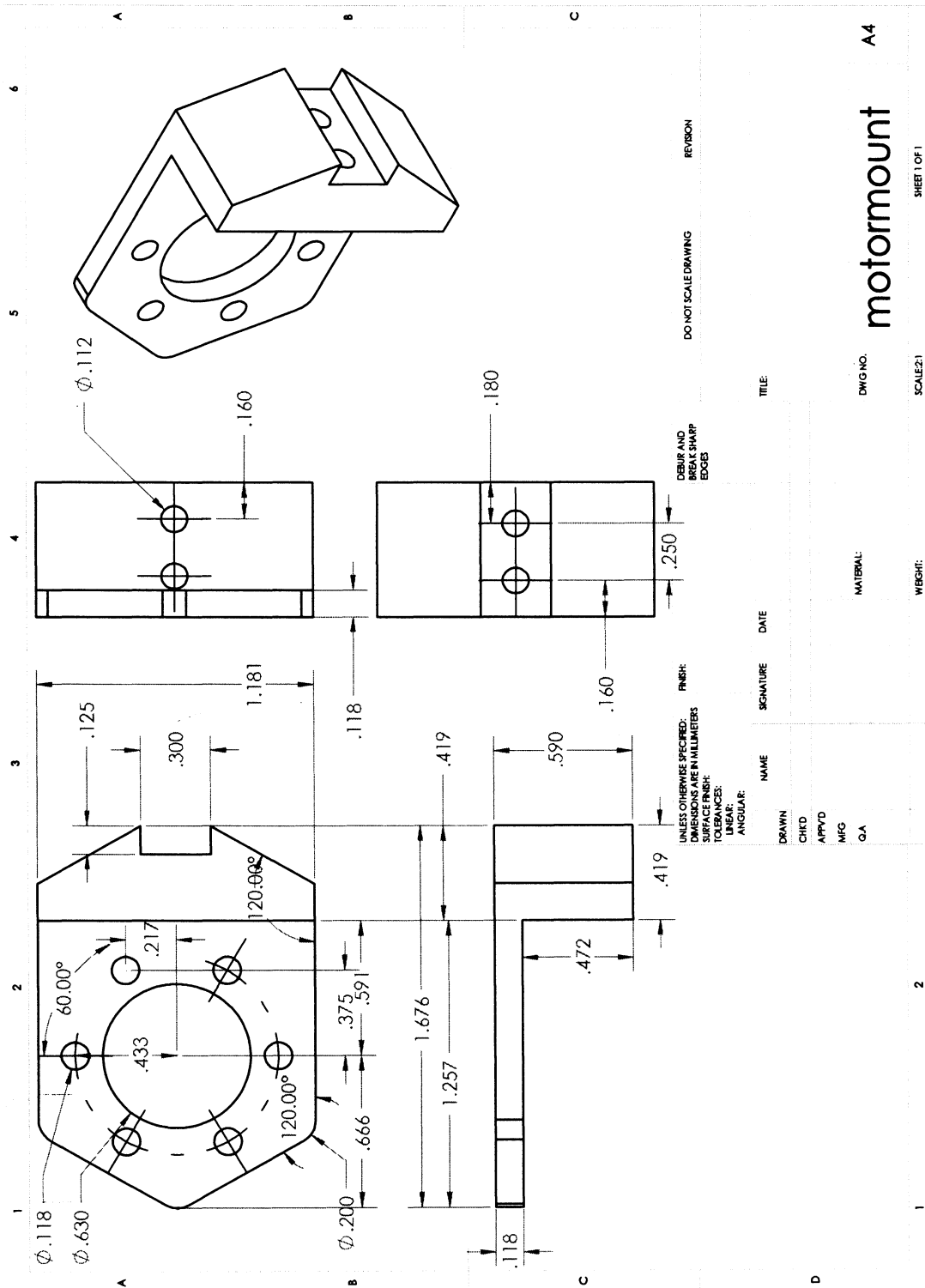
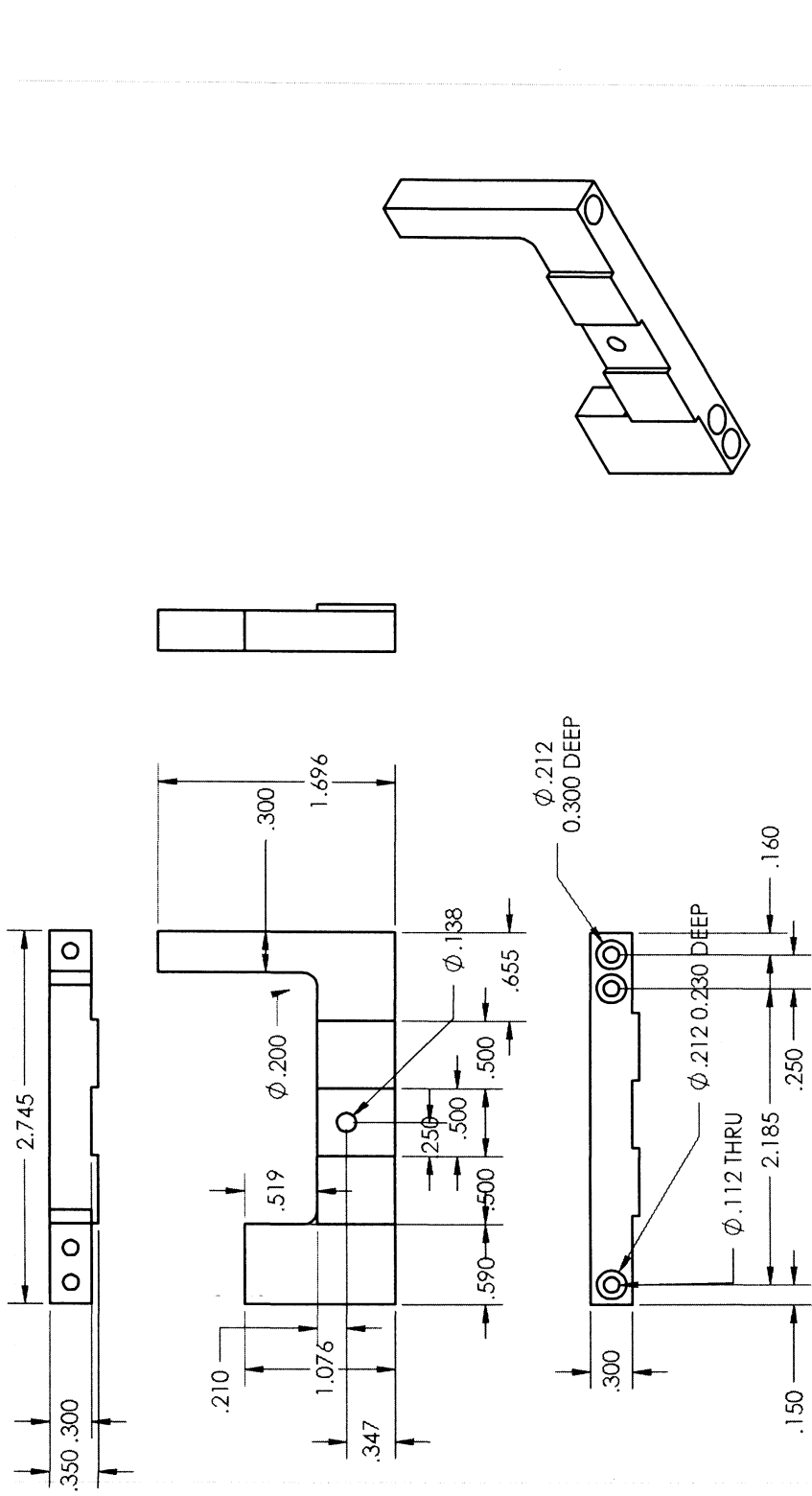
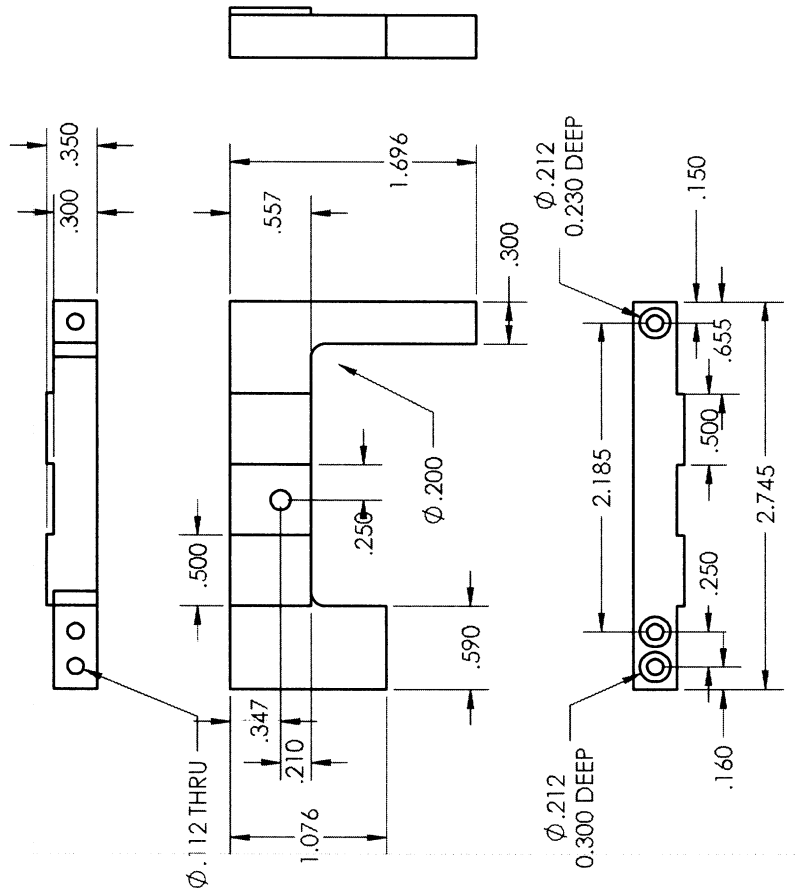


Figure A.3 : Wrist Motor Mount



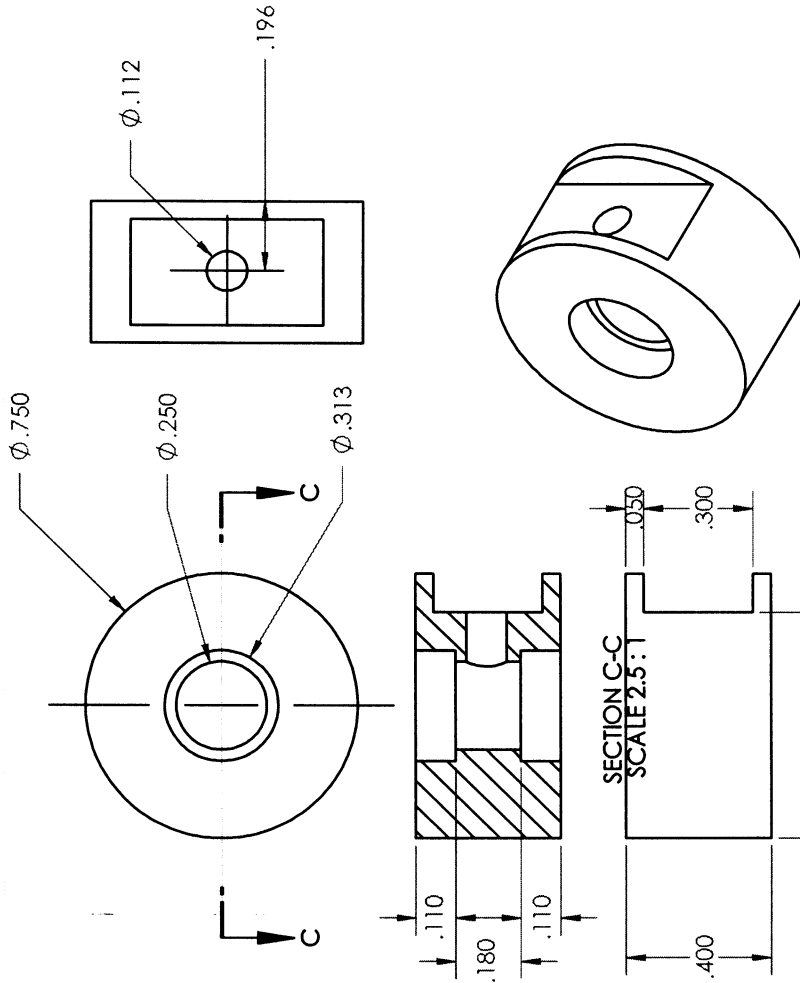
UNLESS OTHERWISE SPECIFIED:		DRAWN		NAME		DATE	
DIMENSIONS ARE IN INCHES		CHECKED					
TOLERANCES:		ENG APPR.					
FRACTIONAL: $\frac{1}{16}$		MFG APPR.					
ANGULAR: MACH $\pm$		G.A.					
TWO PLACE DECIMAL $\pm$		COMMENTS:					
THREE PLACE DECIMAL $\pm$							
INTERPRET GEOMETRIC TOLERANCING PER:							
MATERIAL							
FINISH							
USED ON							
NEXT ASSY							
APPLICATION							
DO NOT SCALE DRAWING							
5		3		2		1	
<p>PROPRIETARY AND CONFIDENTIAL</p> <p>THE INFORMATION CONTAINED IN THIS DRAWING IS THE SOLE PROPERTY OF &lt;INSERT COMPANY NAME HERE&gt;. ANY REPRODUCTION IN PART OR AS A WHOLE WITHOUT THE WRITTEN PERMISSION OF &lt;INSERT COMPANY NAME HERE&gt; IS PROHIBITED.</p>		<p>TITLE:</p>		<p>SIZE DWG. NO. REV</p> <p><b>Apasetomotors</b></p>		<p>SCALE: 1:1 WEIGHT: SHEET 1 OF 1</p>	

Figure A.4 : Bottom Plate to motor connector



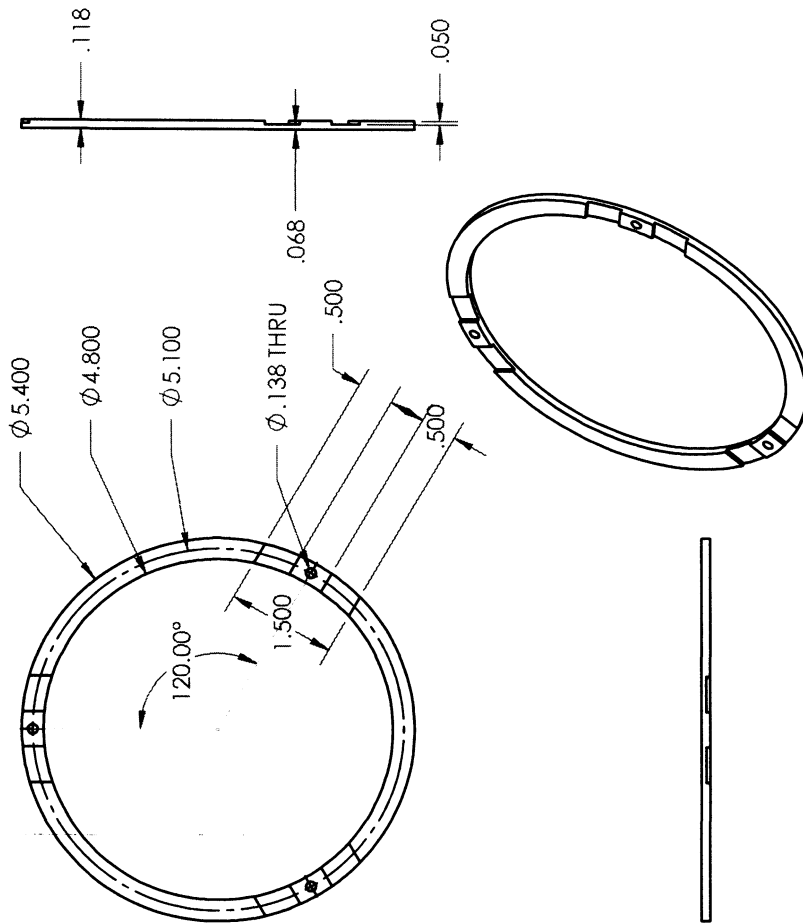
UNLESS OTHERWISE SPECIFIED:		DRAWN		NAME	DATE
DIMENSIONS ARE IN INCHES		CHECKED			
TOLERANCES:		ENG. APPR.			
FRACTIONAL: 1/16		MFG APPR.			
ANGULAR: MACH: BEND 2		G.A.			
TWO PLACE DECIMAL 2		COMMENTS:			
THREE PLACE DECIMAL 2		INTERPRET GEOMETRIC TOLERANCING PER:			
		MATERIAL			
		FINISH			
		USED ON			
		NEXT ASSY			
		APPLICATION			
		DO NOT SCALE DRAWING			
<p><b>PROPRIETARY AND CONFIDENTIAL</b>          THE INFORMATION CONTAINED IN THIS DRAWING IS THE SOLE PROPERTY OF TASCASET MOTORS. ANY REPRODUCTION IN PART OR AS A WHOLE WITHOUT THE WRITTEN PERMISSION OF TASCASET MOTORS IS PROHIBITED.</p>		SIZE	DWG. NO.	REV	
		TASCASET MOTORS			
		SCALE: 1:1	WEIGHT:	SHEET 1 OF 1	
				2	1

Figure A.5 : Bottom Plate to motor connector Reversed



UNLESS OTHERWISE SPECIFIED:		DRAWN		NAME		DATE	
DIMENSIONS ARE IN INCHES		CHECKED					
TOLERANCES:		FRACTIONAL:					
FRACTIONAL:		ANGULAR: MACH:					
ANGULAR: MACH:		BEND:					
TWO PLACE DECIMAL:		MFG APPR:					
THREE PLACE DECIMAL:		G.A.					
INTERPRET GEOMETRIC TOLERANCING PER:		COMMENTS:					
MATERIAL		USED ON					
FINISH		NEXT ASSY					
DO NOT SCALE DRAWING		APPLICATION					
5		4		3		2	
<b>PROPERTY AND CONFIDENTIAL</b> THE INFORMATION CONTAINED IN THIS DRAWING IS THE SOLE PROPERTY OF <INSERT COMPANY NAME HERE>. ANY REPRODUCTION IN PART OR AS A WHOLE WITHOUT THE WRITTEN PERMISSION OF <INSERT COMPANY NAME HERE> IS PROHIBITED.		TITLE:		SCALE: 4:1		WEIGHT:	
		SIZE DWG. NO.		REV		SHEET 1 OF 1	
		<b>Bearingspacer</b>		1		1	

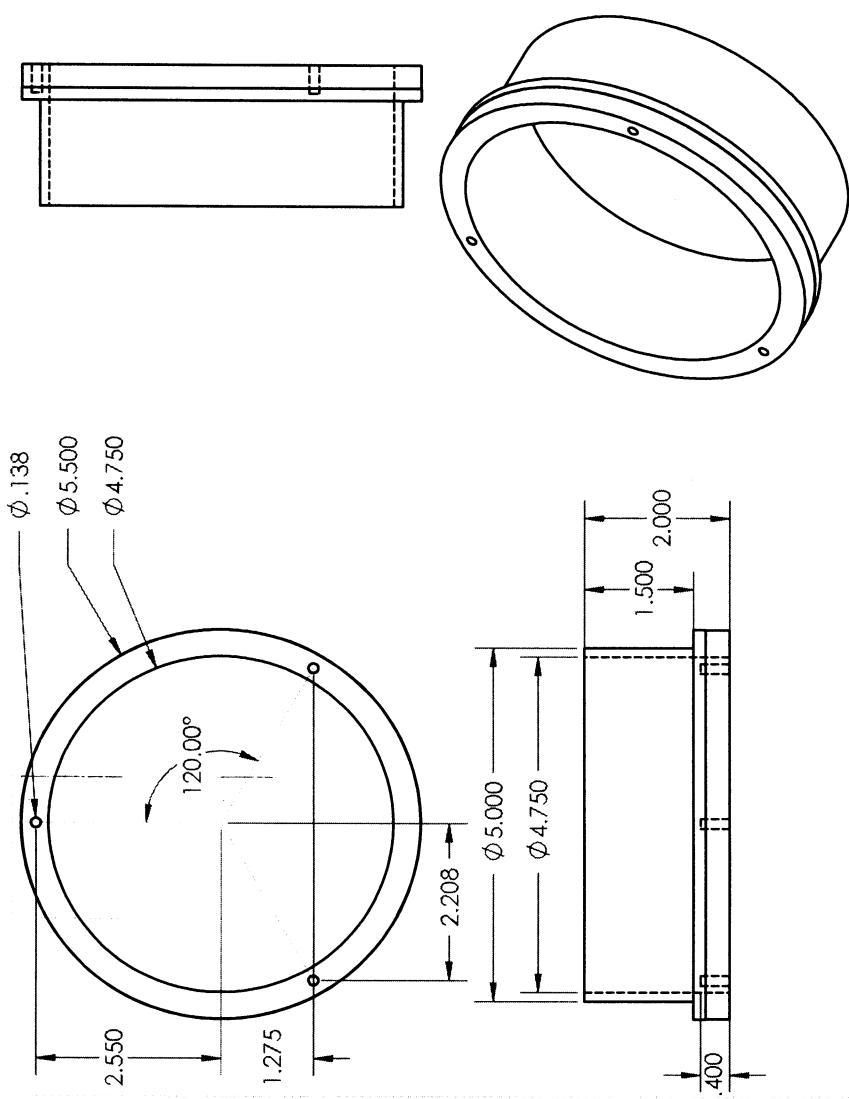
Figure A.6 : Wrist Bearing Spacer



NAME	DATE	TITLE:	SIZE	DWG. NO.	REV
UNLESS OTHERWISE SPECIFIED:			Haasmountpart		
DIMENSIONS ARE IN INCHES			SCALE: 1:2		
TOLERANCES:			WEIGHT:		
FRACTIONAL:	CHECKED	FRAC. DECIMAL	SHEET 1 OF 1		
ANGULAR: MACH:	ENG. APPR.	BEND:			
TWO PLACE DECIMAL:	MFG APPR.	THREE PLACE DECIMAL:			
INTERPRET GEOMETRIC TOLERANCING PER:			G.A.		
MATERIAL:			COMMENTS:		
FINISH:					
USED ON:					
NEXT ASSY:					
APPLICATION:					
DO NOT SCALE DRAWING					
5			2		
4			3		
1			1		

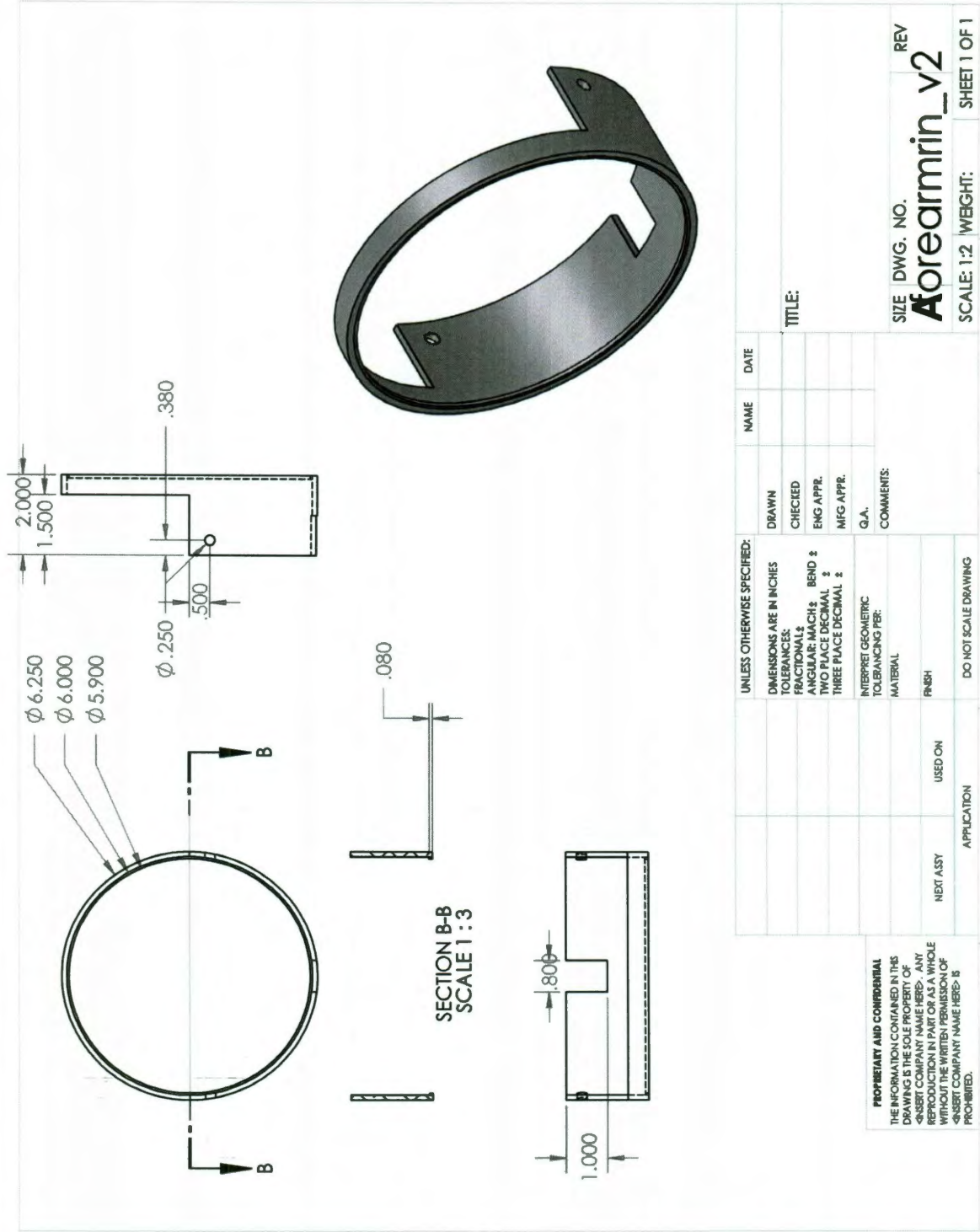
**PROPRIETARY AND CONFIDENTIAL**  
 THE INFORMATION CONTAINED IN THIS DRAWING IS THE SOLE PROPERTY OF HAAS MOUNT PART. ANY REPRODUCTION IN PART OR AS A WHOLE WITHOUT THE WRITTEN PERMISSION OF HAAS MOUNT PART IS PROHIBITED.

Figure A.7 : Bottom Plate Ring



UNLESS OTHERWISE SPECIFIED:		DRAWN		NAME		DATE	
DIMENSIONS ARE IN INCHES		CHECKED					
TOLERANCES:		ENG. APPR.					
FRACTIONAL: $\pm$		MFG APPR.					
ANGULAR: MACH: BEND: $\pm$		G.A.					
TWO PLACE DECIMAL: $\pm$		COMMENTS:					
THREE PLACE DECIMAL: $\pm$		MATERIAL					
INTERPRET GEOMETRIC TOLERANCING PER:		FINISH					
		USED ON					
NEXT ASSY		APPLICATION					
APPLICATION		DO NOT SCALE DRAWING					
5		3		2		1	
TITLE:		SIZE DWG. NO.		REV		SHEET 1 OF 1	
Anewinnerpart		SCALE: 1:2		WEIGHT:			

Figure A.8 : Forearm Inner Drum



UNLESS OTHERWISE SPECIFIED:		NAME	DATE
DIMENSIONS ARE IN INCHES	DRAWN		
TOLERANCES:	CHECKED		
FRACTIONALS:	ENG APPR.		
ANGULAR: MACH $\pm$	MFG APPR.		
TWO PLACE DECIMAL $\pm$	G.A.		
THREE PLACE DECIMAL $\pm$	COMMENTS:		
INTERPRET GEOMETRIC TOLERANCING PER:			
MATERIAL			
FINISH			
USED ON			
NEXT ASY			
APPLICATION			
DO NOT SCALE DRAWING			

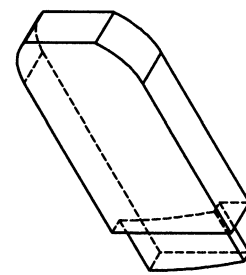
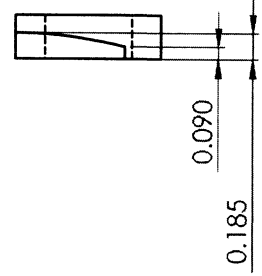
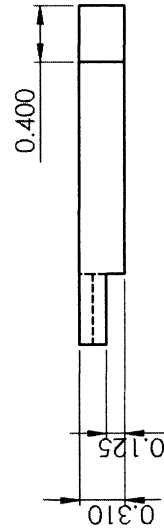
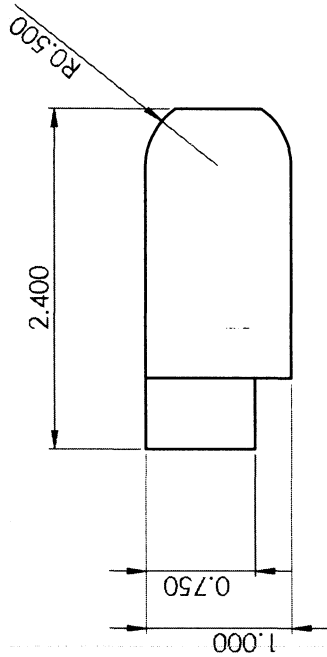
SIZE	DWG. NO.	REV
SCALE: 1:2	WEIGHT:	SHEET 1 OF 1

1	2	3	4	5
---	---	---	---	---

**PROPRIETARY AND CONFIDENTIAL**  
 THE INFORMATION CONTAINED IN THIS DRAWING IS THE SOLE PROPERTY OF <INSERT COMPANY NAME HERE>. ANY REPRODUCTION IN PART OR AS A WHOLE WITHOUT THE WRITTEN PERMISSION OF <INSERT COMPANY NAME HERE> IS PROHIBITED.

Figure A.9 : Forearm Outer Drum



UNLESS OTHERWISE SPECIFIED:		NAME	DATE	REV
DIMENSIONS ARE IN INCHES		TITLE:		
TOLERANCES:		SIZE DWG. NO.		
FRACTIONAL:	CHECKED	elbow_to_forearm_right		
ANGULAR: MACH :	ENG APPR.	SCALE: 1:1		
TWO PLACE DECIMAL :	MFG APPR.	WEIGHT:		
THREE PLACE DECIMAL :	Q.A.	SHEET 1 OF 1		
INTERPRET GEOMETRIC TOLERANCING PER:	COMMENTS:	2		
MATERIAL:	FINISH	3		
DO NOT SCALE DRAWING	USED ON	4		
APPLICATION	NEXT ASSY	5		
<p><b>PROPRIETARY AND CONFIDENTIAL</b>          THE INFORMATION CONTAINED IN THIS DRAWING IS THE SOLE PROPERTY OF GIBERT COMPANY NAME HERE. ANY REPRODUCTION IN PART OR AS A WHOLE WITHOUT THE WRITTEN PERMISSION OF GIBERT COMPANY NAME HERE IS PROHIBITED.</p>				

Figure A.10 : Forearm Elbow Connector Right



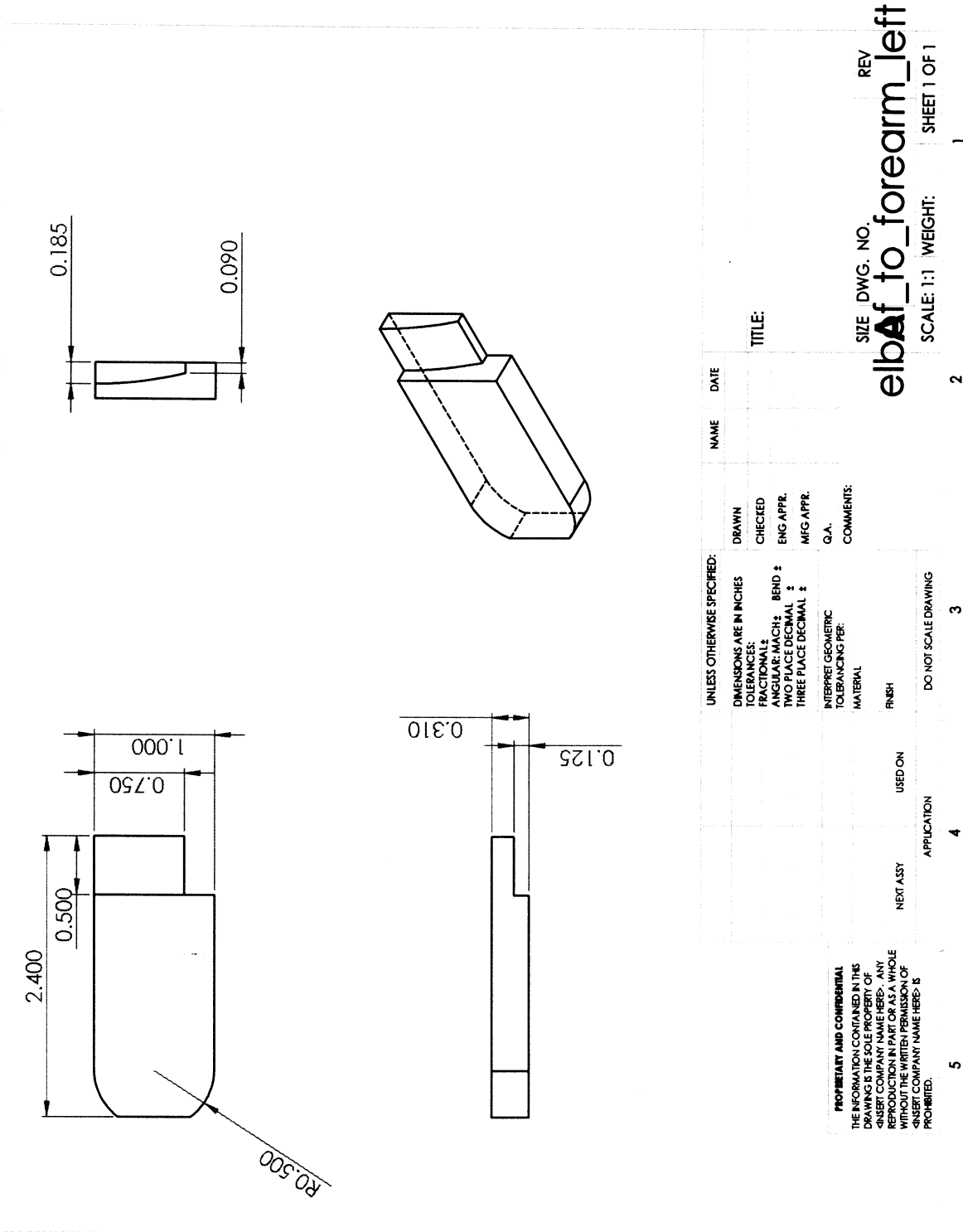
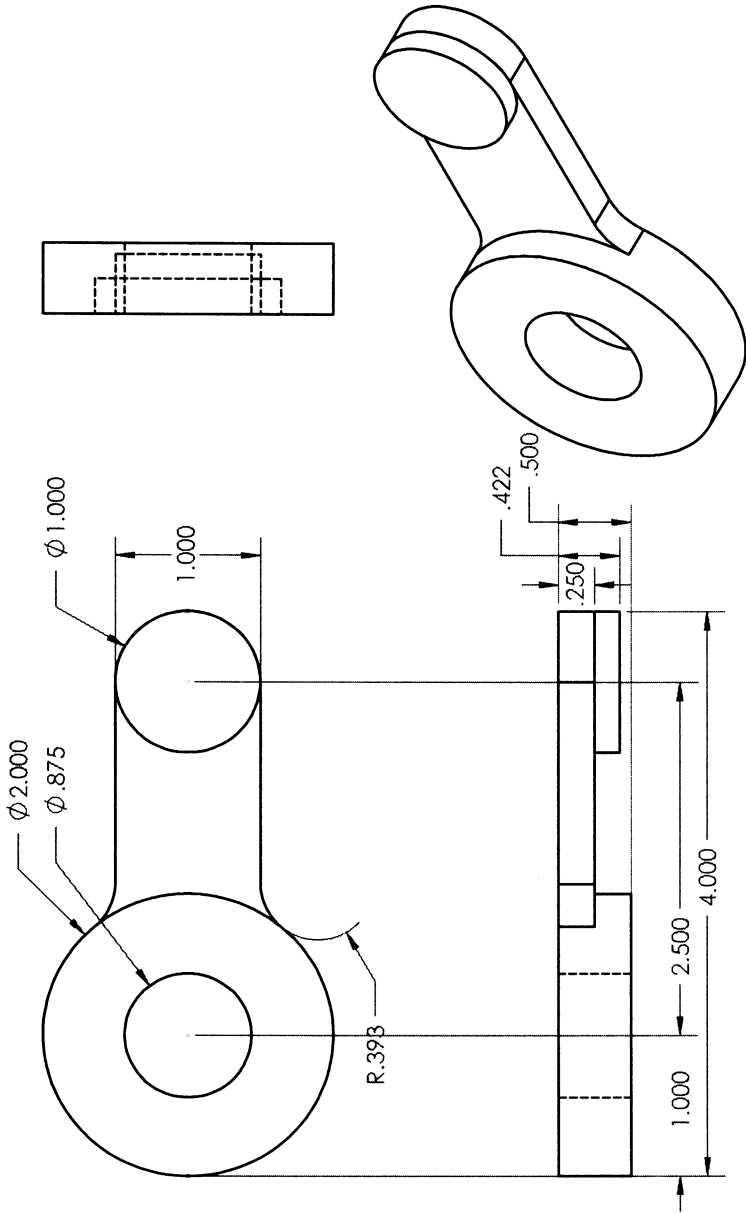


Figure A.11 : Forearm Elbow Connector Left



UNLESS OTHERWISE SPECIFIED:		NAME	DATE
DIMENSIONS ARE IN INCHES	DRAWN		
TOLERANCES:	CHECKED		
FRACTIONAL: 1/16	ENG APPR.		
ANGULAR: MACH 1/4	MFG APPR.		
TWO PLACE DECIMAL 1/2	G.A.		
THREE PLACE DECIMAL 3/4	COMMENTS:		
INTERPRET GEOMETRIC TOLERANCING PER: MATERIAL			
FINISH			
USED ON			
NEXT ASSY			
APPLICATION			
DO NOT SCALE DRAWING			

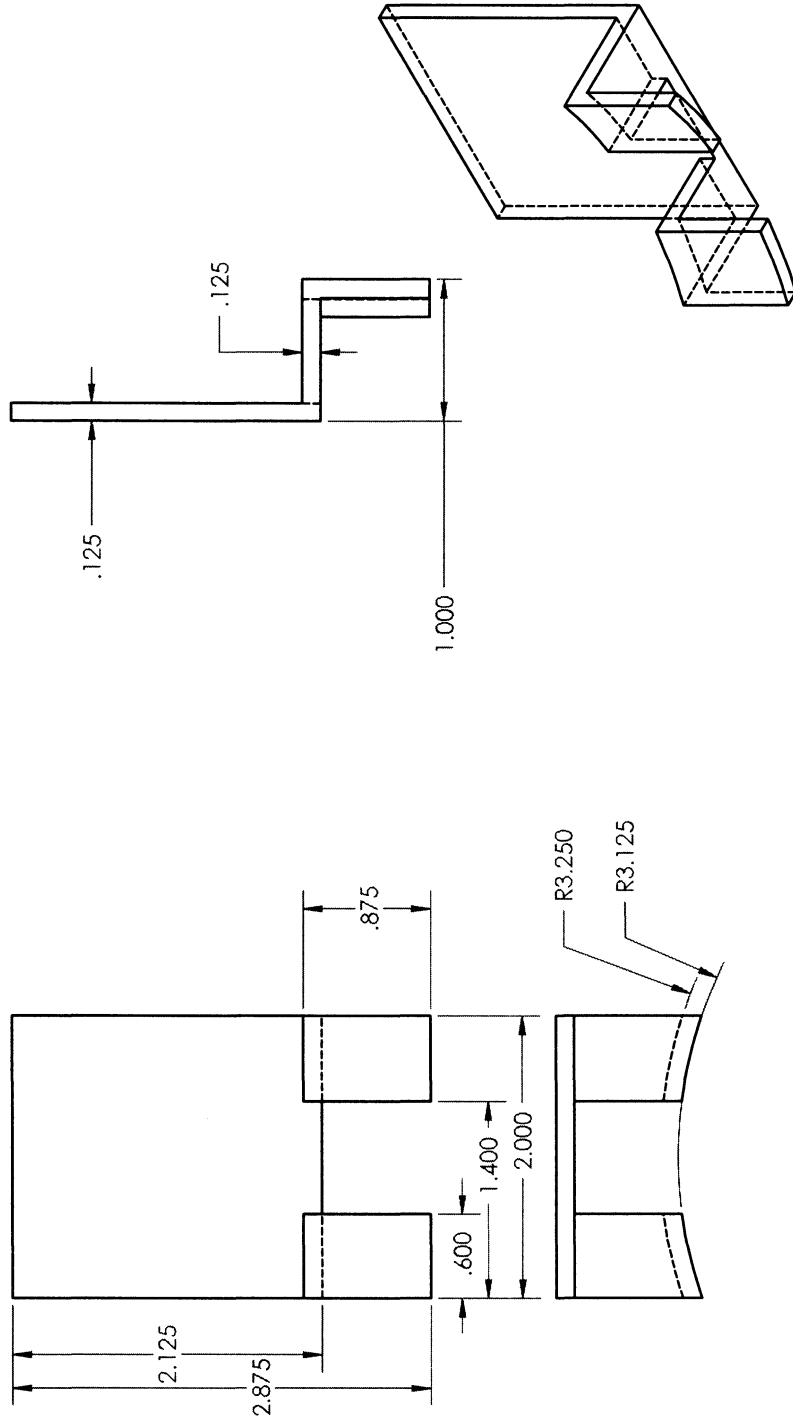
**PROPRIETARY AND CONFIDENTIAL**  
 THE INFORMATION CONTAINED IN THIS DRAWING IS THE SOLE PROPERTY OF EXOFORM. ANY REPRODUCTION IN PART OR AS A WHOLE WITHOUT THE WRITTEN PERMISSION OF EXOFORM COMPANY NAME HERE IS PROHIBITED.

SIZE DWG. NO. REV  
**ExoForeArmMotortoElbowl**

SCALE: 1:2 WEIGHT: SHEET 1 OF 1

5 4 3 2 1

Figure A.12 : Elbow to Forearm Joint



UNLESS OTHERWISE SPECIFIED:		NAME	DATE
DIMENSIONS ARE IN INCHES			
TOLERANCES:		DRAWN	
FRACTIONAL:		CHECKED	
ANGULAR:	MACH: BEND ±	ENG. APPR.	
TWO PLACE DECIMAL:		MFG APPR.	
THREE PLACE DECIMAL:		G.A.	
INTERPRET GEOMETRIC TOLERANCING PER:		COMMENTS:	
MATERIAL			
FINISH			
NEXT ASSY		USED ON	
APPLICATION		DO NOT SCALE DRAWING	
5	4	3	2

SIZE DWG. NO. REV  
**Aoutershellpart**  
 SCALE: 1:1 WEIGHT: SHEET 1 OF 1

Figure A.13 : Forearm Motor Mount

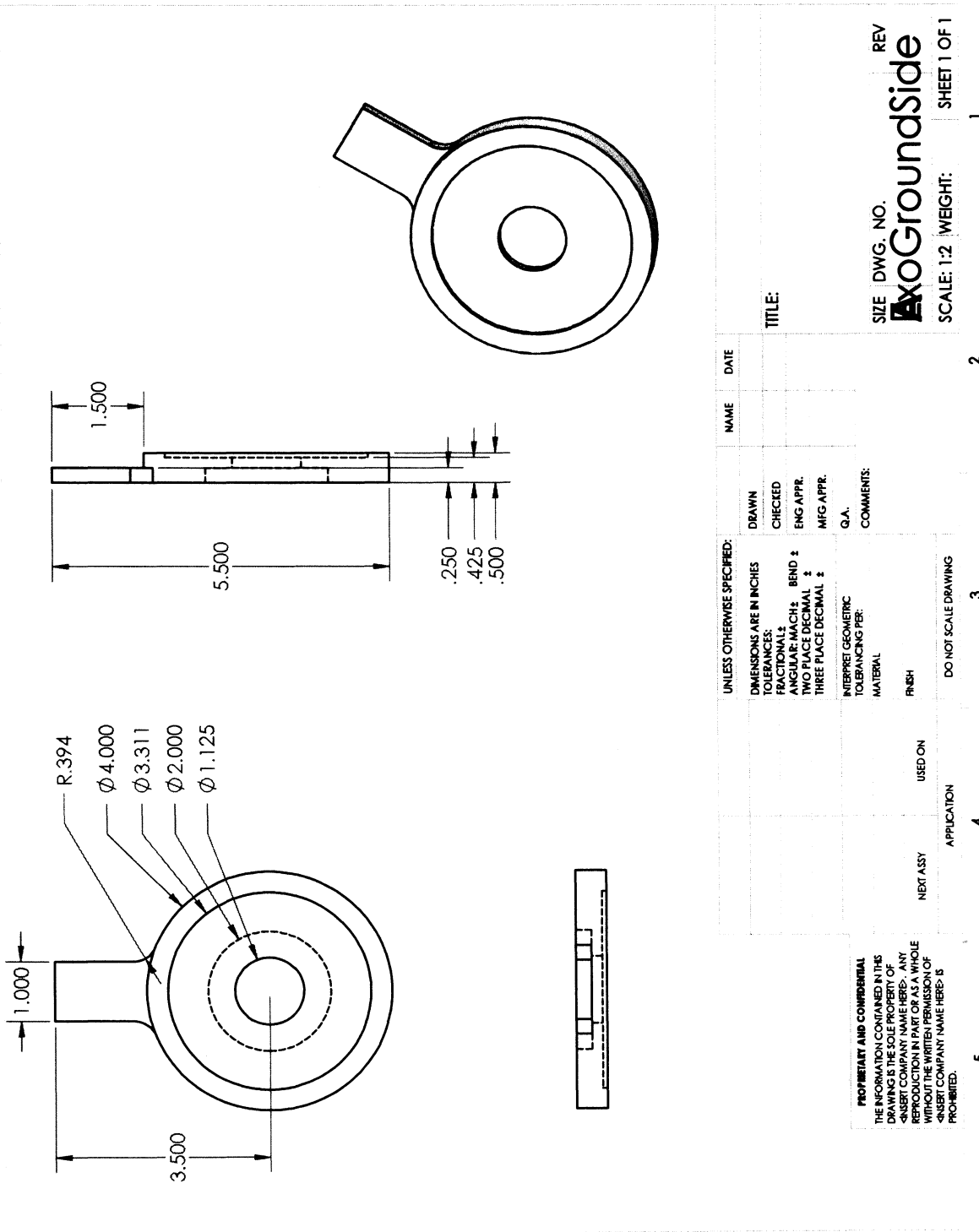


Figure A.14 : Elbow to Ground Joint

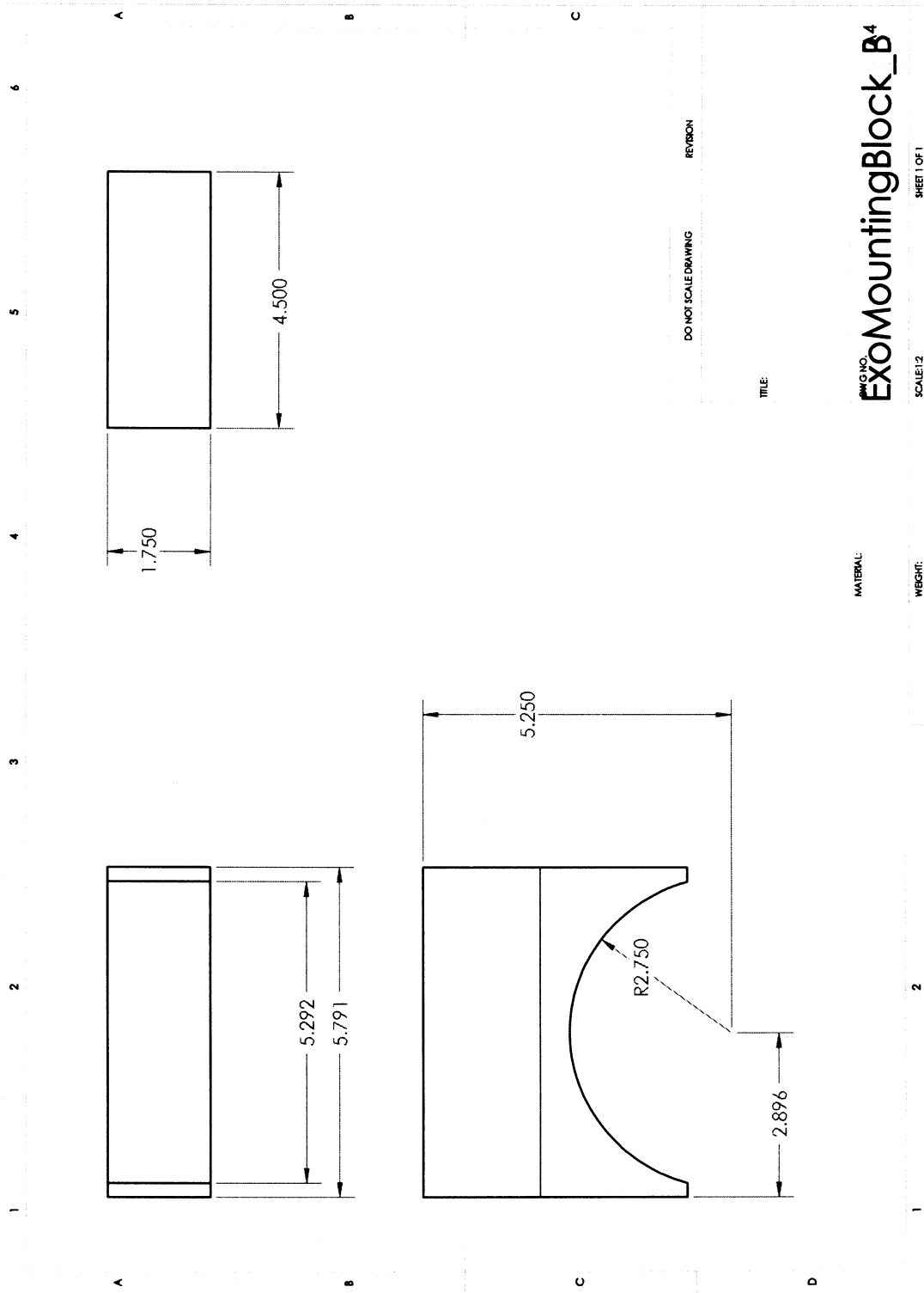


Figure A.15 : Ground Block

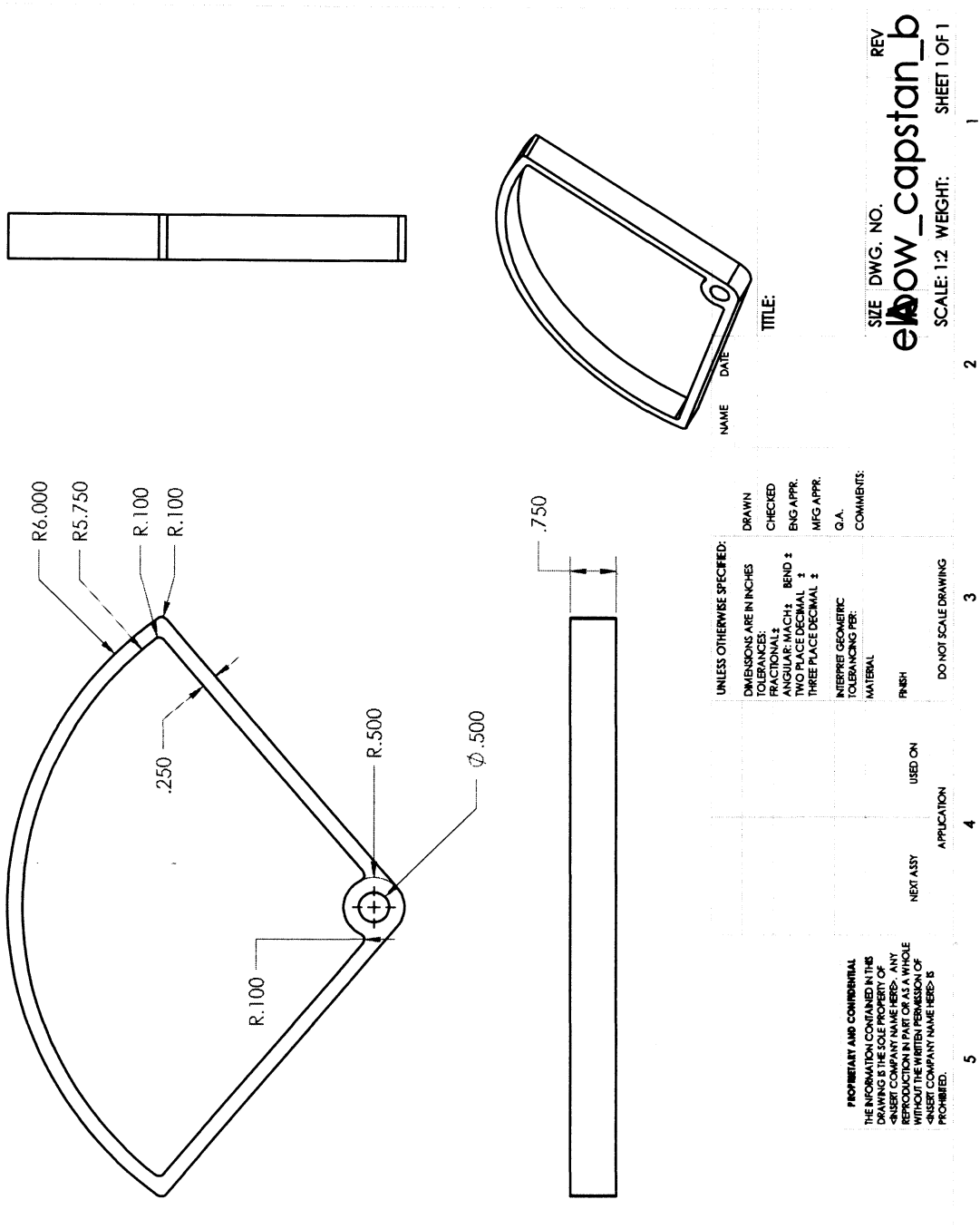
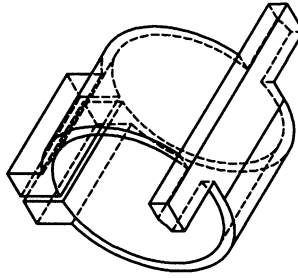
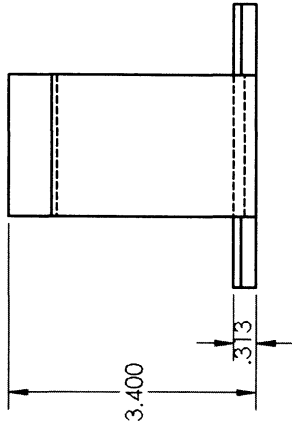
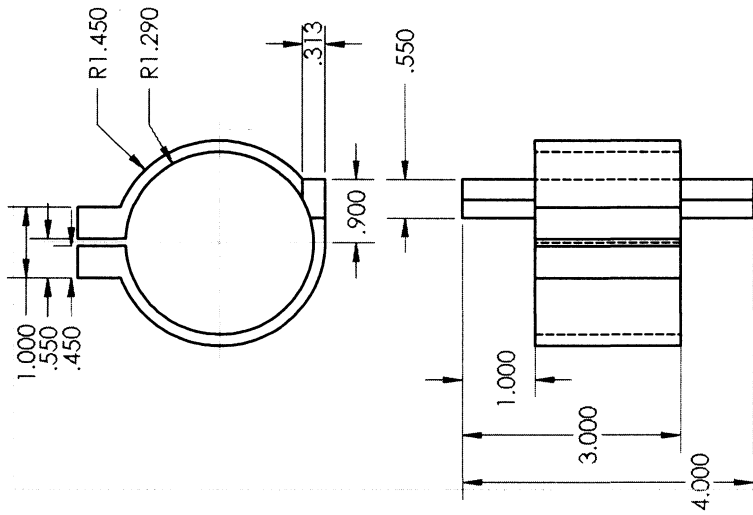


Figure A.16 : Elbow Capstan Arc



<p><b>PROPRIETARY AND CONFIDENTIAL</b>          THE INFORMATION CONTAINED IN THIS DRAWING IS THE SOLE PROPERTY OF INSERT COMPANY NAME HERE. ANY REPRODUCTION IN PART OR AS A WHOLE WITHOUT THE WRITTEN PERMISSION OF INSERT COMPANY NAME HERE IS PROHIBITED.</p>	<p>UNLESS OTHERWISE SPECIFIED:          DIMENSIONS ARE IN INCHES          TOLERANCES:          FRACTIONAL: ±          ANGULAR: MACH ± BEND ±          TWO PLACE DECIMAL ±          THREE PLACE DECIMAL ±</p>	<p>DRAWN          CHECKED          ENG APPR.          MFG APPR.          G.A.          COMMENTS:</p>	<p>NAME</p>	<p>DATE</p>	<p>TITLE:</p>	<p>SIZE DWG. NO. REV  <b>elbowmount_up_new</b></p>
	<p>INTERPRET GEOMETRIC TOLERANCING PER: MATERIAL FINISH USED ON NEXT ASSY APPLICATION</p>	<p>DO NOT SCALE DRAWING</p>	<p>SCALE: 1:2 WEIGHT: SHEET 1 OF 1</p>	<p>2</p>	<p>3</p>	<p>4</p>

Figure A.17 : Elbow Motor Mount

## Appendix B

### Autolev and C-Codes for Kinematic and Dynamic Equations

#### B.1 Autolev Code for Kinematic Equations

##### B.1.1 Position Level

```

%   File:  RiceWrist_Kinematics_v1.al
%   Date:  10.15.2011
%   Author:  Ali Utku Pehlivan
%   Problem:  RiceWrist Position Level Kinematics
%-----
%       Default settings
AutoEpsilon 1.0E-14      % Rounds off to nearest integer
AutoZ       on          % Turn ON for large problems
Degrees     off
Digits      7           % Number of digits displayed for numbers
%-----
%       Newtonian, bodies, frames, particles, points
Newtonian   N
Bodies      T, M                %base plate, end-effector
Bodies      A, B, C,           %legs

```



```

Bodies      CA, CB, CC, HC, HA          %ee connectors, handle connector,
Frames      FAT, FBT, FCT, FAM, FBM, FCM    %aux. frames
Points      O, PAT, PBT, PCT            %on the base
Points      E, PAM, PBM, PCM            %on the end-effector
Points      PCA, PCB, PCC              %between legs and connectors

%-----
%      Variables, constants, and specified
Variables   q{3}',L{3}',ALPHA', BETA', GAMMA', THETA', x',y',z'      % Configur
Constants   RHO1, RHO2                                          % base plate and
Constants   jnt
%Constants   cmT, cmCA, cmCB, cmCC, cmA{3}, cmB{3}, cmC{3}, cmM, cmHA{3}, cmHC{3}
%Constants   g
%Specified   dist{4}, cnti{4}          %control input, disturbance at the

%-----
% Mass and inertia properties
%Mass      T = mT, M = mM, A = mA, B = mB, C = mC, HA = mHA, HC = mHC
%Mass      CA = mCA, CB = mCB, CC = mCC
%Inertia   T, IT11, IT22, IT33, IT12, IT23, IT31
%Inertia   M, IM11, IM22, IM33, IM12, IM23, IM31
%Inertia   A, IA11, IA22, IA33, IA12, IA23, IA31
%Inertia   B, IB11, IB22, IB33, IB12, IB23, IB31
%Inertia   C, IC11, IC22, IC33, IC12, IC23, IC31
%Inertia   HA, IHA11, IHA22, IHA33, IHA12, IHA23, IHA31
%Inertia   HC, IHC11, IHC22, IHC33, IHC12, IHC23, IHC31
%Inertia   CA, ICA11, ICA22, ICA33, ICA12, ICA23, ICA31

```

```
%Inertia CB, ICB11, ICB22, ICB33, ICB12, ICB23, ICB31
```

```
%Inertia CC, ICC11, ICC22, ICC33, ICC12, ICC23, ICC31
```

```
%-----
```

```
%      Geometry relating unit vectors
```

```
Simprot(N, T, 3, THETA)
```

```
Simprot(T,FAT, 3, 0)
```

```
Simprot(T,FBT, 3, -2*PI/3)
```

```
Simprot(T,FCT, 3, 2*PI/3)
```

```
Simprot(FAT,A, 2, -q1)
```

```
Simprot(FBT,B, 2, -q2)
```

```
Simprot(FCT,C, 2, -q3)
```

```
Simprot(M,FAM, 3, 0)
```

```
Simprot(M,FBM, 3, -2*PI/3)
```

```
Simprot(M,FCM, 3, 2*PI/3)
```

```
Simprot(FAM, CA, 2, -PI/9)
```

```
Simprot(FBM, CB, 2, -PI/9)
```

```
Simprot(FCM, CC, 2, -PI/9)
```

```
Dircos(N,M,BODY123,ALPHA ,BETA ,GAMMA)
```

```
Simprot(M, HC, 3, 0)
```

```
Simprot(M, HA, 2, -PI/2)
```

```
%-----
```

```
%      Position vectors
```

P\_O\_PAT> =RHO1\*FAT1>

P\_O\_PBT> =RHO1\*FBT1>

P\_O\_PCT> =RHO1\*FCT1>

P\_PAT\_PCA> =L1\*A3>

P\_PBT\_PCB> =L2\*B3>

P\_PCT\_PCC> =L3\*C3>

P\_PCA\_PAM> =jnt\*CA3>

P\_PCB\_PBM> =jnt\*CB3>

P\_PCC\_PCM> =jnt\*CC3>

P\_E\_PAM> =RHO2\*FAM1>

P\_E\_PBM> =RHO2\*FBM1>

P\_E\_PCM> =RHO2\*FCM1>

P\_O\_E> = x\*N1>+y\*N2>+z\*N3>

%-----

% Configuration Constraint Equation(s)

ZEROS1>=P\_O\_PAT> + P\_PAT\_PCA> + P\_PCA\_PAM> - P\_E\_PAM> - P\_O\_E>

ZEROS2>=P\_O\_PBT> + P\_PBT\_PCB> + P\_PCB\_PBM> - P\_E\_PBM> - P\_O\_E>

ZEROS3>=P\_O\_PCT> + P\_PCT\_PCC> + P\_PCC\_PCM> - P\_E\_PCM> - P\_O\_E>

```
ZERO_CONFIG = [dot(ZEROS1>,N1>); dot(ZEROS2>,N1>); dot(ZEROS3>,N1>);&
dot(ZEROS1>,N2>); dot(ZEROS2>,N2>); dot(ZEROS3>,N2>);&
dot(ZEROS1>,N3>); dot(ZEROS2>,N3>); dot(ZEROS3>,N3>)]
```

```
inv_kin = [L1, L2, L3, q1, q2, q3, X, Y, THETA]
```

```
forw_kin = [ALPHA, BETA, GAMMA, q1, q2, q3, x, y, z]
```

```
Code Nonlinear(ZERO_CONFIG, inv_kin) ricewrist_inv_pos_v1.c
```

```
Code Nonlinear(ZERO_CONFIG, forw_kin) ricewrist_for_pos_v1.c
```

```
%Code Nonlinear(ZERO_CONFIG, inv_kin) ricewrist_inv_pos_v1.m
```

```
%Code Nonlinear(ZERO_CONFIG, forw_kin) ricewrist_for_pos_v1.m
```

```
%-----
```

```
% Record Autolev responses
```

```
Save RW_Kin_Pos.all
```

### B.1.2 Velocity Level

```
% File: RiceWrist_Dyn_v1.al
```

```
% Date: 10.15.2011
```

```
% Author: Ali Utku Pehlivan
```

```
% Problem: RiceWrist Velocity Level Kinematics
```

```
%-----
```

```
% Default settings
```

```
AutoEpsilon 1.0E-14 % Rounds off to nearest integer
```

```
AutoZ on % Turn ON for large problems
```

```
Degrees off
```

```

Digits      7          % Number of digits displayed for numbers
%-----
%          Newtonian, bodies, frames, particles, points
Newtonian   N
Bodies      T, M          %base plate, end-effector
Bodies      A, B, C,      %legs
Bodies      CA, CB, CC, HC, HA      %ee connectors, handle

connector, handle

Frames      FAT, FBT, FCT, FAM, FBM, FCM      %aux. frames
Points      O, PAT, PBT, PCT      %on the base
Points      E, PAM, PBM, PCM      %on the end effector
Points      PCA, PCB, PCC      %between legs and connectors
%-----
%          Variables, constants, and specified
Variables   q{3}',L{3}',ALPHA', BETA', GAMMA', THETA', x',y',z'      %

Configuration variables; derivatives

Constants   RHO1, RHO2          % base

plate and end-effector radius

Constants   jnt

Constants   cmT, cmCA, cmCB, cmCC, cmA{3}, cmB{3}, cmC{3}, cmM, cmHA{3},

cmHC{3}    % constants for CoM calculations

```

```

Constants    g
Specified    dist{4}, cnti{4} %control input, disturbance at the end effector
%-----
%           Motion variables for static/dynamic analysis
MotionVariables' u{13}' % Motion variables; derivatives
%-----
%           Geometry relating unit vectors
Simprot(N, T, 3, THETA)
Simprot(T,FAT, 3, 0)
Simprot(T,FBT, 3, -2*PI/3)
Simprot(T,FCT, 3, 2*PI/3)
Simprot(FAT,A, 2, -q1)
Simprot(FBT,B, 2, -q2)
Simprot(FCT,C, 2, -q3)
Simprot(M,FAM, 3, 0)
Simprot(M,FBM, 3, -2*PI/3)
Simprot(M,FCM, 3, 2*PI/3)

Simprot(FAM, CA, 2, -PI/9)
Simprot(FBM, CB, 2, -PI/9)
Simprot(FCM, CC, 2, -PI/9)

Dircos(N,M,BODY123,ALPHA ,BETA ,GAMMA)
Simprot(M, HC, 3, 0)
Simprot(M, HA, 2, -PI/2)

```

```
%-----  
% Angular Velocities  
angvel(N, T)  
angvel(N, M)  
  
angvel(N, FAT)  
angvel(N, FBT)  
angvel(N, FCT)  
  
angvel(N, A)  
angvel(N, B)  
angvel(N, C)  
  
angvel(N, FAM)  
angvel(N, FBM)  
angvel(N, FCM)  
  
angvel(N, CA)  
angvel(N, CB)  
angvel(N, CC)  
  
angvel(N, HA)  
angvel(N, HC)  
%-----  
%      Kinematical differential equations
```

x' = u1

y' = u2

z' = u3

ALPHA' = u4

BETA' = u5

GAMMA' = u6

L1' = u7

L2' = u8

L3' = u9

THETA' = u10

q1' = u11

q2' = u12

q3' = u13

%-----

% Angular Accelerations

ALF\_T\_N> = dt(W\_T\_N>, N)

ALF\_A\_N> = dt(W\_A\_N>, N)

ALF\_B\_N> = dt(W\_B\_N>, N)

ALF\_C\_N> = dt(W\_C\_N>, N)

ALF\_HA\_N> = dt(W\_HA\_N>, N)

ALF\_HC\_N> = dt(W\_HC\_N>, N)

ALF\_CA\_N> = dt(W\_CA\_N>, N)



ALF\_CB\_N> = dt(W\_CB\_N>, N)

ALF\_CC\_N> = dt(W\_CC\_N>, N)

ALF\_M\_N> = dt(W\_M\_N>, N)

%-----

% Position vectors

P\_O\_PAT> =RH01\*FAT1>

P\_O\_PBT> =RH01\*FBT1>

P\_O\_PCT> =RH01\*FCT1>

P\_PAT\_PCA> =L1\*A3>

P\_PBT\_PCB> =L2\*B3>

P\_PCT\_PCC> =L3\*C3>

P\_PCA\_PAM> =jnt\*CA3>

P\_PCB\_PBM> =jnt\*CB3>

P\_PCC\_PCM> =jnt\*CC3>

P\_E\_PAM> =RH02\*FAM1>

P\_E\_PBM> =RH02\*FBM1>

P\_E\_PCM> =RH02\*FCM1>

P\_O\_E> = x\*N1>+y\*N2>+z\*N3>

%-----

% Position vectors to centre of masses

P\_0\_To> = cmT\*T3>

P\_0\_Ao> = P\_0\_PAT> + cmA1\*A1> + cmA3\*A3>

P\_0\_Bo> = P\_0\_PBT> + cmB1\*B1> + cmB3\*B3>

P\_0\_Co> = P\_0\_PCT> + cmC1\*C1> + cmC3\*C3>

P\_0\_CAo> = P\_0\_PAM> - cmCA\*CA3>

P\_0\_CBo> = P\_0\_PBM> - cmCB\*CB3>

P\_0\_CCo> = P\_0\_PCM> - cmCC\*CC3>

P\_0\_Mo> = P\_0\_E> - cmM\*M3>

P\_0\_HCo> = P\_0\_PAM> + cmHC1\*HC1> + cmHC2\*HC2> + cmHC3\*HC3>

P\_0\_HAo> = P\_0\_HCo> + cmHA1\*HA1> + cmHA2\*HA2> + cmHA3\*HA3>

%-----

% Configuration Constraint Equation(s)

ZEROS1>=P\_0\_PAT> + P\_PAT\_PCA> + P\_PCA\_PAM> - P\_E\_PAM> - P\_0\_E>

ZEROS2>=P\_0\_PBT> + P\_PBT\_PCB> + P\_PCB\_PBM> - P\_E\_PBM> - P\_0\_E>

ZEROS3>=P\_0\_PCT> + P\_PCT\_PCC> + P\_PCC\_PCM> - P\_E\_PCM> - P\_0\_E>

ZERO\_CONFIG = [dot(ZEROS1>,N1>); dot(ZEROS2>,N1>); dot(ZEROS3>,N1>)];&

```

dot(ZEROS1>,N2>); dot(ZEROS2>,N2>); dot
(ZEROS3>,N2>);&
dot(ZEROS1>,N3>); dot(ZEROS2>,N3>); dot
(ZEROS3>,N3>)]

%inv_kin = [L1, L2, L3, q1, q2, q3, X, Y, THETA]
%forw_kin = [ALPHA, BETA, GAMMA, q1, q2, q3, x, y, z]
%Code Nonlinear(ZERO_CONFIG, inv_kin) ricewrist_inv_pos_v1.c
%Code Nonlinear(ZERO_CONFIG, forw_kin) ricewrist_for_pos_v1.c
%Code Nonlinear(ZERO_CONFIG, inv_kin) ricewrist_inv_pos_v1.m
%Code Nonlinear(ZERO_CONFIG, forw_kin) ricewrist_for_pos_v1.m
%-----
-
%      Velocity vectors
V_PAT_N> =dt(P_O_PAT>, N)
V_PBT_N> =dt(P_O_PBT>, N)
V_PCT_N> =dt(P_O_PCT>, N)

V_PCA_N> =dt(P_O_PCA>, N)
V_PCB_N> =dt(P_O_PCB>, N)
V_PCC_N> =dt(P_O_PCC>, N)

```

$$V_{PAM\_N} > = dt(P_{O\_PAM} >, N)$$

$$V_{PBM\_N} > = dt(P_{O\_PBM} >, N)$$

$$V_{PCM\_N} > = dt(P_{O\_PCM} >, N)$$

$$V_{E\_N} > = dt(P_{O\_E} >, N)$$

%-----

-

% Velocity and acceleration vector for centre of masses

$$V_{To\_N} > = dt(P_{O\_To} >, N)$$

$$V_{Ao\_N} > = dt(P_{O\_Ao} >, N)$$

$$V_{Bo\_N} > = dt(P_{O\_Bo} >, N)$$

$$V_{Co\_N} > = dt(P_{O\_Co} >, N)$$

$$V_{CAo\_N} > = dt(P_{O\_CAo} >, N)$$

$$V_{CBo\_N} > = dt(P_{O\_CBo} >, N)$$

$$V_{CCo\_N} > = dt(P_{O\_CCo} >, N)$$

$$V_{Mo\_N} > = dt(P_{O\_Mo} >, N)$$

$$V_{HCo\_N} > = dt(P_{O\_HCo} >, N)$$

$$V_{HAo\_N} > = dt(P_{O\_HAo} >, N)$$

A\_To\_N> =dt(dt(P\_O\_To>, N), N)

A\_Ao\_N> =dt(dt(P\_O\_Ao>,N), N)

A\_Bo\_N> =dt(dt(P\_O\_Bo>,N), N)

A\_Co\_N> =dt(dt(P\_O\_Co>,N), N)

A\_CAo\_N>=dt(dt(P\_O\_CAo>,N), N)

A\_CBo\_N>=dt(dt(P\_O\_CBo>,N), N)

A\_CCo\_N>=dt(dt(P\_O\_CCo>,N), N)

A\_Mo\_N> =dt(dt(P\_O\_Mo>,N), N)

A\_HCo\_N>=dt(dt(P\_O\_HCo>,N), N)

A\_HAo\_N>=dt(dt(P\_O\_HAo>,N), N)

%-----

% Motion Constraint Equation(s)

dZEROS1> = dt(ZEROS1>, N)

dZEROS2> = dt(ZEROS2>, N)

dZEROS3> = dt(ZEROS3>, N)

Dependent = [dot(dZEROS1>, N1>); dot(dZEROS2>, N1>); dot(dZEROS3>, N1>); &  
dot(dZEROS1>, N2>); dot(dZEROS2>, N2>); dot(dZEROS3>,

N2>); &

```

dot(dZEROS1>, N3>); dot(dZEROS2>, N3>); dot(dZEROS3>, N3>)]

Constrain(Dependent[u1, u2, u3, u4, u5, u6, u11, u12, u13])
%-----
% Jacobian

% Analytic Jacobian
Ja = [d(u1, u7), d(u1, u8), d(u1, u9), d(u1, u10); &
      d(u2, u7), d(u2, u8), d(u2, u9), d(u2, u10); &
      d(u3, u7), d(u3, u8), d(u3, u9), d(u3, u10); &
      d(u4, u7), d(u4, u8), d(u4, u9), d(u4, u10); &
      d(u5, u7), d(u5, u8), d(u5, u9), d(u5, u10); &
      d(u6, u7), d(u6, u8), d(u6, u9), d(u6, u10)]

J = Rows(Ja, 3:6)
Jtr = transpose(J)
Jinv = inv(J)
Jinvtr = transpose(Jinv)
Encode J, Jtr, Jinv, Jinvtr
Code Algebraic() ricewrist_jacobian.m
Code Algebraic() ricewrist_jacobian.c

```

## B.2 Autolev Code for Dynamics Equations

```
% File: RiceWrist_Dyn_v1.al
```

```

%   Date: 10.15.2011
%   Author: Ali Utku Pehlivan
%   Problem: RiceWrist Dynamics
%-----
%       Default settings
AutoEpsilon 1.0E-14    % Rounds off to nearest integer
AutoZ       on        % Turn ON for large problems
Degrees     off
Digits      7         % Number of digits displayed for numbers
%-----
%       Newtonian, bodies, frames, particles, points
Newtonian   N
Bodies      T, M      %base plate, end-effector
Bodies      A, B, C,  %legs
Bodies      CA, CB, CC, HC, HA    %ee connectors, handle connector,
Frames      FAT, FBT, FCT, FAM, FBM, FCM    %aux. frames
Points      O, PAT, PBT, PCT    %on the base
Points      E, PAM, PBM, PCM    %on the end effector
Points      PCA, PCB, PCC    %between legs and connectors
%-----
%       Variables, constants, and specified
Variables   q{3}',L{3}',ALPHA', BETA', GAMMA', THETA', x',y',z'    % Configur
Constants   RHO1, RHO2    % base plate and
Constants   jnt
Constants   cmT, cmCA, cmCB, cmCC, cmA{3}, cmB{3}, cmC{3}, cmM, cmHA{3}, cmHC{3}

```

```

Constants      g
Specified      dist{4}, cnti{4}                %control input, disturbance at the
%-----
% Mass and inertia properties
Mass   T = mT, M = mM, A = mA, B = mB, C = mC, HA = mHA, HC = mHC
Mass   CA = mCA, CB = mCB, CC = mCC
Inertia T, IT11, IT22, IT33, IT12, IT23, IT31
Inertia M, IM11, IM22, IM33, IM12, IM23, IM31
Inertia A, IA11, IA22, IA33, IA12, IA23, IA31
Inertia B, IB11, IB22, IB33, IB12, IB23, IB31
Inertia C, IC11, IC22, IC33, IC12, IC23, IC31
Inertia HA, IHA11, IHA22, IHA33, IHA12, IHA23, IHA31
Inertia HC, IHC11, IHC22, IHC33, IHC12, IHC23, IHC31
Inertia CA, ICA11, ICA22, ICA33, ICA12, ICA23, ICA31
Inertia CB, ICB11, ICB22, ICB33, ICB12, ICB23, ICB31
Inertia CC, ICC11, ICC22, ICC33, ICC12, ICC23, ICC31
%-----
%           Motion variables for static/dynamic analysis
MotionVariables' u{13}' % Motion variables; derivatives
%-----
%           Geometry relating unit vectors
Simprot(N, T, 3, THETA)
Simprot(T,FAT, 3, 0)
Simprot(T,FBT, 3, -2*PI/3)
Simprot(T,FCT, 3, 2*PI/3)

```



```

Simprot(FAT,A, 2, -q1)
Simprot(FBT,B, 2, -q2)
Simprot(FCT,C, 2, -q3)
Simprot(M,FAM, 3, 0)
Simprot(M,FBM, 3, -2*PI/3)
Simprot(M,FCM, 3, 2*PI/3)

```

```

Simprot(FAM, CA, 2, -PI/9)
Simprot(FBM, CB, 2, -PI/9)
Simprot(FCM, CC, 2, -PI/9)

```

```

Dircos(N,M;BODY123,ALPHA ,BETA ,GAMMA)

```

```

Simprot(M, HC, 3, 0)
Simprot(M, HA, 2, -PI/2)

```

```

%-----
```

```

% Angular Velocities

```

```

angvel(N, T)

```

```

angvel(N, M)

```

```

angvel(N, FAT)

```

```

angvel(N, FBT)

```

```

angvel(N, FCT)

```

```

angvel(N, A)

```

```

angvel(N, B)

```

angvel(N, C)

angvel(N, FAM)

angvel(N, FBM)

angvel(N, FCM)

angvel(N, CA)

angvel(N, CB)

angvel(N, CC)

angvel(N, HA)

angvel(N, HC)

%-----

% Kinematical differential equations

x' = u1

y' = u2

z' = u3

ALPHA' = u4

BETA' = u5

GAMMA' = u6

L1' = u7

L2' = u8

L3' = u9

THETA' = u10

q1' = u11

q2' = u12

q3' = u13

%-----

% Angular Accelerations

ALF\_T\_N> = dt(W\_T\_N>, N)

ALF\_A\_N> = dt(W\_A\_N>, N)

ALF\_B\_N> = dt(W\_B\_N>, N)

ALF\_C\_N> = dt(W\_C\_N>, N)

ALF\_HA\_N> = dt(W\_HA\_N>, N)

ALF\_HC\_N> = dt(W\_HC\_N>, N)

ALF\_CA\_N> = dt(W\_CA\_N>, N)

ALF\_CB\_N> = dt(W\_CB\_N>, N)

ALF\_CC\_N> = dt(W\_CC\_N>, N)

ALF\_M\_N> = dt(W\_M\_N>, N)

%-----

% Position vectors

P\_O\_PAT> =RH01\*FAT1>

P\_O\_PBT> =RH01\*FBT1>

P\_O\_PCT> =RH01\*FCT1>

P\_PAT\_PCA> =L1\*A3>

$$P\_PBT\_PCB> = L2*B3>$$

$$P\_PCT\_PCC> = L3*C3>$$

$$P\_PCA\_PAM> = jnt*CA3>$$

$$P\_PCB\_PBM> = jnt*CB3>$$

$$P\_PCC\_PCM> = jnt*CC3>$$

$$P\_E\_PAM> = RH02*FAM1>$$

$$P\_E\_PBM> = RH02*FBM1>$$

$$P\_E\_PCM> = RH02*FCM1>$$

$$P\_O\_E> = x*N1>+y*N2>+z*N3>$$

%-----

% Position vectors to centre of masses

$$P\_O\_To> = cmT*T3>$$

$$P\_O\_Ao> = P\_O\_PAT> + cmA1*A1> + cmA3*A3>$$

$$P\_O\_Bo> = P\_O\_PBT> + cmB1*B1> + cmB3*B3>$$

$$P\_O\_Co> = P\_O\_PCT> + cmC1*C1> + cmC3*C3>$$

$$P\_O\_CAo> = P\_O\_PAM> - cmCA*CA3>$$

$$P\_O\_CBo> = P\_O\_PBM> - cmCB*CB3>$$

$$P\_O\_CCo> = P\_O\_PCM> - cmCC*CC3>$$

$$P\_O\_Mo> = P\_O\_E> - cmM*M3>$$

$$P\_O\_HCo> = P\_O\_PAM> + cmHC1*HC1> + cmHC2*HC2> + cmHC3*HC3>$$

$$P\_O\_HAo> = P\_O\_HCo> + cmHA1*HA1> + cmHA2*HA2> + cmHA3*HA3>$$

%-----

% Configuration Constraint Equation(s)

$$ZEROS1>=P\_O\_PAT> + P\_PAT\_PCA> + P\_PCA\_PAM> - P\_E\_PAM> - P\_O\_E>$$

$$ZEROS2>=P\_O\_PBT> + P\_PBT\_PCB> + P\_PCB\_PBM> - P\_E\_PBM> - P\_O\_E>$$

$$ZEROS3>=P\_O\_PCT> + P\_PCT\_PCC> + P\_PCC\_PCM> - P\_E\_PCM> - P\_O\_E>$$

$$ZERO\_CONFIG = [dot(ZEROS1>,N1>); dot(ZEROS2>,N1>); dot(ZEROS3>,N1>);&$$

$$dot(ZEROS1>,N2>); dot(ZEROS2>,N2>); dot(ZEROS3>,N2>);&$$

$$dot(ZEROS1>,N3>); dot(ZEROS2>,N3>); dot(ZEROS3>,N3>)]$$

$$\%inv\_kin = [L1, L2, L3, q1, q2, q3, X, Y, THETA]$$

$$\%forw\_kin = [ALPHA, BETA, GAMMA, q1, q2, q3, x, y, z]$$

%Code Nonlinear(ZERO\_CONFIG, inv\_kin) ricewrist\_inv\_pos\_v1.c

%Code Nonlinear(ZERO\_CONFIG, forw\_kin) ricewrist\_for\_pos\_v1.c

%Code Nonlinear(ZERO\_CONFIG, inv\_kin) ricewrist\_inv\_pos\_v1.m

%Code Nonlinear(ZERO\_CONFIG, forw\_kin) ricewrist\_for\_pos\_v1.m

%-----

% Velocity vectors

V\_PAT\_N> =dt(P\_O\_PAT>, N)

V\_PBT\_N> =dt(P\_O\_PBT>, N)

V\_PCT\_N> =dt(P\_O\_PCT>, N)

V\_PCA\_N> =dt(P\_O\_PCA>, N)

V\_PCB\_N> =dt(P\_O\_PCB>, N)

V\_PCC\_N> =dt(P\_O\_PCC>, N)

V\_PAM\_N> =dt(P\_O\_PAM>,N)

V\_PBM\_N> =dt(P\_O\_PBM>,N)

V\_PCM\_N> =dt(P\_O\_PCM>,N)

V\_E\_N> =dt(P\_O\_E>,N)

%-----

% Velocity and acceleration vector for centre of masses

V\_To\_N> = dt(P\_O\_To>, N)

V\_Ao\_N> = dt(P\_O\_Ao>,N)

V\_Bo\_N> = dt(P\_O\_Bo>,N)

V\_Co\_N> = dt(P\_O\_Co>,N)

V\_CAo\_N> = dt(P\_O\_CAo>,N)

V\_CBo\_N> = dt(P\_O\_CBo>,N)

V\_CCo\_N> = dt(P\_O\_CCo>,N)

$$V_{Mo\_N} = dt(P_{O\_Mo}, N)$$

$$V_{HCo\_N} = dt(P_{O\_HCo}, N)$$

$$V_{HAo\_N} = dt(P_{O\_HAo}, N)$$

$$A_{To\_N} = dt(dt(P_{O\_To}, N), N)$$

$$A_{Ao\_N} = dt(dt(P_{O\_Ao}, N), N)$$

$$A_{Bo\_N} = dt(dt(P_{O\_Bo}, N), N)$$

$$A_{Co\_N} = dt(dt(P_{O\_Co}, N), N)$$

$$A_{CAo\_N} = dt(dt(P_{O\_CAo}, N), N)$$

$$A_{CBo\_N} = dt(dt(P_{O\_CBo}, N), N)$$

$$A_{CCo\_N} = dt(dt(P_{O\_CCo}, N), N)$$

$$A_{Mo\_N} = dt(dt(P_{O\_Mo}, N), N)$$

$$A_{HCo\_N} = dt(dt(P_{O\_HCo}, N), N)$$

$$A_{HAo\_N} = dt(dt(P_{O\_HAo}, N), N)$$

%-----

% Motion Constraint Equation(s)

$$dZEROS1 = dt(ZEROS1, N)$$

$$dZEROS2 = dt(ZEROS2, N)$$

```

dZEROS3> = dt(ZEROS3>, N)

Dependent = [dot(dZEROS1>, N1>); dot(dZEROS2>, N1>); dot(dZEROS3>, N1>); &
             dot(dZEROS1>, N2>); dot(dZEROS2>, N2>); dot(dZEROS3>, N2>); &
             dot(dZEROS1>, N3>); dot(dZEROS2>, N3>); dot(dZEROS3>, N3>)]

Constrain(Dependent[u1, u2, u3, u4, u5, u6, u11, u12, u13])
%-----
% Jacobian

% Analytic Jacobian
% Ja = [d(u1, u7), d(u1, u8), d(u1, u9), d(u1, u10); &
%       d(u2, u7), d(u2, u8), d(u2, u9), d(u2, u10); &
%       d(u3, u7), d(u3, u8), d(u3, u9), d(u3, u10); &
%       d(u4, u7), d(u4, u8), d(u4, u9), d(u4, u10); &
%       d(u5, u7), d(u5, u8), d(u5, u9), d(u5, u10); &
%       d(u6, u7), d(u6, u8), d(u6, u9), d(u6, u10)]

% J = Rows(Ja, 3:6)
% Jtr = transpose(J)
% Jinv = inv(J)
% Jinvtr = transpose(Jinv)
% Encode J, Jtr, Jinv, Jinvtr
% Code Algebraic() ricewrist_jacobian.m

```



```

% Code Algebraic() ricewrist_jacobian.c
%-----
% Generalized Torques
Gravity(-g*N1>)
Force_E> = dist1*N3>
Torque_M> = dist2*N1> + dist3*N2> + dist4*N3>
%-----
% Control Input

Torque_T> = cnti4*N3>
Force_PAT> = -cnti1*A3>
Force_PBT> = -cnti2*B3>
Force_PCT> = -cnti3*C3>

Force_PAM> = cnti1*A3>
Force_PBM> = cnti2*B3>
Force_PCM> = cnti3*C3>
%-----
%      Units system for CODE input/output conversions
UnitSystem  kg,meter,sec
%-----
%      Quantities to be output form the Code
Output  u7' m/s^2, u8' m/s^2, u9' m/s^2, u10' rad/s^2
%-----
%      Equations of motion

```

```
Zero = Fr() + FrStar()
Kane() % Simplify and/or solve
solve_for_X = [u7', u8', u9', u10']
solve(Zero, solve_for_X)
M = -[coef(Zero, u7'), coef(Zero, u8'), coef(Zero, u9'), coef(Zero, u10')]

CG = -(Zero + M*transpose(solve_for_X))
%-----
% Quantities to be output from the CODE
Encode M, CG
Code Dynamics() ricewrist_dynamics.c
%-----
% Record Autolev responses
% Save RW_Dyn.all
```

## Bibliography

- [1] A. Gupta and M. K. O'Malley, "Design of a haptic arm exoskeleton for training and rehabilitation," *IEEE/ASME Transactions on Mechatronics*, vol. 11, no. 3, pp. 280–289, 2006.
- [2] N. Tsagarakis, D. Caldwell, and G. Medrano-Cerda, "A 7 dof pneumatic muscle actuator (pma) powered exoskeleton," in *Robot and Human Interaction, 1999. RO-MAN'99. 8th IEEE International Workshop on*. IEEE, 1999, pp. 327–333.
- [3] J. C. Perry, J. Rosen, and S. Burns, "Upper-limb powered exoskeleton design," *IEEE/ASME Transactions on Mechatronics*, vol. 12, no. 4, pp. 408–417, 2007.
- [4] D. Lloyd-Jones, R. Adams, M. Carnethon, G. De Simone, T. B. Ferguson, K. Flegal, E. Ford, K. Furie, A. Go, K. Greenlund *et al.*, "Heart disease and stroke statistics–2009 update: A report from the American Heart Association Statistics Committee and Stroke Statistics Subcommittee," *Circulation*, vol. 119, no. 3, p. e21, 2009.
- [5] Anon., "Spinal cord injury: facts and figures at a glance," *National Spinal Cord Injury Statistical Center*, February 2010.
- [6] M. Berkowitz, *Spinal cord injury: An analysis of medical and social costs*. Demos Medical Pub, 1998.
- [7] R. Riener, T. Nef, and G. Colombo, "Robot-aided neurorehabilitation of the

- upper extremities,” *Medical and Biological Engineering and Computing*, vol. 43, no. 1, pp. 2–10, 2005.
- [8] C. Bütetisch, H. Hummelsheim, P. Denzler, and K. Mauritz, “Repetitive training of isolated movements improves the outcome of motor rehabilitation of the centrally paretic hand,” *Journal of the Neurological Sciences*, vol. 130, no. 1, pp. 59–68, 1995.
- [9] T. Nef, M. Mihelj, G. Kiefer, C. Perndl, R. Muller, and R. Riener, “ARMin-exoskeleton for arm therapy in stroke patients,” in *IEEE 10th International Conference on Rehabilitation Robotics (ICORR 2007)*. IEEE, 2008, pp. 68–74.
- [10] C. Senanayake and S. Senanayake, “Emerging robotics devices for therapeutic rehabilitation of the lower extremity,” in *Advanced Intelligent Mechatronics, 2009. AIM 2009. IEEE/ASME International Conference on*. IEEE, 2009, pp. 1142–1147.
- [11] A. Frisoli, L. Borelli, A. Montagner, S. Marcheschi, C. Procopio, F. Salsedo, M. Bergamasco, M. Carboncini, M. Tolaini, and B. Rossi, “Arm rehabilitation with a robotic exoskeleton in virtual reality,” in *Rehabilitation Robotics, 2007. ICORR 2007. IEEE 10th International Conference on*. IEEE, 2007, pp. 631–642.
- [12] H. I. Krebs, N. Hogan, M. L. Aisen, and B. T. Volpe, “Robot-aided neurorehabilitation,” *Rehabilitation Engineering, IEEE Transactions on*, pp. 75–87.
- [13] P. S. Lum, C. G. Burgar, P. C. Shor, M. Majmundar, and M. Van der Loos, “Robot-assisted movement training compared with conventional therapy tech-

- niques for the rehabilitation of upper-limb motor function after stroke.” *Arch Phys Med Rehabil*, vol. 83, no. 7, pp. 952–9, 2002.
- [14] T. G. Sugar, J. He, E. J. Koeneman, J. B. Koeneman, R. Herman, H. Huang, R. S. Schultz, D. E. Herring, J. Wanberg, S. Balasubramanian, P. Swenson, and J. A. Ward, “Design and control of RUPERT: a device for robotic upper extremity repetitive therapy,” *Neural Systems and Rehabilitation Engineering, IEEE Transactions on*, vol. 15, no. 3, pp. 336–346, 2007.
- [15] O. Celik, M. K. O’Malley, C. Boake, H. S. Levin, N. Yozbatiran, and T. A. Reistetter, “Normalized movement quality measures for therapeutic robots strongly correlate with clinical motor impairment measures,” *IEEE Transactions on Neural Systems and Rehabilitation Engineering*, vol. 18, no. 4, pp. 433–444, 2010.
- [16] A. Schiele and G. Hirzinger, “A new generation of ergonomic exoskeletons—the high-performance x-arm-2 for space robotics telepresence,” in *Intelligent Robots and Systems (IROS), 2011 IEEE/RSJ International Conference on*. IEEE, 2011, pp. 2158–2165.
- [17] R. Gopura, K. Kiguchi, and D. Bandara, “A brief review on upper extremity robotic exoskeleton systems,” in *Industrial and Information Systems (ICIIS), 2011 6th IEEE International Conference on*. IEEE, 2011, pp. 346–351.
- [18] V. Hayward and K. MacLean, “Do it yourself haptics: Part i,” *Robotics & Automation Magazine, IEEE*, vol. 14, no. 4, pp. 88–104, 2007.
- [19] L. Marchal-Crespo and D. Reinkensmeyer, “Review of control strategies for robotic movement training after neurologic injury,” *Journal of neuroengineering and rehabilitation*, vol. 6, no. 1, p. 20, 2009.

- [20] A. Pehlivan, O. Celik, and M. O'Malley, "Mechanical design of a distal arm exoskeleton for stroke and spinal cord injury rehabilitation," in *Rehabilitation Robotics (ICORR), 2011 IEEE International Conference on*. IEEE, 2011, pp. 1–5.
- [21] A. Sledd and M. K. O'Malley, "Performance enhancement of a haptic arm exoskeleton," in *Proc. of the Symposium on Haptic Interfaces for Virtual Environment and Teleoperator Systems (HAPTICS 2006)*. IEEE Computer Society, 2006, pp. 375–381.
- [22] D. Reinkensmeyer, M. Maier, E. Guigon, V. Chan, O. Akoner, E. Wolbrecht, S. Cramer, and J. Bobrow, "Do robotic and non-robotic arm movement training drive motor recovery after stroke by a common neural mechanism? experimental evidence and a computational model," in *Engineering in Medicine and Biology Society, 2009. EMBC 2009. Annual International Conference of the IEEE*. IEEE, 2009, pp. 2439–2441.
- [23] S. Riccardo, M. Marie-Helene, R. Giulio, and R. David, "Effect of visual distraction and auditory feedback on patient effort during robot-assisted movement training after stroke," *Journal of NeuroEngineering and Rehabilitation*, vol. 8, pp. 21–30, 2011.
- [24] R. Sanchez Jr, E. Wolbrecht, R. Smith, J. Liu, S. Rao, S. Cramer, T. Rahman, J. Bobrow, and D. Reinkensmeyer, "A pneumatic robot for re-training arm movement after stroke: Rationale and mechanical design," in *Rehabilitation Robotics, 2005. ICORR 2005. 9th International Conference on*. IEEE, 2005, pp. 500–504.
- [25] J. Roy, H. Moffet, B. McFadyen, and J. MacDermid, "The kinematics of upper

- extremity reaching: a reliability study on people with and without shoulder impingement syndrome,” *Sports Medicine, Arthroscopy, Rehabilitation Therapy & Technology*, vol. 2, no. 1, pp. 1–12, 2010.
- [26] J. Meythaler, S. Guin-Renfroe, P. Grabb, and M. Hadley, “Long-term continuously infused intrathecal baclofen for spastic-dystonic hypertonia in traumatic brain injury: 1-year experience,” *Archives of physical medicine and rehabilitation*, vol. 80, no. 1, pp. 13–19, 1999.
- [27] J. Rosen, J. Perry, N. Manning, S. Burns, and B. Hannaford, “The human arm kinematics and dynamics during daily activities-toward a 7 dof upper limb powered exoskeleton,” in *Advanced Robotics, 2005. ICAR'05. Proceedings., 12th International Conference on*. IEEE, 2005, pp. 532–539.
- [28] K. Lee and D. Shah, “Kinematic analysis of a three-degrees-of-freedom in-parallel actuated manipulator,” *Robotics and Automation, IEEE Journal of*, vol. 4, no. 3, pp. 354–360, 1988.
- [29] A. Schiele and F. C. T. van der Helm, “Kinematic design to improve ergonomics in human machine interaction,” *IEEE Transactions on Neural Systems and Rehabilitation Engineering*, vol. 14, no. 4, pp. 456–469, 2006.
- [30] M. OMalley, A. Sledd, A. Gupta, V. Patoglu, J. Huegel, and C. Burgar, “The ricewrist: A distal upper extremity rehabilitation robot for stroke therapy,” in *ASME International Mechanical Engineering Congress and Exposition*, 2006.
- [31] E. Wolbrecht, V. Chan, V. Le, S. Cramer, D. Reinkensmeyer, and J. Bobrow, “Real-time computer modeling of weakness following stroke optimizes robotic

- assistance for movement therapy,” in *Neural Engineering, 2007. CNE'07. 3rd International IEEE/EMBS Conference on*. IEEE, 2007, pp. 152–158.
- [32] P. Lum, C. Burgar, M. Van der Loos, P. Shor, M. Majmundar, and R. Yap, “The mime robotic system for upper-limb neuro-rehabilitation: Results from a clinical trial in subacute stroke,” in *Rehabilitation Robotics, 2005. ICORR 2005. 9th International Conference on*. IEEE, 2005, pp. 511–514.
- [33] D. Feygin, M. Keehner, and R. Tendick, “Haptic guidance: Experimental evaluation of a haptic training method for a perceptual motor skill,” in *Haptic Interfaces for Virtual Environment and Teleoperator Systems, 2002. HAPTICS 2002. Proceedings. 10th Symposium on*. IEEE, 2002, pp. 40–47.
- [34] N. Hogan, H. Krebs, B. Rohrer, J. Palazzolo, L. Dipietro, S. Fasoli, J. Stein, R. Hughes, W. Frontera, D. Lynch *et al.*, “Motions or muscles? some behavioral factors underlying robotic assistance of motor recovery,” *Journal of rehabilitation research and development*, vol. 43, no. 5, pp. 605–618, 2006.
- [35] F. Amirabdollahian, W. Harwin, and R. Loureiro, “Analysis of the fugl-meyer outcome measures assessing the effectiveness of robot-mediated stroke therapy,” in *Rehabilitation Robotics, 2007. ICORR 2007. IEEE 10th International Conference on*. IEEE, 2007, pp. 729–735.
- [36] E. Wolbrecht, “Adaptive, assist-as-needed control of a pneumatic orthosis for optimizing robotic movement therapy following stroke,” Ph.D. dissertation, University of California, Irvine, 2007.
- [37] J. Stein, H. Krebs, W. Frontera, S. Fasoli, R. Hughes, and N. Hogan, “Comparison of two techniques of robot-aided upper limb exercise training after stroke,”



*American journal of physical medicine & rehabilitation*, vol. 83, no. 9, pp. 720–728, 2004.

- [38] J. D. Irwin, *The industrial electronics handbook*. CRC, 1997.
- [39] R. Dickstein, Y. Heffes, Y. LAUFER, N. ABULAFFIO, and L. ESTHER, “Repetitive practice of a single joint movement for enhancing elbow function in hemiparetic patients,” *Perceptual and motor skills*, vol. 85, no. 3, pp. 771–785, 1997.
- [40] N. Yozbatiran, J. Berliner, C. Boake, M. O’Malley, Z. Kadivar, and G. Francisco, “Robotic training and clinical assessment of forearm and wrist movements after incomplete spinal cord injury: A case study,” in *Rehabilitation Robotics (ICORR), 2011 IEEE International Conference on*. IEEE, 2011, pp. 1–4.
- [41] F. Hummel, P. Celnik, P. Giraux, A. Floel, W. Wu, C. Gerloff, and L. Cohen, “Effects of non-invasive cortical stimulation on skilled motor function in chronic stroke,” *Brain*, vol. 128, no. 3, pp. 490–499, 2005.
- [42] M. McDonnell, “Action research arm test,” *Aust J Physiother*, vol. 54, no. 3, pp. 220–220, 2008.
- [43] J. Slotine and W. Li, “On the adaptive control of robot manipulators,” *The International Journal of Robotics Research*, vol. 6, no. 3, pp. 49–59, 1987.
- [44] F. Ghorbel, O. Chételat, R. Gunawardana, and R. Longchamp, “Modeling and set point control of closed-chain mechanisms: theory and experiment,” *Control Systems Technology, IEEE Transactions on*, vol. 8, no. 5, pp. 801–815, 2000.

- [45] R. Ortega and M. Spong, “Adaptive motion control of rigid robots: A tutorial,” *Automatica*, vol. 25, no. 6, pp. 877–888, 1989.
- [46] F. Ghorbel, “Adaptive control of flexible joint robot manipulators: a singular perturbation approach,” 1991.
- [47] M. Buhmann, *Radial basis functions: theory and implementations*. Cambridge Univ Pr, 2003, vol. 12.
- [48] F. Girosi and T. Poggio, “Networks and the best approximation property,” *Biological Cybernetics*, vol. 63, no. 3, pp. 169–176, 1990.
- [49] D. Schaechter, D. Levinson, and T. Kane, *Autolev user’s manual*. Online Dynamics, 1988.